REACTION OF CALCITE AND DOLOMITE WITH IN-SITU GELLED ACIDS, ORGANIC ACIDS, AND ENVIRONMENTALLY FRIENDLY CHELATING AGENT (GLDA)

A Dissertation

by

AHMED IBRAHIM RABIE

Submitted to the Office of Graduate Studies of
Texas A&M University
in partial fulfillment of the requirements for the degree of

DOCTOR OF PHILOSOPHY

Approved by:

Chair of Committee,	Hisham A. Nasr-El-Din
Committee Members,	A. Daniel Hill
	Jerome J. Schubert
	Mahmoud El-Halwagi
Head of Department,	A. Daniel Hill

December 2012

Major Subject: Petroleum Engineering

ABSTRACT

Well stimulation is the treatment remedy when oil/gas productivity decreases to unacceptable economical limits. Well stimulation can be carried out through either “Matrix Acidizing” or fracturing with both “Hydraulic Fracturing” and “Acid Fracturing” techniques. “Matrix Acidizing” and “Acid Fracturing” applications involve injecting an acid to react with the formation and dissolve some of the minerals present and recover or increase the permeability. The permeability enhancement is achieved by creating conductive channels “wormholes” in case of “Matrix Acidizing” or creating uneven etching pattern in case of “Acid Fracturing” treatments.

In both cases, and to design a treatment successfully, it is necessary to determine the distance that the live acid will be able to penetrate inside the formation, which in turn, determines the volume of the acid needed to carry out the treatment. This distance can be obtained through lab experiments, if formation cores are available, or estimated by modeling the treatment. The successful model will depend on several chemical and physical processes that take place including: the acid transport to the surface of the rock, the speed of the reaction of the acid with the rock, which is often referred to as “Reaction Rate”, and the acid leak-off. The parameters describing these processes such as acid diffusion coefficient and reaction kinetics have to be determined experimentally to ensure accurate and reliable modeling.

Hydrochloric acid and simple organic acids such as acetic and citric acids have been used extensively for stimulation treatments. The diffusion and reaction kinetics of these acids, in a straight form, were investigated thoroughly in literature. However, solely these acids are used in a simple form in the field. Acid systems such as gelled, crosslinked gelled, surfactant-based, foam-based, or emulsified acids are used to either retard the reaction rate or to enhance acid diversion. Literature review shows that additional work is needed to understand the reaction and report the diffusion and kinetics of these systems with carbonate. In addition, a new chelating agent (GLDA) was recently introduced as a stand-alone stimulating fluid. The kinetics and the mass transfer properties of this acid were not studied before.

Therefore, the objective of this work is to study the reaction of different acid systems with calcite and dolomite and report the mass transport and kinetic data experimentally. Lactic acid, a chelating agent (GLDA), and in-situ gelled HCl-formic acids were investigated in this study. In some cases, rheology measurements and core flood experiments were conducted. The data were combined with the reaction study to understand the behavior of these acids and examine their efficiency if injected in the formation.

ACKNOWLEDGEMENTS

I would like to thank my advisor and committee chair, Dr. Hisham A. Nasr-El-Din, for his support and for his academic guidance.

Appreciation is extended to the members of my committee, Dr. A. Daniel Hill, Dr. Jerome J. Schubert, and Dr. Mahmoud El-Halwagi.

I also would like thank my colleagues for their friendship and my family for their support during my graduate study.

Finally, I would like to acknowledge the financial support of the Texas Engineering Experiment Station of Texas A&M University (TEES), all companies that support the Middle East Carbonate Project (MEC), AkzoNobel, and Saudi Aramco Company for partially funding this work.

TABLE OF CONTENTS

Page

LIST OF FIGURES

LIST OF TABLES

1. INTRODUCTION

Well stimulation is the treatment remedy when oil productivity decreases to unacceptable limits due to formation damages. Well stimulation can be carried out through either “Matrix Acidizing” or fracturing with both “Hydraulic Fracturing” and “Acid Fracturing” techniques. “Matrix Acidizing” and “Acid Fracturing” applications involve the injection of a stimulating acid into the formation in order to dissolve some of the minerals/damage present and hence, recover or increase the permeability. In acid fracturing, high-pressure viscous fluid is injected to initiate and propagate fractures. Acid solution is then pumped to create non-uniform etched rock surfaces in the fractured channels. The uneven surface pattern provides conductive flow paths after the fracture closure. In matrix acidizing, acids are pumped below the fracture pressure to initiate and propagate highly permeable channels, known as “wormholes”, that bypass the damage near the wellbore area and regain the well productivity.

In both cases of “Matrix Acidizing” and “Acid Fracturing”, and to design a treatment successfully, it is necessary to determine the distance that live acid will be able to penetrate inside the formation. This distance will determine the volume of the acid needed to carry out the treatment and can be obtained through lab experiments if formation cores are available or estimated by modeling. These models involve several physical and chemical phenomena that take place during the treatment such as the acid diffusion to the formation surface, chemical reaction on the surface, and the acid leak-off

through the channel walls (Schechter 1992).

The parameters describing these processes such as acid diffusion coefficient and reaction kinetic data have to be determined experimentally to ensure accurate and reliable modeling. For instance, Hung et al. (1989) introduced a mathematical model that describes the growth and the propagation of wormholes in matrix acidizing and stated that wormhole characteristics are controlled by reaction, diffusion, and leak-off rate. The authors in this work showed a significant difference in the predicted length of wormholes when the acid diffusion was altered by 1 order of magnitude, which is very typical in such parameter, especially when the type of the acid changes between straight, gelled, cross-linked gelled, and emulsified acids.

Fredd and Fogler (1998c) also introduced a generalized model that describes the dissolution of calcite in several types of acids including HCl, weak acids, and chelating agents. The authors showed that the optimal injection rate and type of wormholes depend on a dimensionless group, referred to as "Damköhler number". The generalized model relates the Damköhler number to an overall reaction rate constant, which is in turn a function of the reactant and product mass transfer coefficients and the reaction rate constants.

Several researchers investigated the reaction and the diffusion of hydrochloric acid and simple organic acids such as acetic and citric acids when reacting with

carbonate. These acids have been used extensively for stimulation treatments. The diffusion and reaction kinetics of these acids, in a straight form, were investigated thoroughly in literature (Nierode and Williams 1971; Roberts and Guin 1974; Lund et al. 1975; Fogler et al. 1975; Kline and Fogler 1981; Busenberg and Plummer 1982; Gautelier at al. 1999; Buijse et al. 2004; Pokrovsky et al. 2005; 2009; Al-khaldi et al. 2007; 2010a, b).

However, these acids are solely used in a simple form in the field. Acid systems such as gelled, crosslinked gelled, surfactant-based, foam-based, or emulsified acids are used either to retard the reaction rate or to enhance acid diversion. Literature review shows that additional work is needed to understand the reaction and report the diffusion and kinetics of these systems with carbonate. In addition to these existing acid systems, chelating agents have been recently introduced in the oil field as stand-alone stimulating fluids. While there were some efforts to investigate existing chelants such as EDTA and HEDTA, the reaction and the mass transport of new chelating agents such GLDA with calcite and dolomite were not studied before.

The diffusion and the kinetic data have to be measured experimentally and the experimental set up should be designed and controlled carefully in order to provide the conditions to measure each of them separately. The two common methods known with this respect are the well-stirred reactor (slurry reactor) and the rotating disk reactor (RDR). The rotating disk reactor has become more popular and has been widely-used in

the last 20 years for measuring the kinetics of dissolution of various minerals under various conditions, both by hydrogeologists and researchers in the petroleum industry (Economides and Nolte 1989). The virtue of the rotating disk reactor is that the theory of mass transfer in the vicinity of a disk rotating in a semi-infinite volume of liquid has been studied extensively and reported (Levich 1962; Newman 1966; Ellison 1969). Therefore, studying the effect of both mass transport and reaction kinetics can be done under very well defined conditions of the transport process.

By controlling the temperature and the disk rotational speed, the dissolution can be exclusively limited by the transport process to the surface. In that case, the experimental data can be used to determine the acid diffusion coefficients. In the cases that the dissolution is completely independent on the rotational speed, the data can be used to drive the reaction kinetics such as the rate expression, the reaction rate constant, the reaction order, and the activation energy.

1.1 Objective and Thesis Overview

Because of the importance of reaction kinetics and mass transfer process in acidizing treatments and to provide the literature with measured data that are necessary for successful modeling, the objective of this study will be to utilize the rotating disk reactor to study the reaction of different acidizing systems with calcite and dolomite. A chelating agent (GLDA), in-situ gelled HCl-formic acids, and lactic acid were investigated. In two of the three case studies, results from rheology and core flood

experiments were combined with the reaction rate study to understand the behavior of these acids and evaluate their efficiency when injected in the formation at the reservoir temperature.

Section 2 of this study serves as an introduction to the rotating disk apparatus, a typical procedure to conduct an experiment, mathematical description for the mass transfer theory and how to analyze the data for both mass transfer and reaction kinetic limited reactions. This chapter also includes a brief description of the core flood setup and the HP/HT viscometer used in measuring the viscosity of HCl-formic acids studied in Section 4.

Section 3 describes the work done on an environmentally friendly chelating agent (GLDA). The reaction of GLDA with calcite are reported over a temperature range of 77-250°F and disk rotational speed of 100-1800 rpm. The two possible mechanisms of reaction (Hydrogen attack vs. chelating mechanism) were investigated.

Section 4 is an extension for Section 3 in which the reaction of GLDA with dolomite was addressed. The objectives were to utilize the rotating disk reactor to determine the effect of disk rotational speed, temperature, and acid concentration on the reaction of GLDA with dolomite and to report the conditions under which the reaction is diffusion/surface reaction limited.

Section 5 discusses the second study on cross-linked HCl-formic acids as diverting agents for carbonate. The RDR was used as a qualitative method to compare the reaction rate of different HCl-formic cross-linked and HCl-polymer based acids. Core flood study and viscosity measurements were combined with the RDR data to reach a conclusion on the efficiency of using mixtures of HCl and formic acids as diverting agents.

Section 6 presents a kinetic and mass transfer study of the reaction of lactic acid with calcite. The results obtained over a temperature range of 77-250°F and disk rotational speed of 100-1800 rpm were used to determine the acid diffusivity and fitted to the best power law kinetic expression. The reaction rate constants and the activation energy were reported.

Section 7 summarizes the main conclusions and provides some outlines for further expansion of the current work.

2. EXPERIMENTAL STUDY

This chapter is intended to serve as an introduction to the rotating disk apparatus, a typical procedure to conduct an experiment, mathematical description for the mass transfer theory and how to analyze the data for both mass transfer and reaction kinetic limited reactions. This chapter also includes a brief description of the core flood setup and the HP/HT viscometer used in measuring the viscosity of HCl-formic acids studied in chapter 4.

2.1 Rotating Disk Apparatus

The rotating disk reactor system (RDR) is used for primarily two important applications in the oil and gas industry. First, RDR is used to conduct corrosion tests of tubular samples (coupons) under static or dynamic conditions at elevated temperatures and pressures that imitate the downhole conditions. The effect of parameters such as acid type, acid concentration, temperature, type/concentration of additives, mainly corrosion inhibitors, and type of metal tubular on the corrosion rate can be determined using the RDR.

The RDR can also be used also to conduct a kinetics/diffusion study at the designated pressure and temperature. The availability of the fundamental equations that describe the mass transport phenomena in the reactor vicinity allowed several researchers to measure the diffusion coefficient for different acids at various conditions.

The kinetic and diffusion data are necessary information for any successful design of matrix acidizing or acid fracturing treatments.

The RDR consists mainly of two vessels; reservoir vessel and reactor vessel, as well as booster, rotating assembly, and controlling panel as shown in **Fig. 2.1**. The reservoir vessel is used mainly as pre-heating stage in which the fluid is loaded and heated up to the desired temperature. The reactor vessel contains the rotating shaft that provides the sample with the rotational motion, a sample holder (1 and 1.5 inch in diameter) that is attached to the sample using shrinkable Teflon tubing, **Fig. 2.2**.

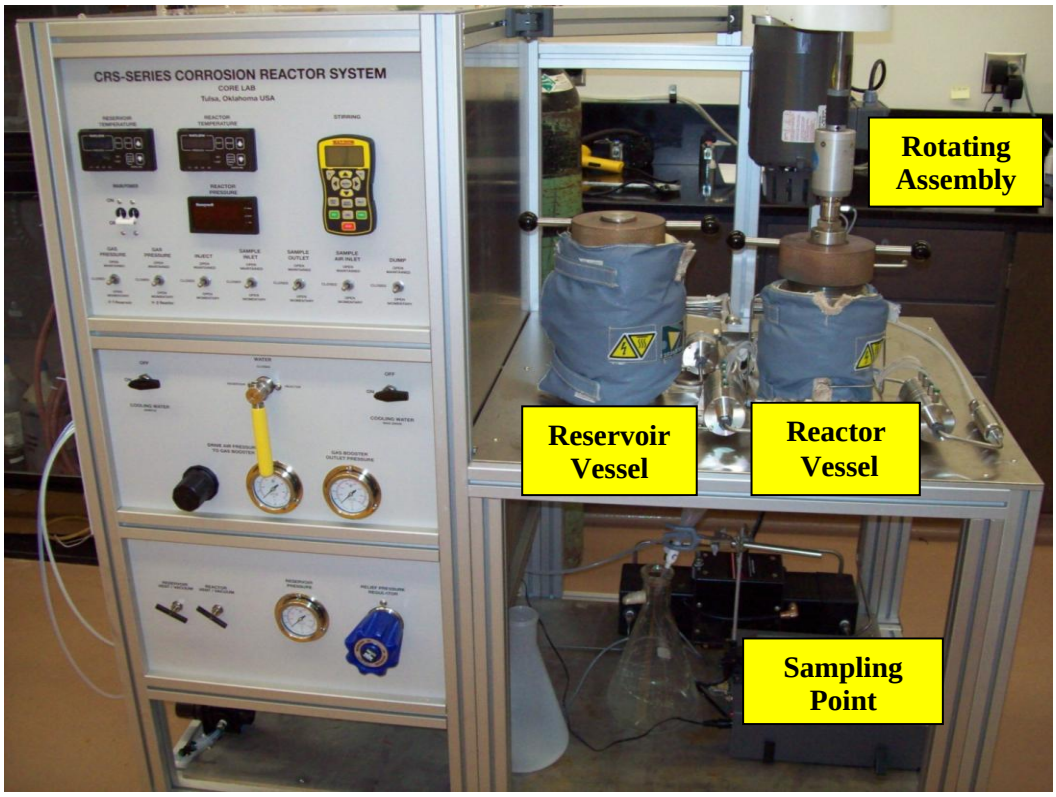

Fig. 2.1: The Rotating Disk Reactor.

The booster which is operated by low-pressure air is used to compress inert gas (N_2) in the space over the liquid surface in the reservoir and/or the reactor vessel and therefore, provides the necessary pressure required. The rotating assembly consists of a motor, two pulleys, connecting belt, and a rotating shaft. This assembly gives the rotational motion to the sample up to 1800 rpm. The controlling panel contains all the switches that operate the sampling valves and several displays for the temperature and the pressure in the reservoir and the reactor as well.

Fig. 2.2: A sample attached to the sample holder using the heat-shrinkable Teflon tubing.

All acid-contacting parts are manufactured from materials that resist corrosion that can occur due to exposure to the testing fluids. The reactor, reservoir, and the tubing parts are made of Hastelloy B. All the reactor vessel fluid plumbing and vessel body are mounted in a stationary fashion. The reactor and the reservoir vessels are heated with external electric band heaters. The temperature of the two vessels (reactor and reservoir) is set and read independently by separate auto-tuned temperature controllers.

2.2 Typical Procedure

The test on the RDR is carried out through 5 stages: Sample preparation, filling and pressurizing, heating, running and sampling, and termination. Below is a description of each one of these steps.

2.2.1 Sample Preparation

All the core samples were cut from carbonate blocks (Pink Desert limestone, Indiana limestone, and dolomite) into disks of 1.5 inch in diameter and 0.65-0.75 inch in thickness. Samples were dried at 120°C and weighed then saturated with deionized water for 24 hours under vacuum and re-weighed to determine the initial porosity.

All samples were then soaked in 0.1N HCl for 30 to 40 minutes then rinsed thoroughly with deionized water before reaction. This method ensures good reproducibility and eliminates problems associated with preparing the disk surfaces (Fredd and Fogler 1998c).

2.2.2 Filling and Pressurizing

If only a rotational motion is to be given to the fluid (no samples), fluid can be loaded directly to the reactor. However, if a sample (metal or rock) has to be used and liquid samples are to be taken periodically in time, the fluid has to be loaded first in the reservoir vessel and then transferred to the reactor. This procedure gives full control on the temperature of both specimen and fluid at the beginning of the experiment. The

internal volume of the reservoir vessel is 1100 cc and the reactor is 600 cc. The internal volume of the reactor is designed to keep the sample submerged in acid even after removing 200 cc of liquid samples during the test.

Throughout this study, a typical pressure of 1200 psi was kept in the reactor vessel during the test. This should be enough to keep CO_2 dissolved in the reaction fluids and therefore, does not affect the mass transfer to the rock surface. The reservoir pressure is set initially between 1500 and 2000 psi. This pressure is enough to transfer the fluid to the reactor and result in a pressure of 1000 psi in the reactor. To keep the reactor pressure at 1200 psi (or higher), compressed nitrogen is directed to the reactor directly. It also should be noted that heating after the initial pressurization may increase the pressure in the reservoir. A vent line is used to control the pressure as desired.

2.2.3 Heating

Controlling the temperature of the experiment is crucial for the accuracy of the results, the safety of the personnel running the experiment, and for the integrity of the mechanical parts of the instrument. Controlling the temperature can be achieved by using separate auto-tuned temperature controllers with built-in digital-displays. Each of these controllers automatically controls the temperature of the individually heated device by controlling its heaters. Although the maximum practical temperature in this study did not exceed 300°F, the maximum operating temperature of the heating elements is 200°C (392°F).

2.2.4 Running and Sampling

Once the temperature stabilizes to the desired values in the reactor and the reservoir, the rotational speed is then set up in the reactor to the selected value and the acid is allowed to transfer from the reservoir to reactor under pressure by manually controlling an "inject" valve. The time-recording start immediately at the moment the inject valve is opened. An initial sample is taken and discarded at the very beginning seconds to eliminate the effect of any residual cleaning water from the previous run.

Samples, each of approximately 2-3 cm^3, have to be taken afterwards accurately as a function of time. Normally, each experiment was run for 20-30 minutes, which is enough to collect 10-15 samples. Larger sampling time was avoided to eliminate the effect of changing the surface area on determining the rate of dissolution. The initial surface area of the sample was used to determine the dissolution rate.

2.2.5 Test Termination

Terminating the experiment correctly is very important to meet the safety requirements and maintain the machine in good shape for future use. Test termination includes releasing the pressure, draining the fluid, and post cleaning. To release the pressure, all the heaters are set off by changing the set point temperatures to some temperature below ambient. The residual pressure in the reservoir is first released by slowly opening the "vent" valve, which directs the compressed nitrogen and/or any

trapped acid fumes safely to a circulating-air fume hood. The same procedure is then applied to release the pressure in the reactor.

Once the temperature is lowered to a safely operating value, the residual fluid in the reactor is directed to a drainage vessel. The reactor lid can be opened to remove the sample. Samples after reaction have to be rinsed with deionized water, dried, and re-weighed for post analysis.

To clean the system, the reactor is closed again and running water is circulated through the reservoir, connecting tubes, reactor, and sampling tube for few minutes to ensure elimination of all residual fluids. Compressed nitrogen is then used to flush and dry all parts in the system.

2.3 Mathematical Description

RDR are used to study the heterogeneous reactions in which both mass transport to the surface and the kinetics play role in determining the rate of reaction. The overall reaction occurs through 3 main steps: (1) transfer of the reactant(s) from the bulk of solution to the surface, (2) chemical reaction on the surface, and (3) back diffusion of the product(s) to the bulk of the solution. An illustration of these steps is shown in **Fig. 2.3**.

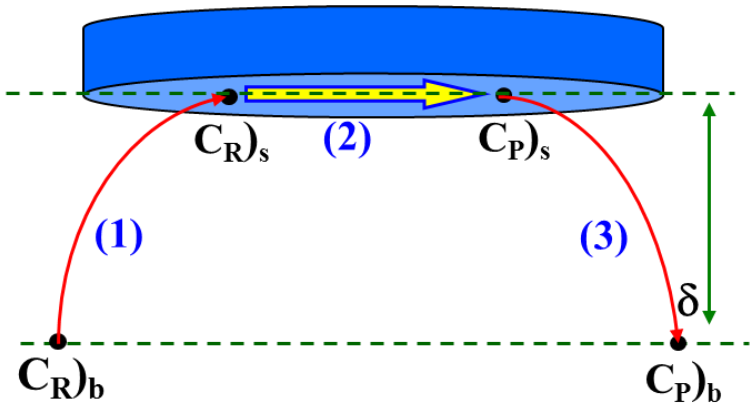

Fig. 2.3: Three steps for heterogeneous reactions: (1) mass transfer to the surface, (2) chemical reaction on the surface, and (3) mass transfer to the bulk of solution.

The overall rate of reaction is controlled by the slowest step of these steps which is referred to as "rate limiting step". To identify this step, the reaction rate should be measured over a wide range of the disk rotational speeds. If the reaction is mainly affected by the mass transfer to the surface, it is then called "mass-transfer limited". On the other hand, if the kinetics of the reaction on the surface controls the overall rate of reaction, it is then called, "surface-reaction limited".

The virtue of the rotating disk reactor is that the theory of mass transfer in the vicinity of a disk rotating in a semi-infinite volume of liquid has been studied extensively and reported (Levich 1962; Newman 1966; Ellison 1969). Therefore, studying the effect of both mass transport and reaction kinetics can be done under very well defined conditions of the transport process. The diffusion problem of a solute transferring to a surface has been formulated and solved analytically for certain geometries: Cylindrical, Single Plate, and Rotating Disk (Barron et al. 1962; Nierode

and Williams 1971; Roberts and Guin 1974; Levich 1962; Newman 1966; Ellision 1969) In the vicinity of a rotating disk reactor, the diffusion equation can be written as:

$$\frac{\partial C}{\partial t} + u\nabla C = D\nabla^2 C \quad \text{..... [2.1]}$$

The solution was introduced by Levich (1962) for Newtonian fluids describing the mass flux, J, as a function of mass transfer coefficient k_m and the concentration difference between the bulk of solution the and the surface:

$$J = k_M * A * \left(C_b - C_s\right) \quad \text{..... [2.2]}$$

$$\boldsymbol{k_M} = \frac{0.62048\boldsymbol{Sc}^{-2/3}\sqrt{\boldsymbol{\nu\omega}}}{\left[1 + 0.298\boldsymbol{Sc}^{-1/3} + 0.1459\boldsymbol{Sc}^{-2/3}\right]} \quad \text{..... [2.3]}$$

$$\boldsymbol{Sc} = \frac{\boldsymbol{\mu}}{\boldsymbol{\rho D_e}} \quad \text{..... [2.4]}$$

For non-Newtonian fluids, Hansford and Litt (1968) solved the convective diffusion equation and introduced modified Reynolds and Schmidt numbers to take into account the shear dependence of the viscosity power-law:

$$\boldsymbol{\mu} = \boldsymbol{K}\dot{\boldsymbol{\gamma}}^{\boldsymbol{n}-1} \quad \text{..... [2.5]}$$

and the mass transfer coefficient k_M is:

$$k_M = \left[\varphi'(n) \left(\frac{K}{\rho}\right)^{\frac{-1}{3(1+n)}} (r_s)^{\frac{(1-n)}{3(1+n)}} (\omega)^{\frac{1}{1+n}} D^{2/3} \right] \quad \text{..... [2.6]}$$

2.4 Mode of Operation

Analyzing the rotating disk reactor data is performed on two main steps. First, the rate of dissolution of each run has to be determined from the measured calcium and/or magnesium concentrations versus time. Secondly, the rate of dissolution at specific temperature or pH has to be plotted as a function of the disk rotational speed. From the later plot, a mode of operation is to be detected including mass transfer-limited, surface reaction limited, or a region of a mutual influence of both mass transfer and surface kinetics.

Fig. 2.4 shows an example of how the first step is conducted. The figure shows a particular case of the reaction of 5 wt% HCl in-situ gelled acids with Pink Desert limestone at 100 rpm and 150°F. The acid is used in the field for diversion purposes in which the acid, by reacting with the formation, forms a gel-like structure that plugs the high permeable zone to.

In the rotating disk experiments, when the acid reacts with the rock sample, pH on the surface increases due the fact that the acid gets spent and calcium and CO_2 are produced. At pH near to 2, a gel layer is formed on the surface. This was observed when

the rock sample was removed from the reactor after the run was completed. A thin slippery layer was noted in all in-situ gelled acid experiments.

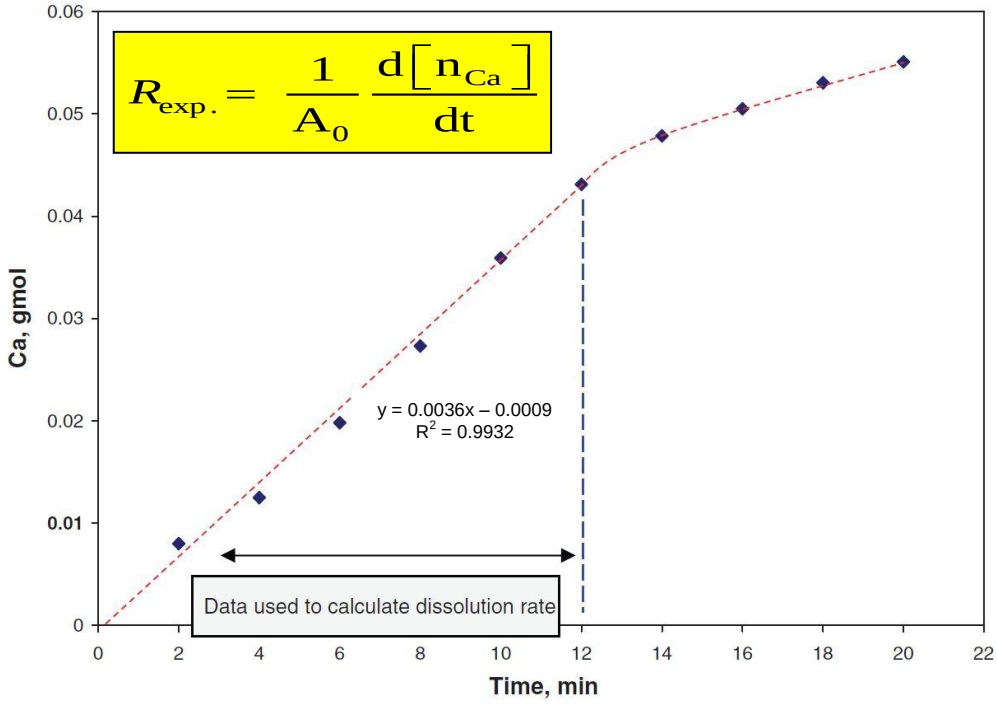

Fig. 2.4: Change of calcium concentration with time for the reaction of 5 wt% in-situ gelled HCl and Pink Desert limestone at 100 rpm and 150°F, (Rabie et al. 2011a).

The formation of this layer during the reaction is believed to act as a physical barrier, that even if preamble, will reduce the acid diffusivity to the rock surface and reduce the rate of reaction as seen from the change in the slope in Fig. 2-4 after 12 minutes. Therefore, the first data points (up to 12 minutes) were used and were fitted to the best straight line and the slope was divided by the initial area of the rock sample in order to calculate the dissolution rate at these specific conditions of disk rotational speed and temperature.

As mentioned in the previous section, the mass flux to the surface in the rotating disk depends on the mass transfer coefficient, which in turn depends on the rotational speed. Therefore, in the case that the overall reaction is mainly controlled by the mass transfer to the surface "mass-transferred limited", the overall rate of dissolution will depend on the disk rotational speed. On the other hand, if the overall reaction is mainly dependent on the kinetics of the surface reaction, changing the rotational speed does not affect the rate. This is the basis of how the results are analyzed as explained in more details below.

2.4.1 Mass-Transfer Limited Reactions

At relatively low rotational speeds, the rate of mass transfer of the reactant to the surface is remarkably slower than the surface reaction. The overall rate of dissolution, Rd, can then be determined directly from the mass flux equation:

$$R_d = J = k_m (C_b - C_s) \quad \text{[2.7]}$$

Substituting Eq. 2.3 for Newtonian fluids or Eq. 2.6 for non-Newtonian will yield the mathematical relation that describes the dependence of the dissolution rate, R_d, on the disk rotational speed, ω. In that case, the reaction rate is proportional to the rotating speed raised to the power (1/2) for Newtonian fluid and 1/(1+ n) in the case of non-Newtonian fluid. One assumption that can be made here is to neglect the concentration

on the surface with regard to the bulk concentration. This assumption is based on the fact that the rate of the surface reaction is much faster than the mass transfer rate.

For a certain initial bulk concentration, C_b, and assuming that this concentration will not change significantly during the reaction, plotting the rate of dissolution versus the disk rotational speed to the appropriate power should yield a straight line with a slope "A" that is proportional to the acid diffusivity raised to the power 2/3. **Fig. 2.5** shows the rate of dissolution of Pink Desert limestone in 0.6M chelating agent (GLDA) at 200^{o}F and pH of 1.7, 3.8, and 13, (Rabie et al. 2011b). The rate was plotted versus the disk rotational speed raised to the power (1/2) as the acid solution is a Newtonian fluid. It is also noted that over the whole range of investigated disk rotational speed (100 – 1800) rpm, the results were fitted accurately to a straight line, indicating a sole dependence of the rate of dissolution on the mass transfer.

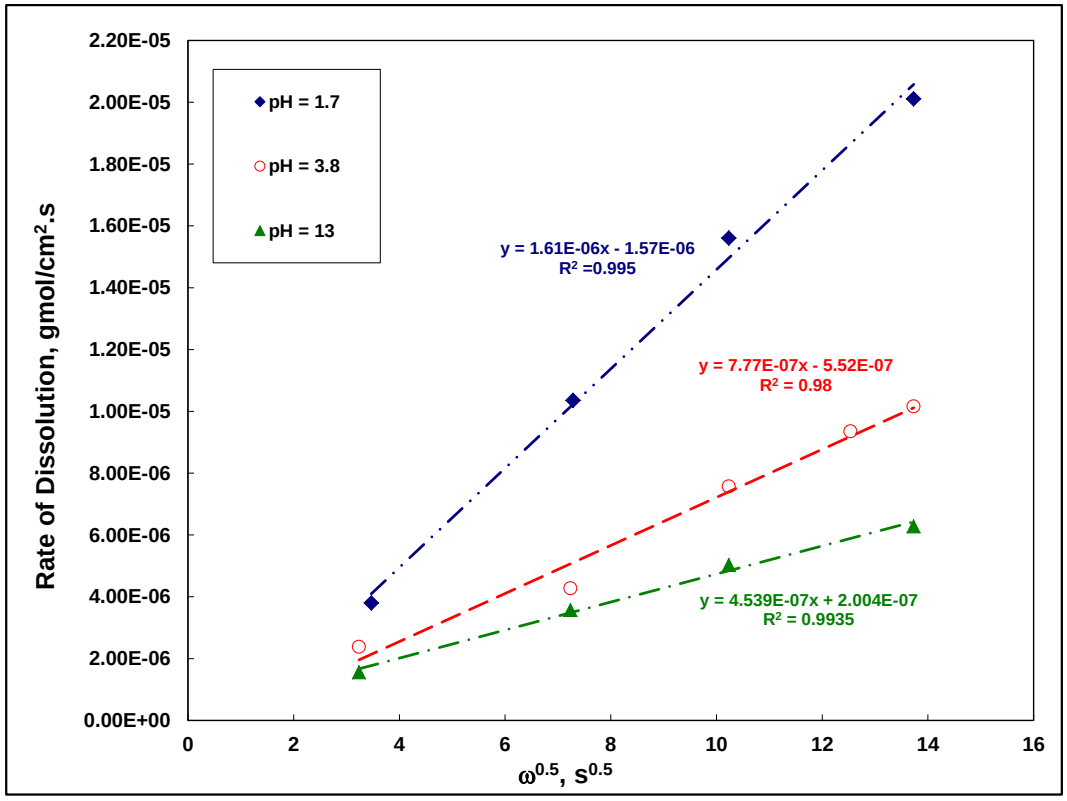

Fig. 2.5: Effect of disk rotational speed on the calcite dissolution of Pink Desert limestone in 0.6M GLDA at 200^{o}F and pH of 1.7, 3.8, and 13, (Rabie et al. 2011b).

Fig. 2.6 shows another example of the rate of dissolution of Pink Desert limestone in 5 wt% cross-linked HCl at 150°F. Because the acid solution is a non-Newtonian fluid, the rate was plotted versus the disk rotational speed raised to the power (1/1 + n), n = 0.69. Two distinguished regions can be observed in Fig. 2.6, a linear dependence on the disk rotational speed up to 1000 rpm, and a plateau between 1000 and 1800 rpm. The second region indicates a transition zone in which both mass transfer and kinetics of surface reaction controls the dissolution process.

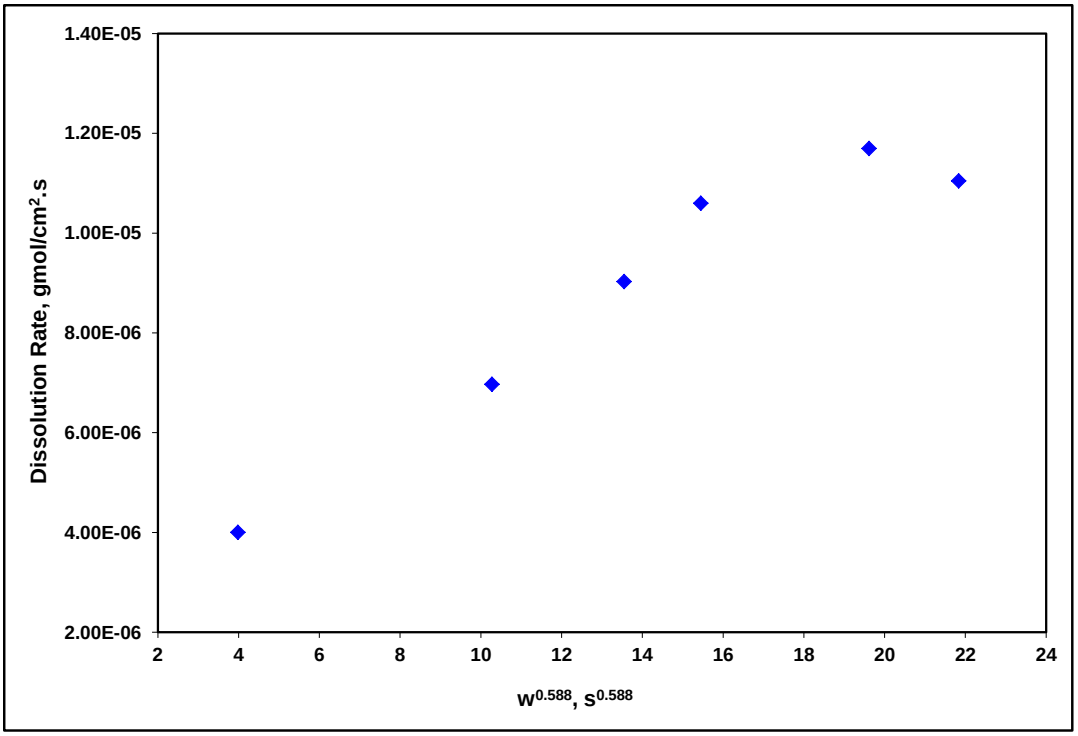

Fig. 2.6: Effect of disk rotational speed on the dissolution rate of Pink Desert limestone in 5 wt% in-situ gelled HCl at 150^{o}F, (Rabie et al. 2011a).

2.4.2 Reactions Limited by Surface Reaction

At relatively high disk rotational speeds, especially at low temperature, the mass transfer boundary layer decreases and, as a result, the mass transfer resistance decreases and the effect of surface reaction becomes more pronounced. If the rate of mass transfer becomes much faster than the surface reaction, the overall dissolution reaction is no longer proportional to the disk rotational speed and it should be obtained from the rate expression that describes the rate of reaction as a function of the reactant and product concentrations at the surface and the temperature of reaction.

For solid-liquid reactions at the interface of the solid surface, progression of reaction does not change the amount of solid per unit volume of the solid. Therefore, the solid concentration becomes constant and is usually lumped into the reaction rate constant as in the case of the carbonate reaction. In the case that the surface reaction is the rate limiting step, the mass transfer resistance is considered very small, especially at high rotational speeds. Therefore, the acid concentration on the rock surface is assumed to be equal to the acid concentration in the bulk concentration. The rate expression can then be written as a function of the acid bulk concentration assuming simple power-law expression that was reported for HCl with calcite (Nierode and Williams 1971; Lund et al. 1973; 1975). The general expression can be formulated as follows:

$$R_d = k_r [H_b^+]^m \quad \text{.....} \quad [2.8]$$

Where k_r is the reaction rate constant, $[H_b^+]$ is the acid concentration in the bulk solution, and m is the reaction rate order. The dependence of the reaction rate constant on temperature is described by Arrhenius equation:

$$k_r = k_o \, e^{\frac{-E_a}{RT}} \quad \text{.....} \quad [2.9]$$

Where k_o is the pre-exponential factor and E_a is the activation energy. Plotting Log k_r (the reaction rate constant) versus the reciprocal of the absolute temperature yields a straight line that has a slope of ($-E_a/R$).

2.5 Core Flood Setup

Core flood experiments were conducted in two of the chosen case studies to either investigate the optimum injection rate (GLDA) or the efficiency of the acid system as a diverting agent (in-situ HCl-formic). **Fig. 2.7** shows a schematic diagram for the setup.

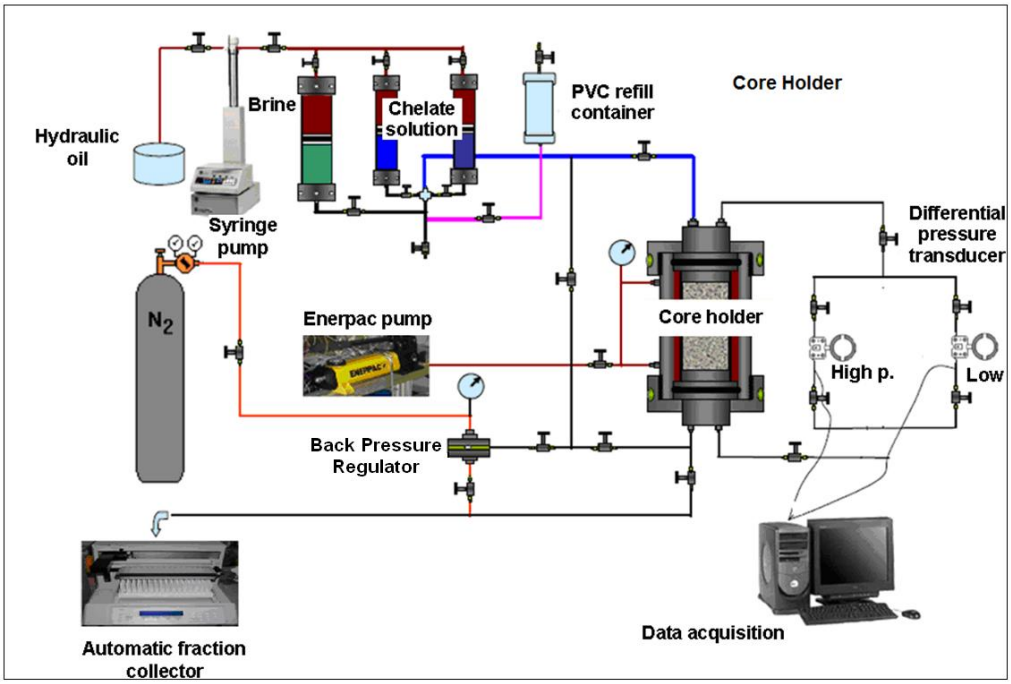

Fig. 2.7: Core Flood Setup

As shown in the figure, a syringe pump is connected to three accumulators to inject the acids into 6-inch length, 1.5-inch diameter cores that were placed horizontally in a core holder. A Back pressure regulator is used to keep back pressure of 1,100 psi on the outlet of the core. Pressure transducers were used to measure the deferential pressure across the core during the experiments every five seconds. Another hand-pump is used

to generate and keep overburden pressure of 2000 psi. A new core was used in each experiment. The cores were imaged using a CT scan technique after each acid injection. A heat jacket was placed around the core holder and was used to heat up the sample to 250 and 300^{o}F.

2.6 HP/HT Viscometer

The viscosity of different HCl-formic cross-linked gelled acids was measured as a function of temperature (77-250°F) and shear rate (0.1-1020) s^{-1} using HP/HT viscometer at live and partially neutralized (pH 4-5) conditions. To resist corrosion by the acids, both the rotor (R1) and the bob (B1) of the viscometer were made of Hastelloy C. The operation specifications of HP/HT viscometer is shown below in **Table 2.1**.

Table 2.1: Specifications of the HP/HT rheometer used for the viscosity measurements.

Sample size	52 ml
Speed Range	0.0001 – 1,100 rpm continuous
Shear Rate	0.00004 – 1870 S^{-1}
Frequency Range	0.01 – 5 Hz (with dynamic option)
Amplitude Range	0.1% – 500% (with dynamic option)
Temperature Range	Ambient (20^{o}F w/chiller) to 500^{o}F
Pressure Range	1 atm to 1,000 psi
Viscosity Range	0.5 – 5,000,000 Centipoise
Torque Range	14 μN.m to 100 mN.m
Shear Stress	1 to 15,000 dyne/cm^2
Resolution	0.01% of full scale range or better
Repeatability	±0.5% of full scale range or better

3. REACTION OF GLDA WITH CALCITE: REACTION KINETICS AND MASS TRANSPORT STUDY*

Chelating agents have been used in the oil industry as iron control, scale removers, and recently as effective stand-alone stimulating fluids in matrix acidizing, especially for deep wells where using hydrochloric acid is restricted due to its corrosion problems. The ultimate goal in matrix acidizing treatment is to create highly conductive wormholes that connect the formation to the wellbore. Glutamic acid diacetic acid (GLDA) is a new chelating agent that can be used for this purpose.

The objective of this work is to study the reaction of GLDA with calcite to investigate the optimum injection condition based on both kinetics and transport studies that have been performed experimentally in the laboratory.

The reaction of GLDA with calcite was investigated by measuring the rate of dissolution using the rotating disk apparatus. The effect of initial pH (1.7, 3.8, and 13) and disk rotational speed (100-1800 rpm) on the rate of reaction was studied at 150, 220 and 300°F. Pink Desert limestone cores 1.5 in. diameter and 0.65 in. length were used in this study.

---

* Reprinted with permission from "Reaction of GLDA with Calcite: Reaction Kinetics and Mass Transport Study" by A.I. Rabie, M.A. Mahmoud, and H.A. Nasr-El-Din, 2011. SPE Paper 139816 presented at the SPE International Symposium on Oilfield Chemistry held in The Woodlands, Texas, USA, 11–13 April.

GLDA transport and its effect on wormhole creation were investigated in core flood experiments using samples of 1.5 in. diameter and 6 in. length. The cores were scanned using CT-scan before and after the injection of GLDA solutions into the cores. Core flood experiments were conducted at temperatures of 200 and 300^{o}F.

The calcite dissolution rate was found to be a strong function of temperature and increased significantly by increasing the temperature from 80 to 300^{o}F. Increasing the pH from 1.7 to 13 resulted in a reduction in the rate of dissolution. GLDA reacted with calcite by one of two mechanisms; hydrogen ion attack and calcium complexation reaction. The GLDA chelation ability (expressed as a percentage of the total rate of dissolution) decreased by increasing temperature, but was not affected much by changing the disk rotational speed.

Acid diffusivity was determined at pH 1.7, 3.8, and 13 and the data was used with core flood results to determine the Damköhler number. An optimal Damköhler number was found in all experiments that correspond to a minimum pore volume required to break through the cores. Increasing temperature or reducing the pH increased the optimum Damköhler number with a reduction in the minimum pore volume required to break through.

3.1 Introduction

Chelating agents have been used in various applications because of their ability to form stable metal complexes that are soluble in water. Such applications include washing and treatment of contaminated soil/sediment (Peters 1999; Khodadoust et al. 2005; Polettini et al. 2006), softener for commercial detergents, in the food industry and medicine as heavy metal detoxification agents, and dissolution of calcium anhydrate sulphate scale from reboilers and heater tubes (Moore et al. 1972; Jamialahmadi and Muller-Steinhagen 1991). In the petroleum industry, chelating agents have been used as iron controlling agents (Taylor and Nasr-El-Din 1999), sulphate scale removal agents, and recently as stand-alone stimulating fluids for matrix acidizing (Fredd and Fogler 1998b; c; Frenier et al. 2001; 2004; Mahmoud et al. 2010a; b;2011).

Chelation agents include aminopolycarboxlic acids such as ethylenediaminetetraacetic acid (EDTA), nitrilotriacetic acid (NTA), diethylenetriaminepentacetic acid (DTPA), hydroxyethylethylenediaminetriacetic acid (HEDTA), and L-glutamic acid diacetic acid (GLDA). EDTA and DTPA have limited solubility in HCl solutions and are not readily degradable. Hydroxyethyliminodiacetic acid (HEIDA) was shown to be biodegradable, yet has lower calcium and iron stability constants and has a lower calcite dissolution capacity, if compared with EDTA and DTPA (Polettini et al. 2006).

Several studies addressed the application of different chelates as stand-alone stimulating fluids. After the pioneering work done by Fredd and Fogler (1998 a;b;c) on acetic acid, EDTA and DTPA, other research groups have been investigating other fluid systems such as HEDTA, citric acid, and GLDA (Frenier et al. 2001; 2004; Al-Khaldi et al., 2007; Mahmoud et al. 2011).

Fredd and Fogler (1998b) studied the kinetics of calcite dissolution in the presence of EDTA, DTPA, and [1,2 cyclohexandiaminetetraacetic acid] (CDTA) over a pH range of 3.3–12 using a rotating disk apparatus. They showed that the rate of dissolution increased significantly by the presence of chelating agents such as CDTA, DTPA, and EDTA and the rate of dissolution is influenced by the combined effects of the hydrogen ion reaction, the chelating reactions (involving various ionic species), and the water reaction. The pH of the solution and the concentration and type of chelating agent present, determine the reaction mechanism that dominates the dissolution reaction.

In another study, Fredd and Fogler (1998c) performed linear core flood experiments on Indiana limestone cores to investigate the dependence of the formation of wormholes on the transport and the reaction through the porous media. They showed that all the tested stimulating fluids including EDTA at pH= 4, and 13, and DTPA at pH of 4.3 showed the same optimum Damköhler number (a parameter that is inversely proportional to the flow rate) that is corresponding to the minimum pore volume required to break through the core.

Fernier et al. (2001 and 2004) examined HEDTA as a stimulating fluid and showed that it was able to form wormholes in limestone cores at 150^{o}F. Following the model proposed by Fredd and Fogler (1998a) and using the rotating disk reactors, diffusion and kinetics parameters were obtained to predict the optimum Damköhler number which was close to the observed one.

Huang et al. (2003) tested 10 wt% solutions of acetic acid, Na_4EDTA and long-chained carboxylic acid (LCA) using Indiana limestone cores of 1 in. diameter and 4 in. length. These cores have porosity of 15 vol% and permeability of 2 to 3 md. The dissolving power of 10 wt% LCA was measured to be 0.45 lb/gal at room temperature. They performed core flow tests at 250^{o}F using different flow rates to determine the optimum one that will be at the minimum pore volume to break through the core. All three chemicals used formed wormholes in the tested cores.

Several studies in our group have adopted a new promising environmentally friendly stimulation fluid that is driven from L-glutamic acid (MSG- mono-sodium glutamate). The new chemical was introduced by LePage et al. (2011) as polyacidic chelate L-glutamic acid, N, N-diacetic acid (GLDA). GLDA has showed very promising stimulating properties when compared to other chelating agents. In addition, and unlike HEDTA and HEIDA, GLDA has better solubility in HCl over a wide pH range. The new chemical is easily biodegradable, GLDA can achieve more than 60% biodegradation

within 28 days according to the standard OECD 301D test (Van Ginkel et al. 2005). The biodegradation level for EDTA and HEDTA in the same test is less than 5%. LePage et al. (2011) also reported that the thermal stability of GLDA is in the same order as HEDTA, which is considered to have very good thermal stability at high temperatures.

Mahmoud et al. (2010 a;b;2011) studied the ability of GLDA to dissolve calcium at different pH values and using a slurry reactor and reported the effect of the presence of sodium salt on the dissolution reaction. According to Mahmoud et al. (2010a), GLAD at pH of 1.7 was able to form a single dominate wormhole in a 20 in. core sample with flow rate of 2 cm^3/min at 200^oF.

In another work (Mahmoud et al. 2010b) investigated the optimum injection rate to break through the sample with minimum pore volume of stimulating fluid at different pH (1.7, 3) and examined the optimum fluid concentration and the effect of increasing the temperature on the optimum injection rate. The authors reported 1 cm^3/min as optimum injection rate for Indiana limestone (low permeability) and 3 cm^3/min for Pink Desert limestone (high permeability). 20 wt% was the optimum injection concentration and increasing the temperature from 180 to 250^oF did not affect the optimum injection rate, but did decrease the minimum pore volume required for breakthrough. The best interpretation of these results should be based on understanding the reaction between GLDA and carbonate rocks at different pH and temperatures.

3.2 Objectives

The objectives of this work are to: (1) investigate the effect of temperature, disk rotational speed, and pH on the rate of calcite dissolution using GLDA solutions, (2) identify the mechanism by which the acid reacts with the rock by measuring the percentage of complexation at different temperatures and disk rotational speeds, and (3) utilize the diffusion and the mass transport information from the rotating disk reactor with core flood experiments to determine the optimum Damköhler number and identify the flow conditions for optimal performance.

3.3 Effect of pH on the Dissociation of GLDA

GLDA is a member of the aminopolycarboxlic acids. Members of this group have the ability to form stable complexes with different metal ions, especially the alkaline–earth metals such as calcium and magnesium. The chemical structure of GLDA is shown in **Fig. 3.1**.

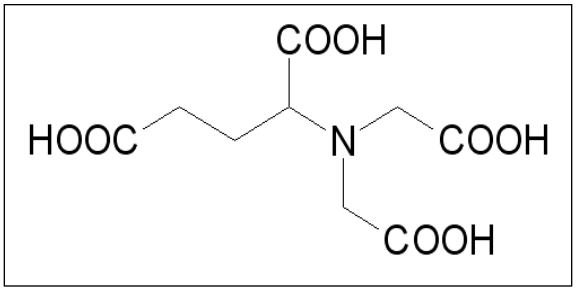

Fig. 3.1: Chemical structures of L-Glutamic acid, N, N-diacetic acid, (GLDA)

Aminopolycarboxlic acids undergo dissociation reactions in which the acid losses hydrogen ions and changes from totally acidic form at low pH into totally deprotonated form at high pH. The dissociation reactions for GLDA are:

$$H_4GLDA \leftrightarrow H_3GLDA^- + H^+ \quad \text{[3.1]}$$

$$H_3GLDA^- \leftrightarrow H_2GLDA^{-2} + H^+ \quad \text{[3.2]}$$

$$H_2GLDA^{-2} \leftrightarrow HGLDA^{-3} + H^+ \quad \text{[3.3]}$$

$$HGLDA^{-3} \leftrightarrow GLDA^{-4} + H^+ \quad \text{[3.4]}$$

Where $GLDA^{-4}$ represents the totally deprotonated part of the GLDA (i.e $C_9H_9NO_8$). The dissociation reactions are function of pH of the solution and the dissociation coefficients (pKa) of each reaction (LePage et al. 2011).

Table 3.1 gives the stability constants for different ions with GLDA and the values of the dissociation coefficients for the four reactions shown above. The species distribution of the four ligands is shown in **Fig. 3.2**. The full acidic form (H_4GLDA) dominates below pH of 2 while the totally deprotonated form ($GLDA^{-4}$) dominates at pH higher than 11. At neutral conditions (pH=7), the monoprotic form ($HGLDA^{-3}$) dominates.

Table 3.1: GLDA dissociation coefficients and the stability constants for different metal ions.

pK_1	pK_2	pK_3	pK_4	Log(K)[a]	
9.36	5.03	3.49	2.56	Ca^{2+}	5.4
				Mg^{2+}	4.9
				Ba^{2+}	3.54
				Cu^{2+}	7.8
				Zn^{2+}	4.0
				Mn^{2+}	5.4
				Fe^{3+}	13.0

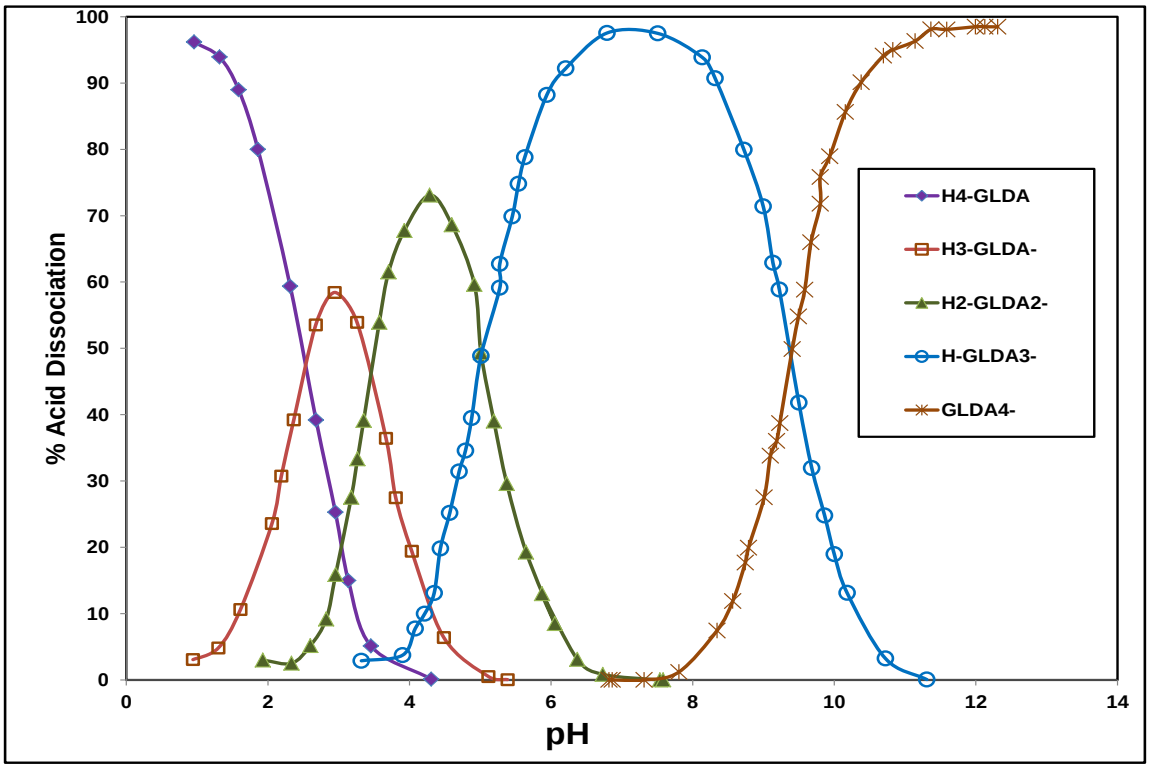

Fig. 3.2: Dissociation of GLDA at 25°C.

3.4 Reaction of GLDA with Calcite

The reaction of calcite with different aqueous solutions has been a subject of interest for many researchers (Lund et al., 1973, 1975; Plummer et al., 1978). Three surface reactions were reported by Plummer et al. (1978) that included the hydrogen ion attack, water reaction, and calcite reaction with carbonic acid. These reactions are shown below:

$$H^+ + CaCO_3 \leftrightarrow Ca^{2+} + HCO_3^- \quad \text{[3.5]}$$

$$H_2CO_3 + CaCO_3 \leftrightarrow Ca^{2+} + 2HCO_3^- \quad \text{[3.6]}$$

$$H_2O + CaCO_3 \leftrightarrow Ca^{2+} + HCO_3^- + OH^- \quad \text{[3.7]}$$

When the partial pressure of CO_2 over the reaction mixture is less than 0.1 atm, the concentration of H_2CO_3 is negligible. Eq. 3.5 (the hydrogen attack) represents the main reaction at low pH. At high pH, Eq. 3.7 represents the dominant reaction and known as water reaction. Reaction represented by Eq. 3.6 is considered only when CO_2 partial pressure is above 0.1 atm and the pH is above 5.

In addition to these reactions, one or more of the following reactions between GLDA and calcite may occur depending on the pH of the solution:

$$H_2GLDA^{-2} + CaCO_3 \leftrightarrow CaH_2GLDA + CO_3^{-2} \quad \text{[3.8]}$$

$$HGLDA^{-3} + CaCO_3 \leftrightarrow CaHGLDA^{-1} + CO_3^{-2} \quad \text{[3.9]}$$

$$GLDA^{-4} + CaCO_3 \leftrightarrow CaGLDA^{-2} + CO_3^{-2} \quad \text{.....} \quad [3.10]$$

Reactions shown by Eqs. 3.8-10 represent the chelation reactions of GLDA that occur when different dissociated species attack the calcium site rather than the carbonate site on the surface, grab the calcium ion and form a stable complex.

3.5 Experimental Studies

3.5.1 Materials

Pink Desert limestone was used to conduct core flood tests. The same rock was used to run tests in the rotating disk apparatus. Core samples from blocks of Pink Desert limestone, **Table 3.2**, were cut into disks with a diameter of 3.81 cm (1.5 in.) and a thickness of 2.54 cm (1 in.).

The procedure reported by Fredd and Fogler (1998c) was followed to ensure good reproducibility. 0.6M GLDA solutions at pH values of 1.7, 3.8, and 13 (measured at 25°C) were prepared by dilution from three concentrated solutions of 40 wt% at the same pH values that were obtained from AkzoNobel and therefore no pH adjustment was needed. Deionized water was used to prepare the GLDA solutions.

Table 3.2: Composition, permeability, and porosity of core samples cut from Pink Desert limestone block.

	Pink Desert limestone
Avg. Porosity, vol%	28
Avg. Permeability, md	80
Composition (wt%)	
Al	0.0707
C	11.9
Ca	39.7
Cl	0.2
Fe	0.0379
K	0.0233
Mg	0.0794
O	47.8
S	0.0329
Si	0.121
Sn	0.0121
Sr	0.0227
$CaCO_3$, wt%	99.4

3.5.2 Free and Chelated Calcium Measurements

GLDA reacts with calcite through different mechanisms according to the type of the dominant reaction on the surface. The latter in turn is determined mainly based on the pH of the reaction medium. Acid attack (or H^+ attack) is the main mechanism at low pH in which GLDA acts as polyprotic acid, while at pH greater than 11 the acid is fully deprotonated and the main mechanism is chelation mechanism. In acid attack reaction, the hydrogen ions (H^+) attack the carbonate component on the surface resulting in dissolving the calcium as free ions in solution.

On the other hand in the chelation reaction, the chelate attacks the calcium site, grabs the ion, and forms a stable complex. Measuring the concentration of the free calcium in solution with time indicates which mechanism occurs and influences the reaction more. Ion selective electrode (Thermo Scientific) and pH meter (M370, Core-Palmer) were used to measure the free calcium for all the collected samples collected.

3.6 Results and Discussion

Rotating disk experiments were conducted over a wide range of disk rotational speed (100-1800) rpm. To study the effect of temperature, the rate of dissolution was measured over a temperature range of 80-300^{o}F at pH 3.8 and 1000 rpm. The concentration of free calcium for all samples at pH of 3.8 and 13 were measured. The results for reactions at pH of 3.8 are only discussed further below. As theoretically expected, no free calcium exists for reaction at pH of 13 due to the chelation reaction.

The rest of this chapter is to discuss the effect of temperature and disk rotational speed on both the overall dissolution rate and the percentage of the rate of chelation reaction. The data obtained from the rotating disk study along with the results from core flood experiments are used to predict the optimum Damköhler number.

3.6.1 Effect of Disk Rotational Speed and pH on the Dissolution Rate

Increasing the disk rotational speed will increase the rate of dissolution in the case that the reaction is controlled by the mass transport process or controlled by both mass transport and surface reaction together. In the case that the reaction is only limited by the mass transfer to the surface, a linear relation should be observed when the measured rate of dissolution is plotted versus $\omega^{1/2}$.

.

Fig. 3.3 shows the rate of dissolution as a function of the disk rotational speed for the reaction of GLDA and calcite (Pink Desert limestone) for a range of disk rotational speeds of 100-1800 rpm at 200^{o}F. Increasing the disk rotational speed from 100 to 1800 rpm has increased the rate of dissolution 5 times at pH of 1.7 and 4 times at pH of 13. On the other hand, increasing the pH of the reacting solution from 1.7 to 13 significantly reduced the rate of dissolution. The three different slopes in Fig. 3.3 indicate that the higher pH of the acid, the lower the diffusion coefficient and hence, the lower the rate of dissolution.

Fredd and Fogler (1998b) have reported a reaction that is primarily controlled by kinetics of the surface reaction of 0.25M EDTA at pH 12 and 4. However, all the reaction experiments in their work were done at room temperature (21±2^{o}C). Increasing the temperature enhances the surface reaction more than the diffusivity to the surface. In addition, the initial acid concentration of the tested fluids in their study was 0.25M while the initial GLDA concentration here is 0.6M.

The rate data obtained at the three different pH values were used to determine the effective diffusion and mass transfer coefficients as a function of disk the rotational speeds. Data are shown in **Table 3.3**.

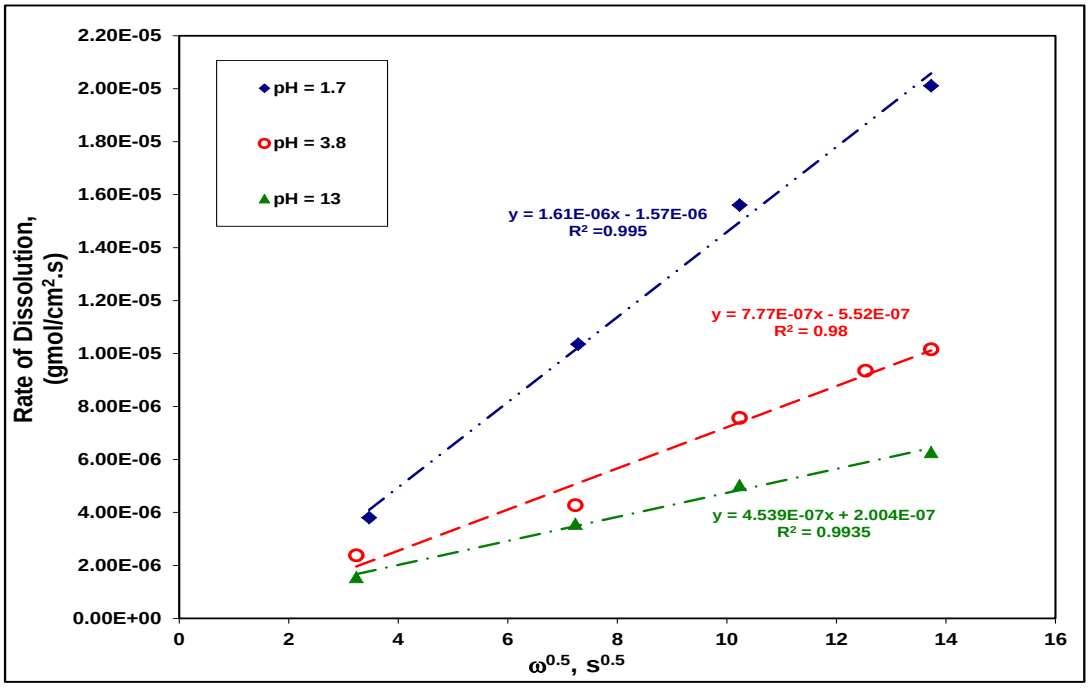

Fig. 3.3: Rate of calcite dissolution in the presence of 0.6M GLDA at 200^{o}F and pH of 1.7, 3.8, and 13.

Table 3.3: Determination of the effective diffusivity for GLDA at different pH values and 200^{o}F.

pH	D_e, cm^2/s	N, rpm	k_m, cm/s
1.7	1.19E-04	100	8.68E-03
		1000	2.75E-02
		1800	3.68E-02
3.8	3.97E-05	100	4.19E-03
		1000	1.33E-02
		1800	1.78E-02
13	1.64E-05	100	2.45E-03
		1000	7.74E-03
		1800	1.04E-02

3.6.2 Effect of Temperature on the Dissolution Rate of GLDA with Calcite

Increasing the temperature increases the overall rate of dissolution. **Fig. 3.4** shows the measured rate of reaction as a function of the disk rotational speed for two different temperatures at 80 and 200^{o}F, both at pH 3.8.

At 1000 rpm, the rate of reaction at 200^{o}F was 6 times the reaction at 80^{o}F. This difference becomes more noticeable at higher rotational speeds. The reaction rate at 1800 rpm and 200^{o}F is almost one order of magnitude higher than the reaction at 80^{o}F (27^{o}C). The data for the reaction at 80^{o}F was used to determine the diffusion coefficient at this temperature and was found to be $3.1*10^{-6}$ cm^2/s. This value matches with the

diffusion coefficient estimated from Einstein-Stokes equation that gives $2.56*10^{-6}$ cm^2/s and also is in agreement with that was reported by Fredd and Fogler for DTPA and EDTA at 20°C ($4*10^{-6}$, $3.7*10^{-6}$ cm^2/s, respectively).

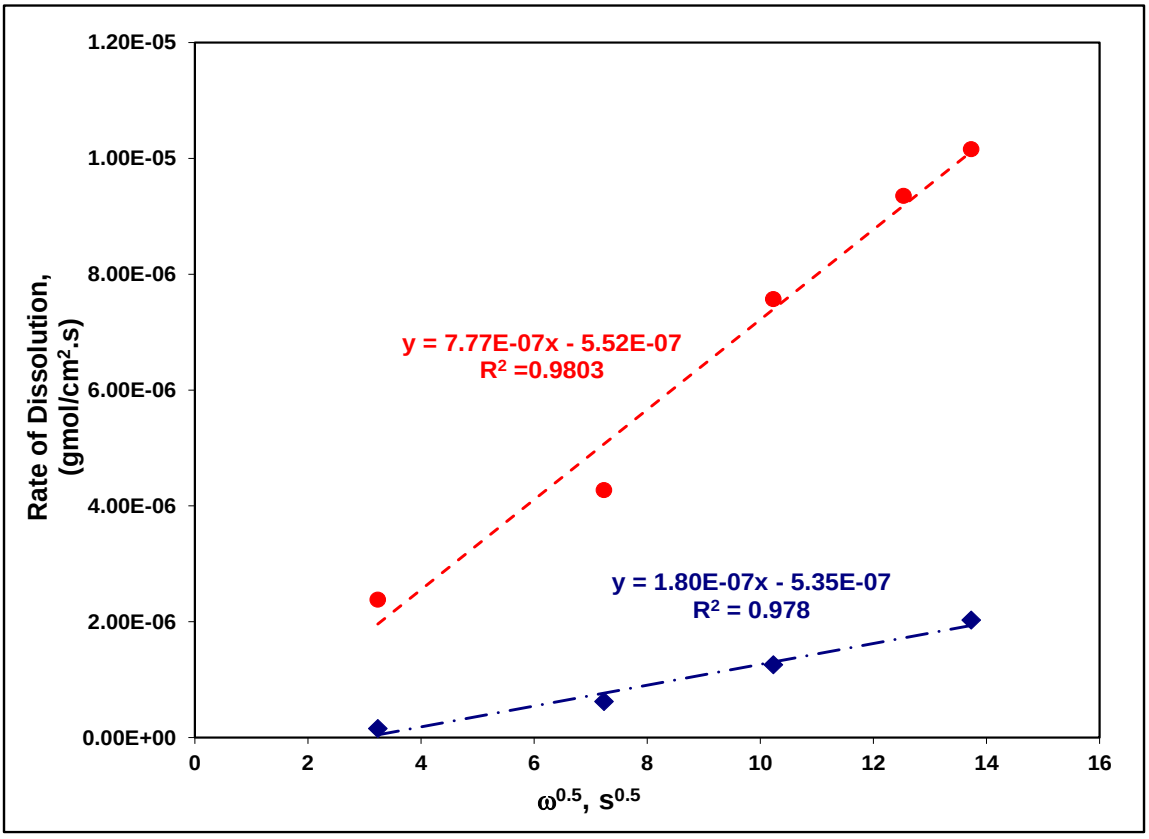

Fig. 3.4: Rate of calcite dissolution in the presence of 0.6M GLDA at pH =3.8, 1000 rpm, and 80 and 200°F.

Fig. 3.5 shows the measured rate of reaction of GLDA (0.6M and pH 3.8) over a range of temperatures from 80 to 300°F. The data was fitted to the best Arrhenius relation and the resulting apparent activation energy for the reaction of GLDA (pH of

3.8) with calcite was found to be 4.81 kcal/mol. Fredd and Fogler (1998b) reported activation energy of 12 kcal/mol for the reaction of EDTA at pH of 4.0.

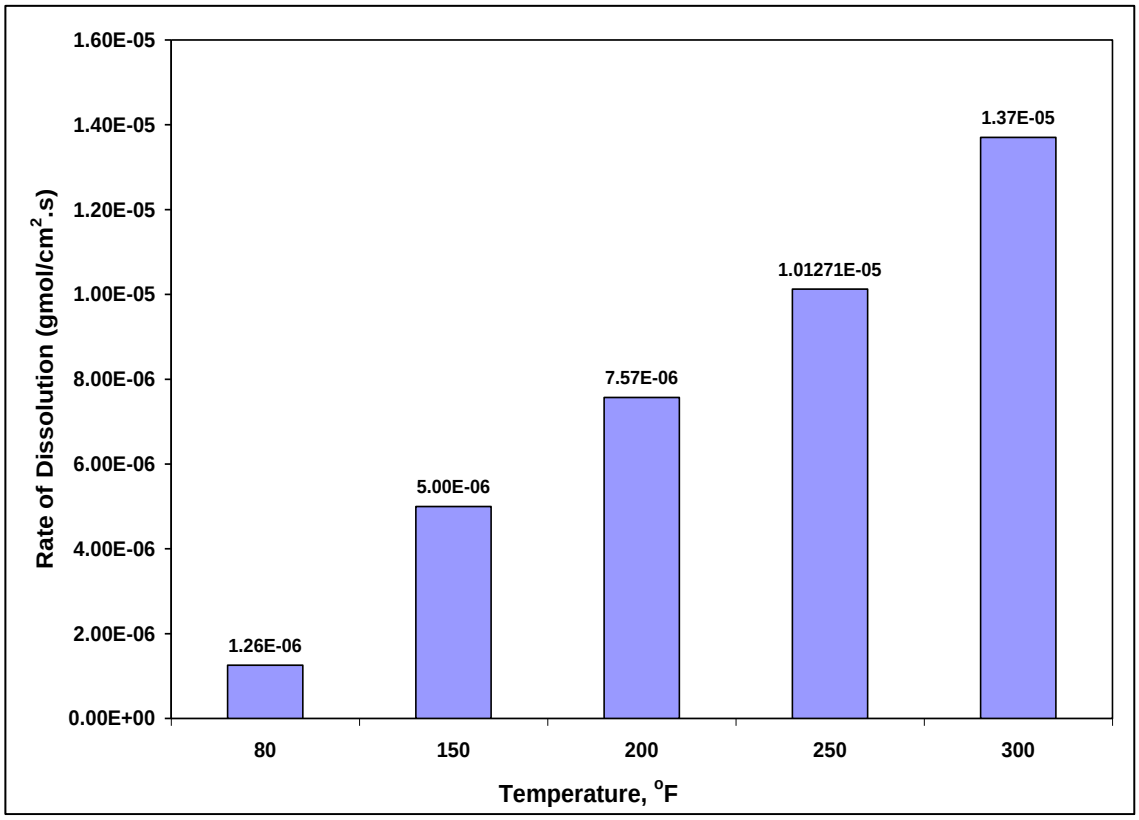

Fig. 3.5: Effect of temperature on the rate of Pink Desert dissolution with 0.6M GLDA at 1000 rpm and pH of 3.8.

Frenier et al. (2001) also measured the reaction rate of 0.25M Na3-HEDTA at 20, 65, and 90°C at 600 rpm with calcite marble at pH values of 2.5, 4, and 12. The results showed that the activation energy was in the range of 10.2-13.2 kcal/mol. The lowest value (10.2 kcal/mol) was an indication of a transition from mass transfer to surface kinetics control, while the higher values match with surface kinetics control. At 90°C, the rate of calcite dissolution was $6*10^{-7}$ and $9*10^{-7}$ gmol/cm^2.s at pH of 12 and 4,

respectively, compared to $4*10^{-6}$ and $5.8*10^{-6}$ gmol/cm^2.s at pH of 13 and 3.8, respectively, obtained from this study at the same conditions.

Fredd and Fogler (1998a) reported activation energy of 6 kcal/gmol for the reaction of acetic acid with calcite, where the reaction was controlled mainly by mass transport processes. Sjoberg and Rickard (1984) stated that the activation energy of the mass transfer reaction limited is much less than the activation energy of the reactions that are controlled by surface reaction. In the latter work, the authors reported a range of 3.12-8.88 kcal/gmol for the activation energy for the reactions limited by mass transfer and 10.8-13.2 kcal/gmol for the reactions limited by the surface kinetics.

3.6.3 GLDA Complexation with Calcium

One main feature of the chelating agents that distinguishes them from mineral acids is their unique chemical structure which enables them to react with metal ions by two different mechanisms, depending on the pH of the reaction medium. At low pH, chelating agent reacts as polyprotic acid and the liberated H^+ ions attack the calcite at the carbonate sites resulting in dissolving the calcium ions as free ions.

At high pH values, especially above pH 11 and based on the structure of chelating agents, the acid is fully deprotonated and the main mechanism is chelation mechanism. In chelation reaction, the chelant ligand attacks the calcium site, grabs the ion, and forms a stable complex.

Like other chelants such as EDTA, DTPA, and CDTA, GLDA forms 1:1 metal complexes with most of the ions especially the alkaline-earth metals. The possible chelation reactions of the three ligands H_2GLDA^{-2}, $HGLDA^{-3}$, and H_2GLDA^{-4} are shown in Eq.3-8 to 3-10.

In order to investigate the mechanism by which the chelating agent reacts with calcite, the total and the free calcium concentrations were measured in the samples taken during the reaction of GLDA at pH of 1.7, 3.8, and 13. The concentration of the total calcium was measured using the ICP technique, while a Ca-selective electrode was used to measure the concentration of the free Ca^{2+} ions. To test the ability of ISE to measure the free calcium in the solution, five standard solutions were prepared by adding 1 ml of 1000 ppm standard Ca^{2+} to 100 ml od DI-water and 2 ml of an ionic strength adjustor to eliminate the effect of any other ions which might be associated with GLDA. Increasing volumes of GLDA were then added to these standard samples and the samples were stirred for 5 minutes and then ISE was used to measure the concentration of the free Ca^{2+}. The results in **Fig. 3.6** demonstrate the ability of the Ca-ISE to record accurately the reduction in the free calcium concentration from initial of 10 ppm and the reduction was in proportion to the GLDA added.

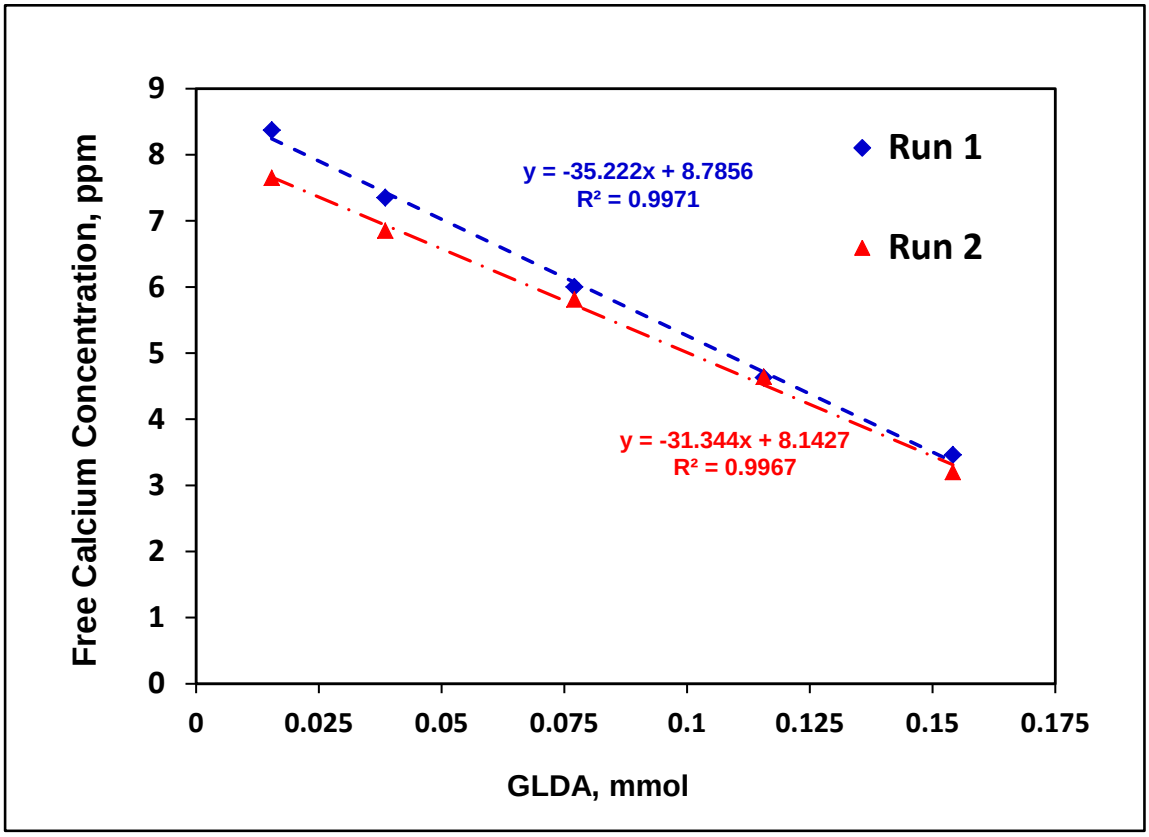

Fig. 3.6: Testing the ability of Ca-SE to measure the concentration of free Ca-ions.

The same procedure was followed with the samples taken from the reaction experiments. The concentration of the chelated calcium in each sample can be determined by conducting a material balance over the volume of each sample using the total and the free calcium concentration. The total calcium concentration was used to determine the total rate of reaction, while the free and the chelated calcium concentrations were used to determine the rate of the hydrogen attack reaction and the rate of chelation reaction, respectively.

The free calcium concentration matched the total calcium concentration at pH 1.7 indicating that the only mechanism possible at this pH is the hydrogen attack reaction and no chelation can occur at this pH value. At pH 13, no free calcium was found due to the dominance of the complexation (chelation) reaction. The results for reactions at pH of 3.8 are discussed further below.

Fig. 3.7 shows the change in the concentration of the free, the chelated, and the total calcium concentration with time for the reaction of 0.6M GLDA with Pink Desert at pH 3.8, 150^{o}F, and 1000 rpm. The data in Fig. 3.6 shows that the concentration of the chelated calcium initially increased with time and then started to level off because of the equilibrium nature of the chelation reaction. The concentration of the chelated calcium was higher than the free calcium throughout the experiment. The first data points in the linear range were fitted to the best straight line for the three data sets (total, free, and chelated calcium). The slope of each line divided by the area of the disk sample gives the rate of the total, hydrogen attack, and chelation reaction, respectively.

The data from Fig. 3.6 is consistent with a rate of chelation of $3.36*10^{-6}$ gmol/cm^2.s and a rate of $1.65*10^{-6}$ gmol/cm^2.s for the hydrogen attack reaction. The percentage of chelation (expressed as the ratio of the rate of the chelation reaction to the total rate of reaction) was 67%.

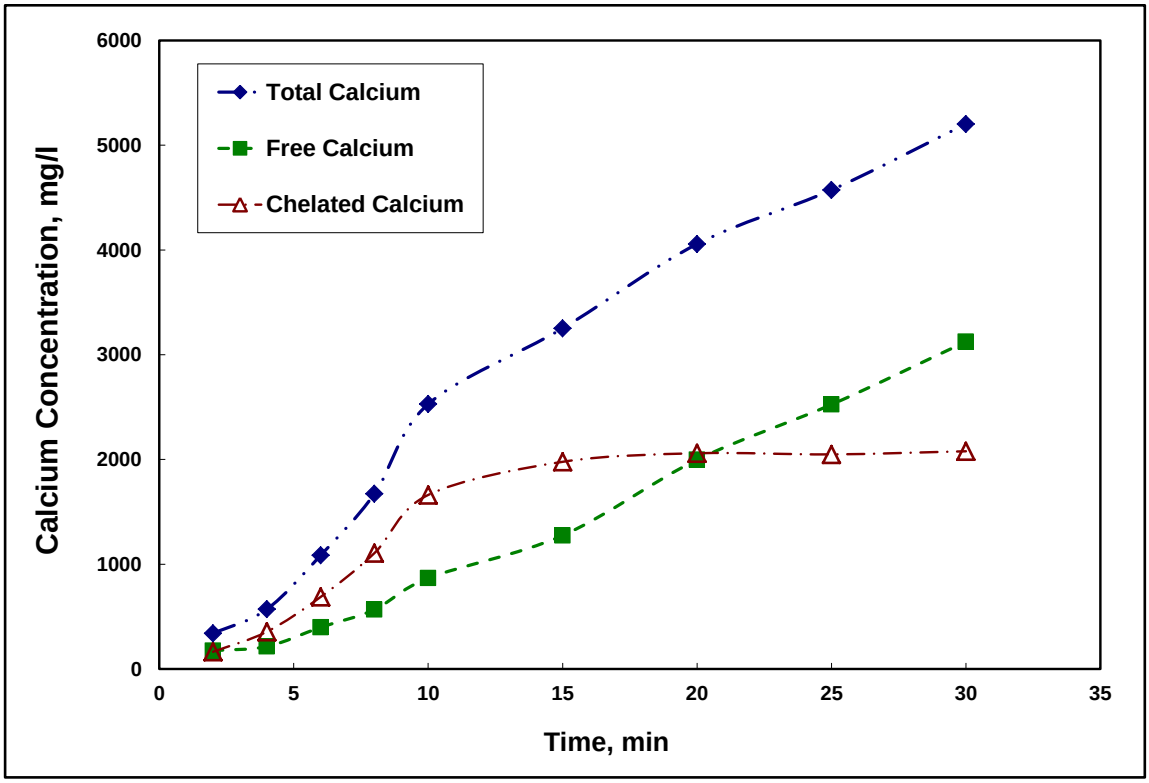

Fig. 3.7: Chelated, free, and total calcium concentrations at pH of 3.8, 1000 rpm, and 150^{o}F.

The rate of chelation and the hydrogen attack reactions increases with temperature. However, increasing temperature had more effect on the rate of the hydrogen attack reaction than the chelation reaction. This resulted in a reduction in the percentage of chelation with increasing the temperature.

The change of the chelated and the free calcium concentration with time at different temperatures (150-300^{o}F) is shown in **Figs. 3.8-9** The data is consistent with rates of chelation of $3.82*10^{-6}$, $5.29*10^{-6}$, and $6.06*10^{-6}$ gmol/cm^{2}.s at 200, 250, and 300^{o}F, respectively. **Fig. 3.10** shows a comparison between the rate of hydrogen reaction

and the chelation reaction, while the numerical values for the rate of each reaction and the percentage of complexation are listed in **Table 3.4** The results obtained are discussed below.

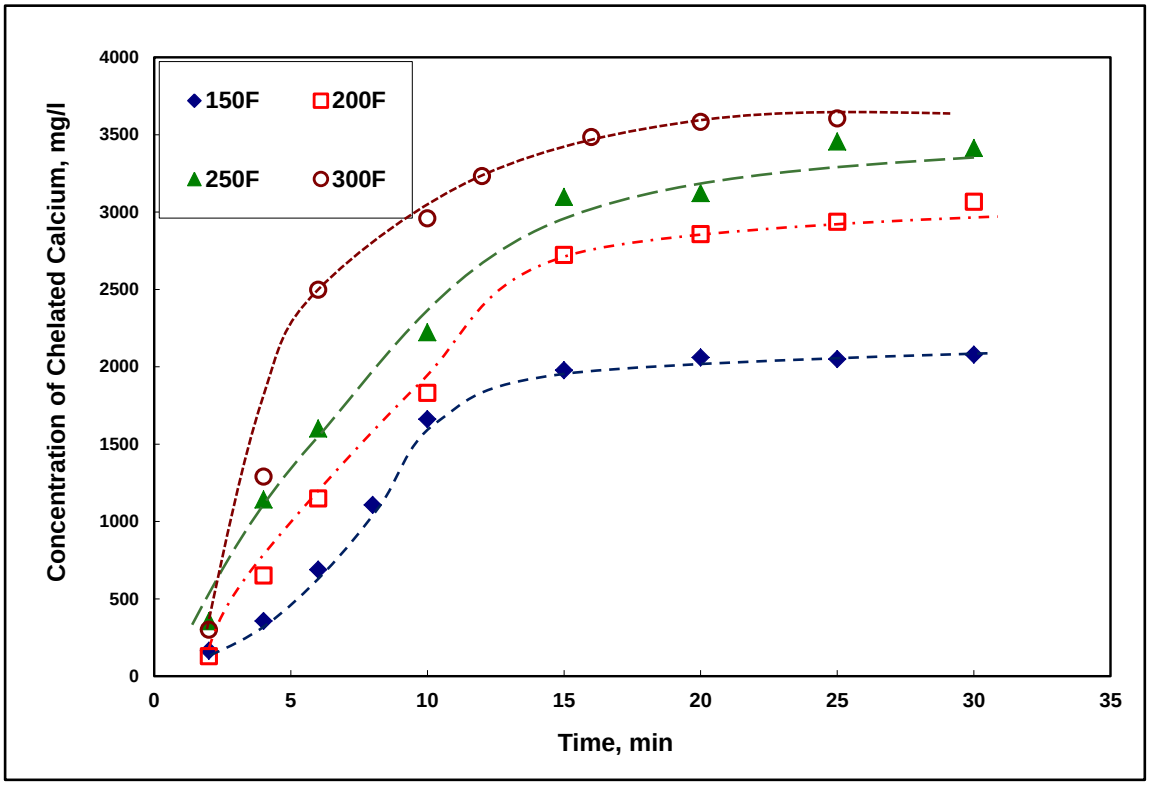

Fig. 3.8: Effect of temperature on the concentration of chelated calcium at pH of 3.8, 1000 rpm.

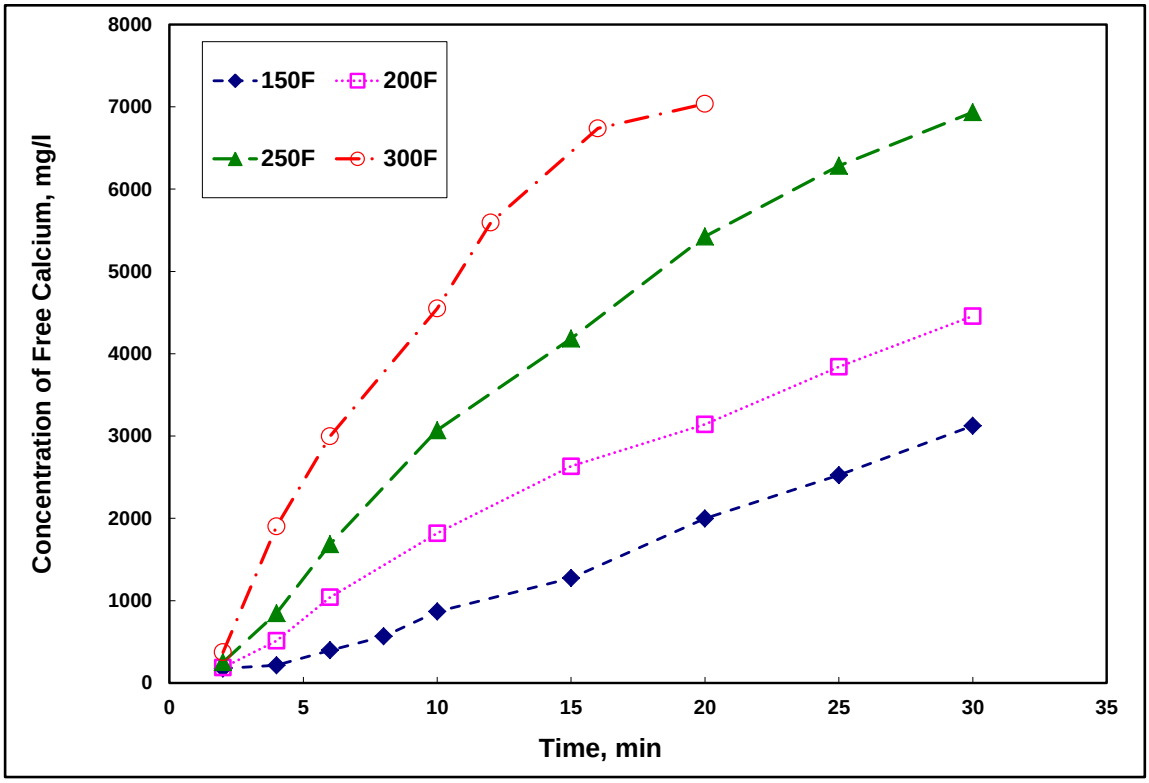

Fig. 3.9: Effect of temperature on the concentration of free calcium at pH of 3.8, 1000 rpm.

Table 3.4: Effect of temperature on the rate of chelation and hydrogen attack reactions at pH 3.8 and 1000 rpm.

Temperature, ^{o}F	Rate of Hydrogen Reaction, gmol/cm^2.s	Rate of Chelation Reaction, gmol/cm^2.s	Percentage Complexation, %
150	1.65E-06	3.36E-06	67.1
200	3.75E-06	3.82E-06	50.5
250	4.83E-06	5.29E-06	52.3
300	7.67E-06	6.06E-06	44.1

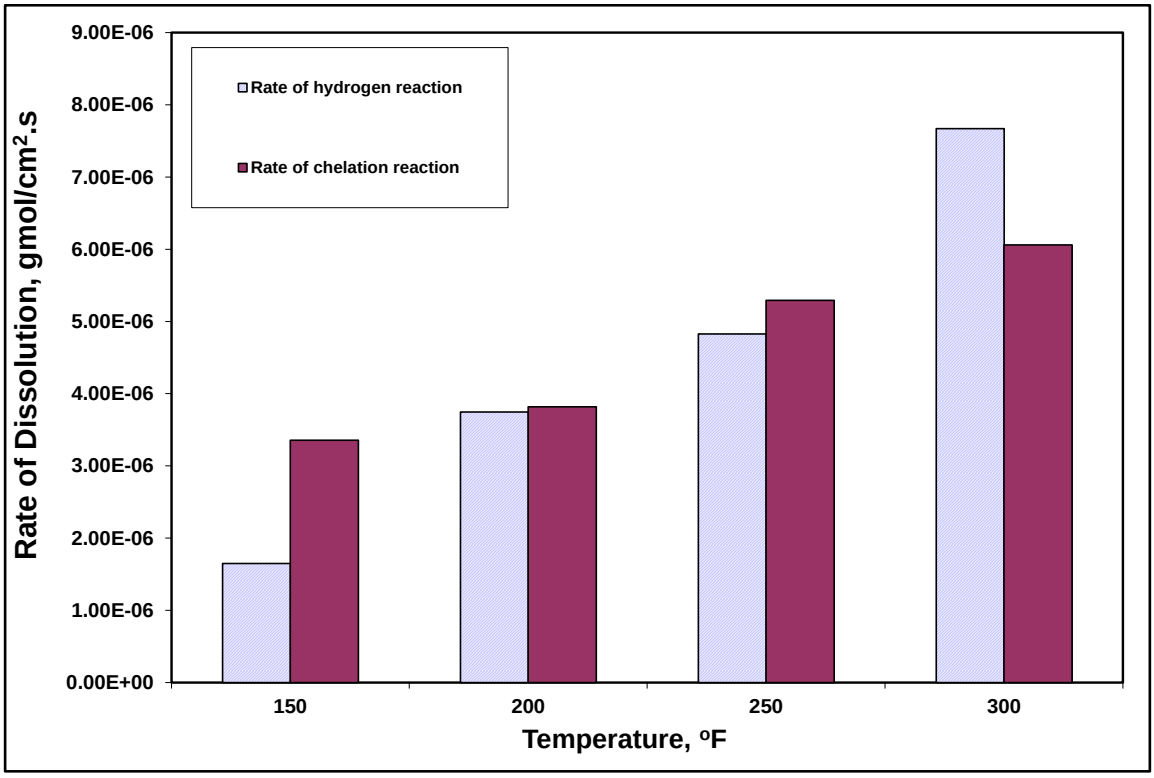

Fig. 3.10: The Effect of temperature on the chelation reaction at pH of 3.8 and 1000 rpm.

Referring to Eqs. 3.8-10, the effect of temperature on the stability (equilibrium) constant of these reactions can be described by the van't Hoff equation, Eq. 3-11. Integration of Eq. 3-11 over intervals of constant change in enthalpy (ΔH) leads to Eq. 3-12 that describes the change of in the chemical equilibrium when the temperature is altered from T_1 to T_2.

$$\frac{d\ln K}{dT} = \frac{\Delta H^\circ}{RT^2} \quad \text{[3-11]}$$

$$\ln\frac{K_2}{K_1} = \frac{-\Delta H^\circ}{R}\left[\frac{1}{T_2} - \frac{1}{T_1}\right] \quad \text{[3-12]}$$

Eq. 3-12 can be used to calculate the stability constant for a particular reaction at temperature T_2 if its value at temperature T_1 and the enthalpy change, $\Delta H°$, are known. If a plot of ln*K* vs 1/T is drawn, the slope of the line is $(-\Delta H°/R)$ which will be positive for an exothermic reaction ($\Delta H°$ is negative) and negative for an endothermic reaction ($\Delta H°$ is positive). A positive slope means that *K* decreases as the temperature is increased and the equilibrium moves away from the products towards the reactants. The opposite occurs in the case of an endothermic reaction. Arena et al (1983) published experimental data for the stability constant and the change of enthalpy reaction of EDTA with calcium and reported Log (K) of 10.75 at 25^{o}C and ΔH of -25.1kJ/mol. The data was confirmed with those published by other researchers (Martell and Calvin 1956; Craggs et al 1979; Anderegg and Podder 1975) who reported 10.59, 10.93, and 10.73, respectively.

The data published by Arena et al. (1983) was used to generate the Log (K) vs. temperature plot as shown in **Fig. 3.11**. It is believed that the similarity between the GLDA and EDTA in the chemical structure and other physical and chemical properties will result in the effect if GLDA is the recanting agent with calcium. The decrease in the stability constant shows that the tendency of the metal-ligand reaction will be towards the reactants (i.e. the free Ca^{2+} ions) and therefore decrease in the percentage of the chelated calcium to the free calcium in solution.

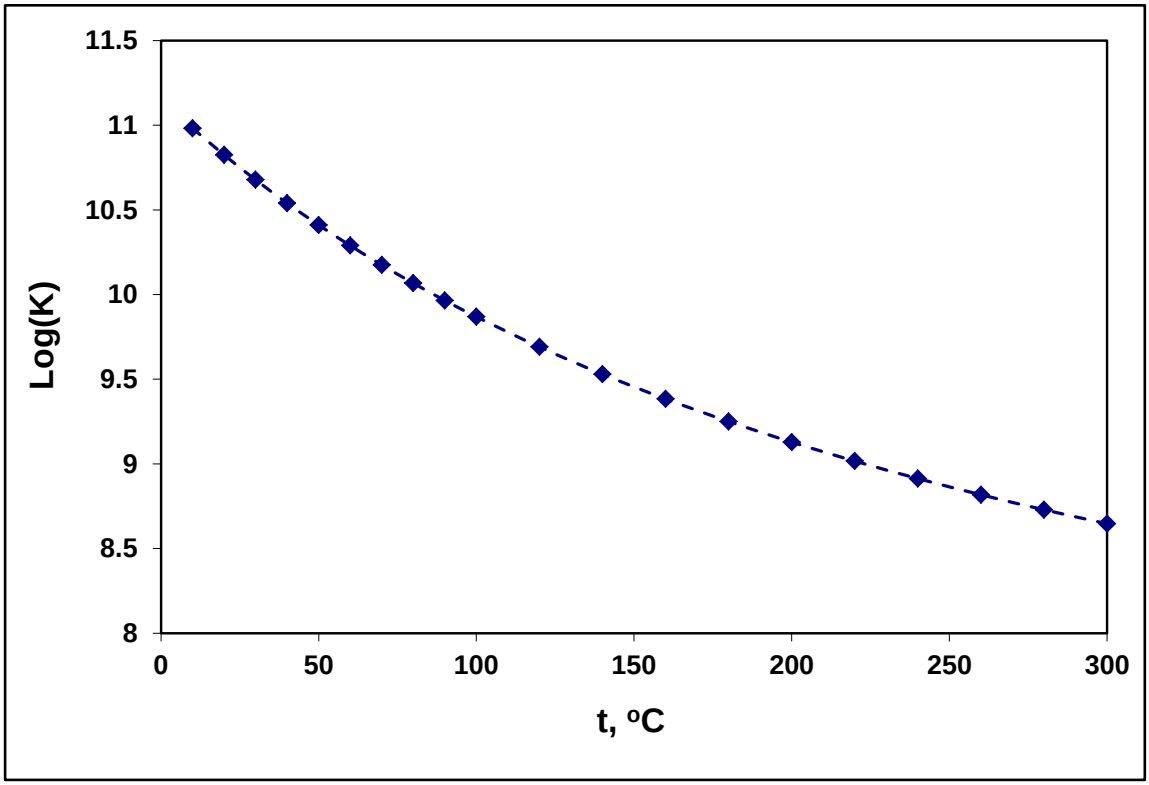

Fig. 3.11: Effect of temperature on the stability constant of the chelation reaction of Ca-EDTA.

On the other hand, increasing the rotational speed did not have a noticeable effect on the rate of the chelation reaction, which was expected because chelation reaction is a surface reaction that is mainly controlled by the kinetics parameters such as temperature and the dissociation coefficients. This can be shown in **Fig. 3.12**, where the chelated calcium concentration is plotted versus time at 1000, 1500, 1800 rpm. The similarity of the slopes of the three lines indicates very close rate of reactions at these rotational speeds.

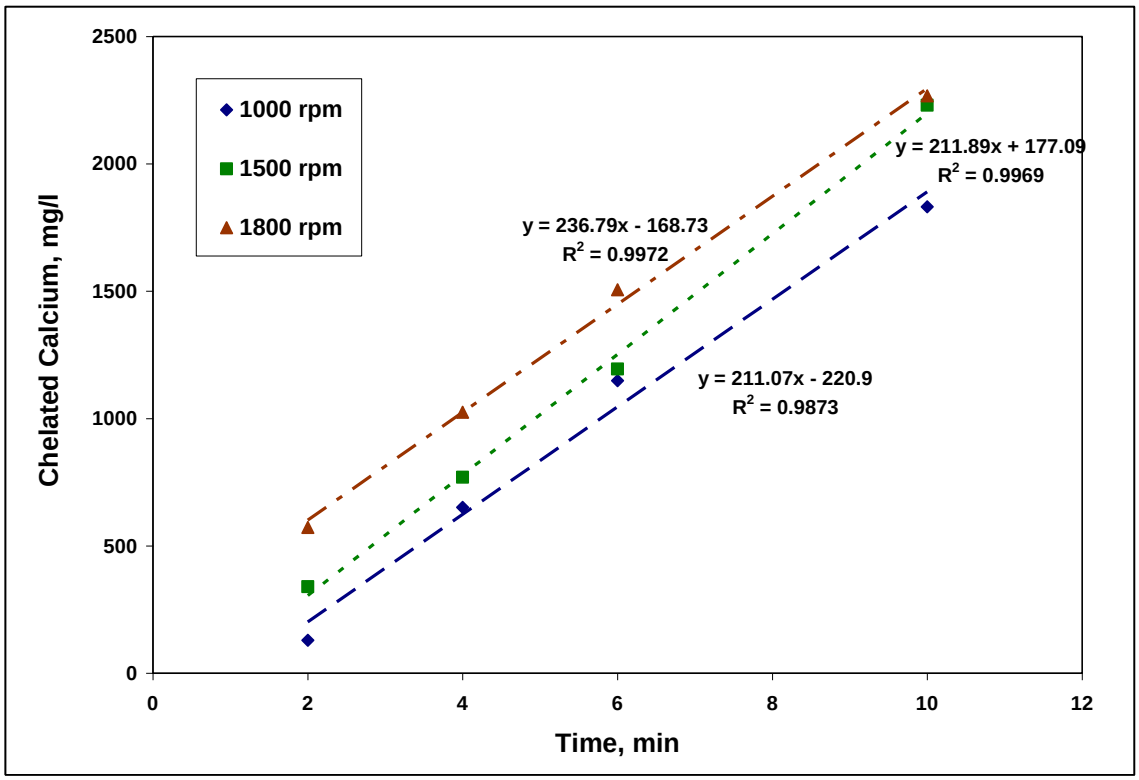

Fig. 3.12: Change of the chelated calcium concentration with time for the reactions at pH of 3.8, 200^{o}F, and different rotational speeds.

3.6.4 Optimum Damköhler Number

The main objective of matrix stimulation is to create high conductive permeable channels, wormholes, which allow oil and gas to flow more readily to the wellbore. The formation and the growth of these wormholes depends on the transport of the fluid through the channels, the reaction of the acid at the tip, and the acid leak-off through the side walls of the wormholes. The transport of the reacting component is a function of its diffusivity and flow rate, while the surface reaction is affected significantly with the surface kinetics.

Several studies have reported that there is an optimum flow rate that results in a minimum volume of injected fluid required to form these wormholes until the breakthrough. It is often a practice to describe this injection volume of the fluid as a pore volume number which represents the ratio of the total volume of the injected fluid to the volume of the pores in a rock sample. The significance of the determination of the minimum pore volume is that it gives a beneficial mean to determine the optimum condition of using the stimulating fluid efficiently and economically. It is also common to express the injection rate that corresponds to the minimum pore volume in term of "Damköhler number", which is defined as follows (Fred and Fogler, 1998b):

$$D_a = \frac{\pi d l k}{Q} \quad \text{[3.13]}$$

Where:

$$k = k_m = 1.86\, D_e^{2/3} \left(\frac{u}{d\, l} \right)^{1/3}$$, in case of mass transfer limited …….. [3.14]

$$k = k_{sr}$$, in case of surface reaction limited …….. [3.15]

Where k_m and k_{sr} are the mass transfer coefficient and the reaction rate constant, respectively. Pink Desert cores with an average permeability of 80 md and average porosity of 28 vol% were examined in three sets of core flood experiments that were run using 0.6M (20 wt%) GLDA at pH of 3.8 at temperatures of 200 and 300^{o}F and for pH

1.7 at 200^{o}F. In each set, the injection rate changed over a range from 0.5 to 5 cm^{3}/min utill the breakthrough and the required acid pore volume was recorded. The cores were imaged using CT-scan technique after each experiment to measure the length and the diameter of the wormhole. **Tables 3.5-7** give the details of each set.

Table 3.5: Flow conditions and wormhole dimensions for set 1 (pH 3.8 and 200°F)

Q, cc/min	PV_{bt}, PV	d, in.	l, in.	1/Da
0.5	4.9	0.22	6.2	1.65
1	4.7	0.20	6.1	2.65
2	4.35	0.14	6.1	4.21
3	**3.74**	**0.14**	**6.05**	**5.54**
4	4.15	0.10	6	6.75
5	6.65	0.08	6	7.83

Table 3.6: Flow conditions and wormhole dimensions for set 2 (pH 3.8 and 300°F)

Q, cc/min	PV_{bt}, PV	d, in.	l, in.	1/Da
0.5	4.55	0.30	6.32	0.90
1	4.15	0.26	6.25	1.44
2	3.65	0.25	6.19	2.23
3	**3.1**	**0.25**	**6.09**	**3.05**
4	3.5	0.18	6	3.73
5	5.22	0.14	6	4.36

Table 3.7: Flow conditions and wormhole dimensions for set 3 (pH 1.7 and 200°F)

Q, cc/min	PV_{bt}, PV	d, in.	l, in.	1/Da
0.5	4.76	0.33	6.5	0.77
1	4.25	0.315	6.35	1.24
2	3.95	0.29	6.12	2.02
3	**3.75**	**0.29**	**6.23**	**2.62**
5	5	0.10	6.05	3.83

It was observed that at each set, there was an optimum injection rate that was corresponding to the minimum acid pore volume required to breakthrough, which was highlighted in bold in each table above. This optimum flow rate is in agreement with what was reported by Frenier et al. (2001) for the injection of Na_3-HEDTA in Indiana limestone at pH values of 2.5, 4, and 13 at 250^{o}F. The results in the mentioned work showed an optimum flow rate of 2 cm^3/min.

Mahmoud et al. also (2011) studied the injection of 0.6M GLDA at 180, 250, and 300^{o}F in Indiana limestone at a pH of 1.7 and 3. The results showed optimum injection flow of 1 cm^3/min. With no previous mass transfer study of GLDA, the Damköhler number was determined based on the diffusion coefficients of EDTA as an approximation.

In the present study, the data of the diffusion coefficients of GLDA that were determined at 200 and 300^{o}F using the rotating disk reactor was used to predict an accurate Damköhler number as a function of the flow rate. Because the reaction of GLDA was found to be solely mass transfer limited over the whole range of the investigated disk rotational speeds as shown in Fig. 3.3, Eqs. 3.13-14 were used to determine the Damköhler number.

Fig. 3.13 illustrates the dependence of the pore volume on the reciprocal of the Damköhler number. Taking the conditions of pH 3.8 and 200^{o}F as a base case, increasing the temperature to 300^{o}F or reducing the pH to 1.7 resulted in shifting the optimum Damköhler number to the left with a decrease in the minimum pore volume required to break through. Increasing the temperature or reducing the pH is associated with increasing the diffusivity coefficient (Table 3.3), which results in increasing in the dissolution rate for a mass transfer limited reaction and hence, lower acid volume to breakthrough.

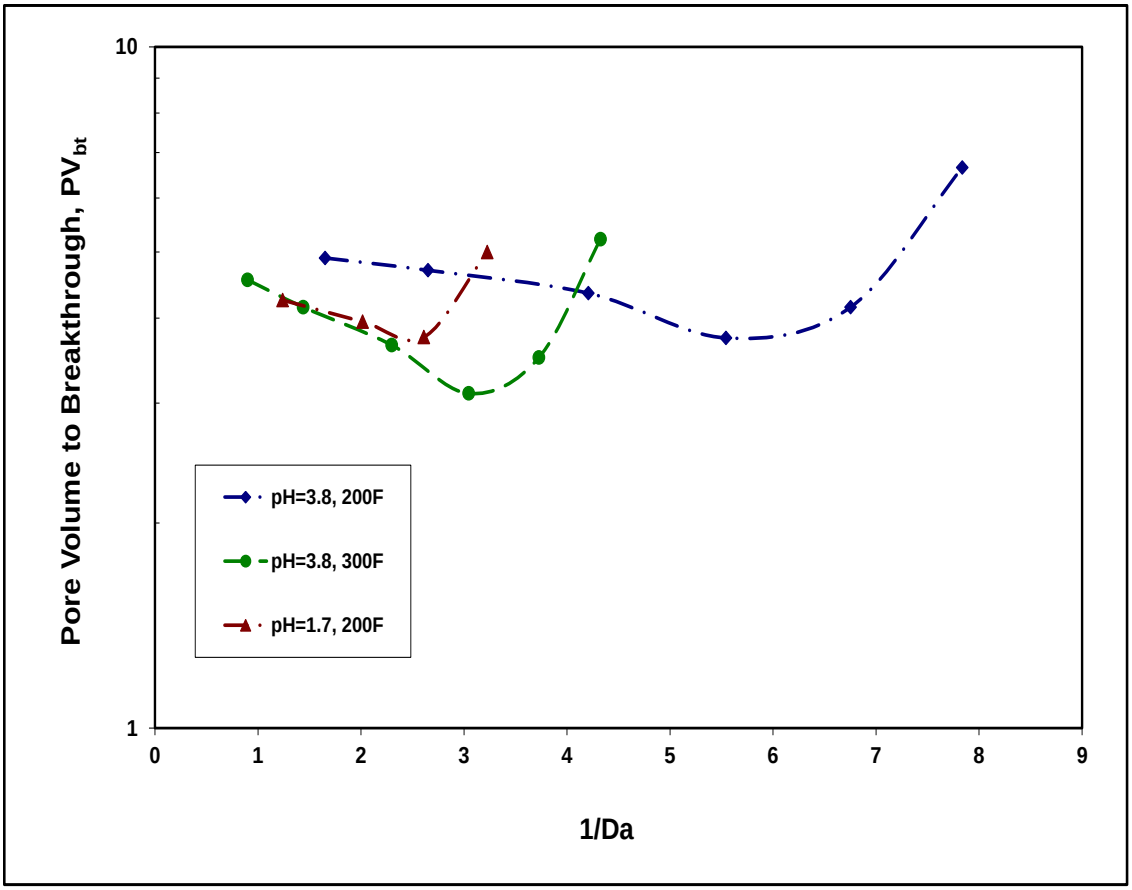

Fig. 3.13: Number of pore volumes to breakthrough for a 0.6M GLDA at pH 3.8 (200, and 300^{o}F), and pH 1.7 (200^{o}F).

4. REACTION OF CHELATING AGENT (GLDA) WITH DOLOMITE

In Chapter 3, the reaction of GLDA with calcite was presented and the rotating disk reactor was utilized to study the mass transfer and reaction mechanism. In this chapter, an extension is made to include the reaction of GLDA with dolomite and to highlight the main differences in reaction rate if GLDA is used to stimulate calcite at the same conditions.

4.1 Introduction

About 80% of the oil and gas reservoirs in North American carbonate rocks are in dolomites and up to 50% of the world's carbonate reservoirs are dolomites (Zenger et al. 1980). However, most of the research efforts for acid stimulation (matrix acidizing and acid fracturing) were given to the reaction of the stimulating fluids with calcite and several acid systems were investigated thoroughly such as hydrochloric acid, organic acids, and chelating agents (Lund et al. 1973; 1975; Plummer et al. 1978; Sjoberg and Rickard 1984; MaGee et al. 1997; Al-khaldi et al. 2010a; b; Pokrovsky et al. 2005; 2009; Finneran and Morse 2008; Taylor and Nasr-El-Din 2002;2003; Nasr-El-Din et al. 2008, Fredd and Fogler 1998a; b; c; Frenier et al. 2001; 2004; Mahmoud et al. 2010a;b;2011; Rabie et al. 2011a;b;c).

Less attention was given to the reaction of these acids with dolomite. Lund et al. (1973) studied the dissolution of dolomite in hydrochloric acid (0.01 to 9 N) using the

rotating disk apparatus over disk rotational speeds (50 to 500 rpm) at 25, 50, and 100°C. At 25°C the dissolution process is surface reaction rate limited even at low disk rotation speeds and the process approaches diffusion limitation as the temperature is increased to 100°C even at relatively high (500 rpm) rotation speeds. The rate of reaction was found to be proportional to a temperature dependent fractional power of the hydrochloric acid concentration.

Roberts and Guin (1974) introduced a mathematical model to determine the distance to which live acid can penetrate into a fracture under conditions in which the overall reaction rate is influenced by finite surface reaction kinetics. Therefore, dolomite laboratory-prepared fractures systems 4.1 to 9.7 ft long were exposed to HCl at 7l, 190, and 290°F. An experimental parameter appearing in the model, termed the effective mixing coefficient, was determined and used to replace the ionic acid diffusion that cannot be used correctly in these applications. The effective mixing coefficient was introduced to account for the effect of the surface reaction rate on the spending of HCI in a dolomite fracture.

Busenberg and Plummer (1982) studied the kinetics of dolomite dissolution far from equilibrium over a pH range from 0 to 10 and a temperature range from 1.5 to 45°C and stated that the dissolution rate is controlled by the surface kinetics of forward and backward reactions. The forward rate depends on 3 reactions and is half order with

respect to the H^+ and H_2CO_3 activity and constant in the absence of both of them. The backward reaction rate depends on first order reaction with respect to HCO^-_3.

Gautelier at al. (1999) studied the dolomite steady-state dissolution rate in HCl solutions in a mixed-flow reactor using the rotating disk techniques. The pH of the bulk solutions changed from 0.39 to 4.44 at temperatures of 25, 50 and 80°C. Dissolution rates were found to depend on disk rotation speed at all temperatures and pH over the experimental conditions. Kinetic expression in the form of $r = k_1 a^n_{(H+)}$ was used to fit the data. The results showed that the rate of dolomite dissolution at these conditions tends to be pH-independent at more acidic conditions indicating the saturation of dolomite surface with rate controlling protonated species.

Taylor et al. (2004) showed that the degree of impurities in reservoir rocks can drastically affect their reaction with acids. The assumption that the calcite reaction is more rapid than dolomite can be wrong in some cases. Rotating disk experiments was used to measure the reaction rate of HCl (1N) with dolomite rocks from a deep gas well that differ in the dolomite composition from 0 to 100%. Minor clay concentration can significantly reduce the reaction rate of calcite to a comparable dolomite rate.

Pokrovsky et al. (2005) used the rotating disk reactor and a mixed-flow reactor to studied the dissolution rates of calcite, dolomite and magnesite at 25°C and pH from 3 to 4 as a function of salinity (0.001M < [NaCl] < 1M) and partial pressure of CO_2 (10-3.5 <

pCO_2 < 55 atm). The authors found that the dolomite dissolution rate increases with increasing the pCO_2 from 1 to 10 atm, but remains constant above that and up to 50 atm. These rates depend slightly on the stirring velocity indication moderate mass transfer effect and independent on the ionic strength between 0.1 and 1 M NaCl and 5 to 50 atm.

Zhang et al. (2007) conducted kinetic experiments of dolomite dissolution in water over a temperature range from 25(77) to 250°C (480°F) using a flow through packed bed reactor and three different size fractions of dolomite samples (18–35 mesh, 35–60 mesh, and 60–80 mesh). The authors noted that the release of Ca and Mg increased with temperature up to 200°C and then decreased afterwards for the 20-40 mesh size, while a maximum rate of dissolution was noted at 100°C when the mesh size was 40-60 or 60-80. Experimental results also showed that the dissolution of dolomite is contradicting in most cases. Dissolution of fresh dolomite was non-stoichiometric, the Ca/Mg ratio released to solution was greater than in the bulk solid, and the ratio increases with rising temperatures from 25 to 250°C. The experiments proved that dissolved Ca is a strong inhibitor for dolomite dissolution.

Sayed and Nasr-El-Din (2012) studied the rheology and reaction of emulsified HCl (15 wt%, 0.7 acid volume fraction) with dolomite. The emulsifier concentration changed between 0.5, 1, and 2.0 vol%. At the experimental conditions (230°F and 100-1500 rpm), the reaction of the emulsified acid with dolomite was controlled by mass

transfer at emulsifier concentration of 0.5 vol%, while both mass transfer and surface reaction influence the rate of dissolution at higher emulsifier concentration.

As can be summarized, reaction of dolomite was reported extensively in HCl and simple organic acids and was found generally to be surface reaction limited unless the temperature is significantly high and the stirring (or disk rotational) speeds are low, conditions at which the influence of mass transfer starts. However, little effort was given to investigate the dissolution of dolomite in chelating agents that showed promising responses as standalone stimulating fluids with calcite (Fredd and Fogler 1998b; c; Fredd 2000; Frenier et al. 2001; 2004; Huang et al. 2003; Mahmoud et al. 2010, 2011a,b).

Fredd (2000) showed that EDTA has a poor ability to dissolve dolomite at ambient temperature and referred that to the low stability of Ca and Mg chelants at this temperature.

4.2 Objectives

The objectives of this study are to utilize the rotating disk reactor to: (1) determine the effect of disk rotational speed, temperature, and acid concentration on the reaction of GLDA with dolomite, (2) investigate the conditions under which the reaction is diffusion/surface reaction limited and, (3) highlight the main difference in reaction rate between calcite and dolomite dissolution by GLDA at the same conditions.

4.3 Reaction of GLDA with Dolomite

Chelating agents are amino carboxylic acids that have the ability to react with calcite and dolomite by two mechanisms depending on the pH of the reaction medium, which in turn determines the dominant reaction on the surface. In the case of GLDA, proton attack (or H^+ rection) is the main mechanism at low pH (< 2), while at higher pH greater than 11, the acid is fully deprotonated and the main mechanism is the chelation mechanism. Deprotonation or dissociation reaction depends on the pH of GLDA solutions.

Three pH values are readily available for GLDA; 1.7, 3.8, and 13. **Table 4.1** gives the percentage ionic distribution at each pH. GLDA at pH 3.8 was used in this study.

Table 4.1: % Ionic distribution of GLDA at 25°C as a function of pH

Species	pH = 1.7	pH = 3.8	pH = 13
H_4-GLDA	87	3	0
H_3-GLDA$^-$	13	28	0
H_2-GLDA^{2-}	0	66	0
H-GLDA^{3-}	0	3	0
GLDA^{4-}	0	0	100

At pH of 3.8, according to the species distribution of the GLDA, both proton attack and chelation reaction occur. The proton attack reaction can be written as:

$$4H^{+} + CaMg(CO_3)_2 \leftrightarrow Ca^{2+}(aq) + Mg^{2+}(aq) + 2CO_2 + 2H_2O \quad \text{..... [4.1]}$$

The dissociated species (H_2-$GLDA^{2-}$) will chelate Ca ion according to the following reaction:

$$2H_2GLDA^{2-} + CaMg(CO_3)_2 \leftrightarrow H_2GLDACa + H_2GLDAMg + 2CO_3^{2-} \quad \text{..... [4.2]}$$

4.4 Experimental Studies

4.4.1 Materials

Silurian dolomite cores were cut into disks of 1.5 in. diameter and 0.65 in. thickness. **Table 4.2** shows the chemical composition of the dolomite mineral used in this study, while **Table 4.3** shows the porosity of each sample. The average porosity was 11 vol.%. A new sample was used for each experiment. GLDA solutions (20 wt%) at pH value of 3.8 were prepared by dilution from initial concentrated solution (40 wt%) at the same pH value. The concentrated solutions were obtained from AkzoNobel. Deionized water was used to prepare the GLDA solutions.

4.4.2 Instruments and Rotating Disk Apparatus

The description of the rotating disk apparatus and the procedure of running a reaction rate experiment were explained in detail in chapter 2 and were published in previous work (Rabie et al. 2011a; c).

Table 4.2: Composition of Silurian Dolomite cores using XRF analysis.

Element	**wt%**
O	51.46
Ca	21.18
C	12.69
Si	0.2
Mg	12.79
Al	0.16
Fe	0.1
K	0.05
Na	1.26
Sn	0.01
% Total	99.9

Table 4.3: Dimensions and porosity of core samples used in the reaction rate experiments.

Exp.	D, cm	H, cm	V_{bulk}, cc	Porosity, %
1	3.8	1.7	19.28	14.63
2	3.8	1.6	18.15	13.72
3	3.8	1.65	18.71	11.05
4	3.8	1.7	19.28	12.70
5	3.8	1.5	17.01	8.38
6	3.9	1.6	19.11	9.08
7	3.8	1.6	18.15	13.39
8	3.9	1.6	19.11	11.66
9	3.8	1.6	18.15	11.56
10	3.8	1.5	17.01	10.80
11	3.8	1.5	17.01	7.43
12	3.9	1.5	17.92	10.08
13	3.8	1.6	18.15	11.17
14	3.8	1.5	17.01	11.68
15	3.8	1.8	20.41	9.69
16	3.8	1.5	17.01	12.69
17	3.8	1.5	17.01	13.87
18	3.8	1.5	17.01	9.26
19	3.9	1.5	17.92	8.01
20	3.8	1.7	19.28	13.38
21	3.8	1.5	17.01	9.26
22	3.8	1.5	17.01	14.28
23	3.8	1.5	17.01	8.20
24	3.8	1.5	17.01	8.26
25	3.8	1.5	17.01	9.85
26	3.8	1.5	17.01	12.45
27	3.8	1.5	17.01	8.32
28	3.8	1.6	18.15	13.61

4.5 Results and Discussion

4.5.1 Dissolution of Dolomite with GLDA

The rotating disk reactor was used to investigate the ability of chelating agent GLDA to dissolve dolomite cores. The reaction experiments were conducted at 150, 200, 250°F at disk rotational speeds 100-1800 rpm. Experimental results showed negligible dolomite dissolution in GLDA at 77°F. The composition of the Silurian dolomite used in this study is shown in Table 4.2 and gives a molar ratio of Ca:Mg of 1.159:1. This indicates that the rock used is mainly dolomite with a negligible amount of free calcite. As a result, dissolving dolomite with GLDA is expected to yield near to equimolar ratio of both ions in solutions.

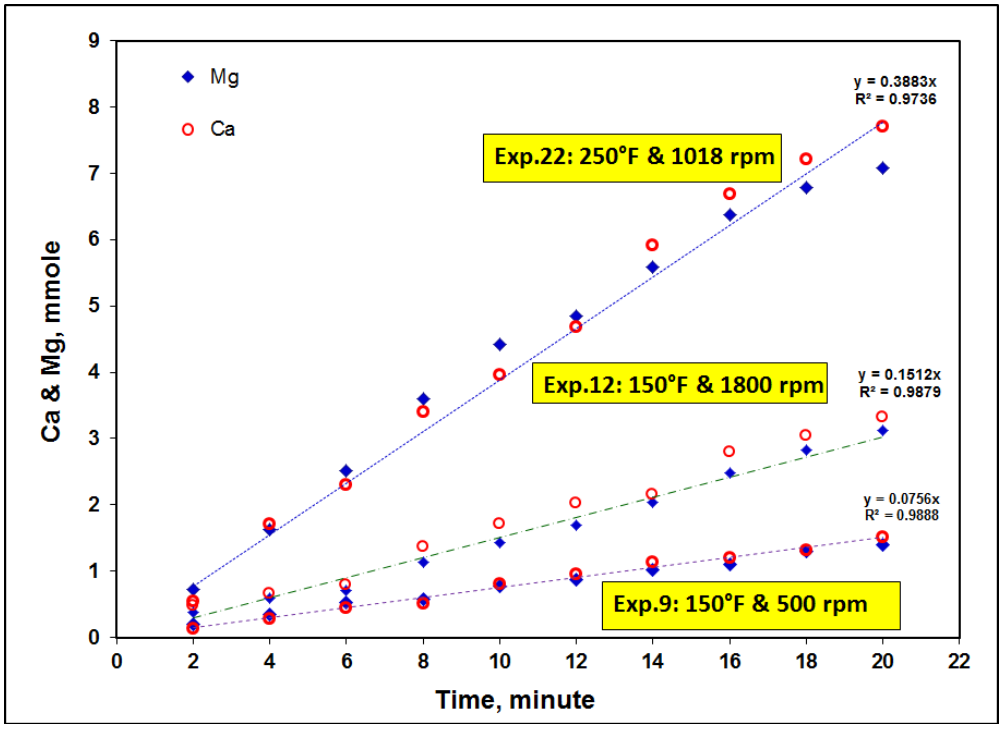

Fig. 4.1: Ca and Mg produced from reaction of GLDA with Silurian dolomite.

Fig. 4.1 shows the produced Ca and Mg in mmole over the reaction time of 20 minutes for three different experiments and the results confirm this claim. Therefore, the dissolution rate calculated from the dissolving of each ion would be the same. **Fig. 4.2** shows the dissolved Ca as a function of time of at 150°F over a range of disk rotational speeds from 100-1800 rpm. The data shows that increasing the disk rotational speed was associated with increasing in the produced calcium up to 1000 rpm. Increasing the disk rotational speed above this value did not yield a higher concentration of Ca ion in solution, which can be seen from the overlapping of the data at 1000, 1500, and 1800 rpm. Data for the calcium produced as a function of time at 200 and 250°F are shown in **Figs. 4.3-4**, which indicate similar behavior.

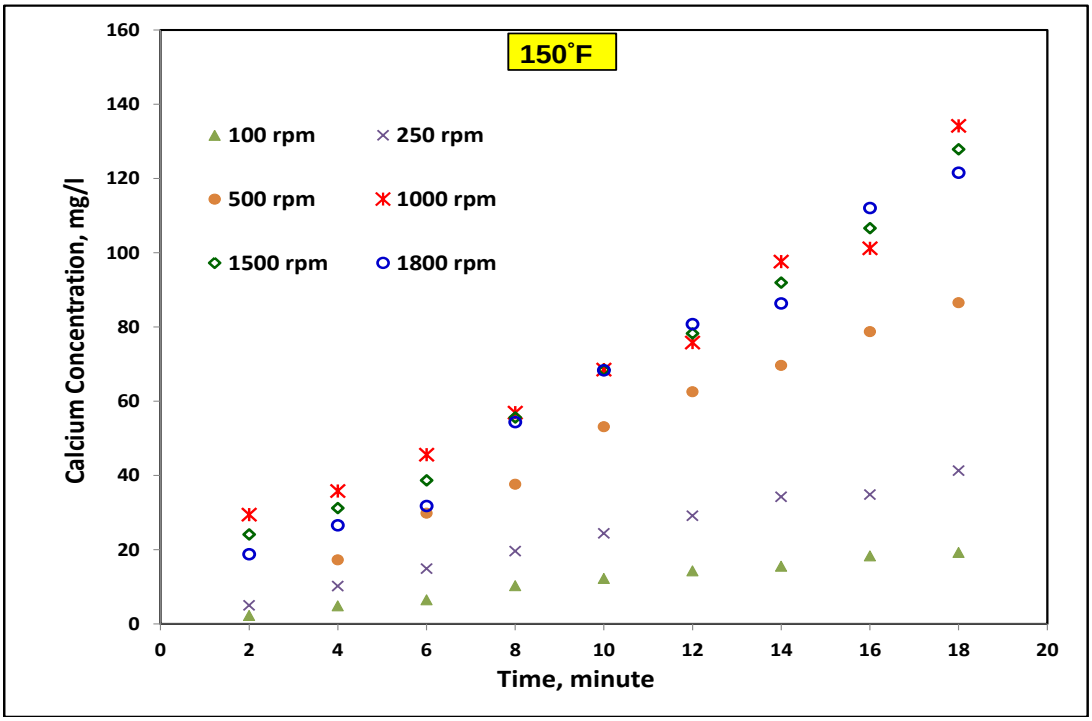

Fig. 4.2: Ca concentration as a function of time for the reaction of GLDA with dolomite at 150°F.

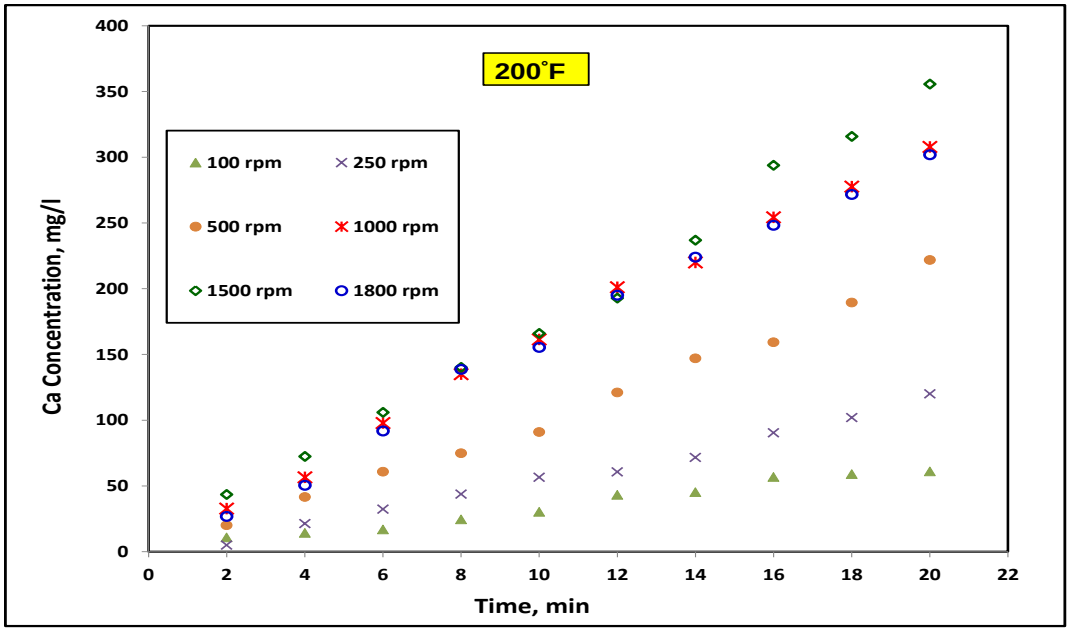

Fig. 4.3: Ca concentration as a function of time for the reaction of GLDA with dolomite at 200°F.

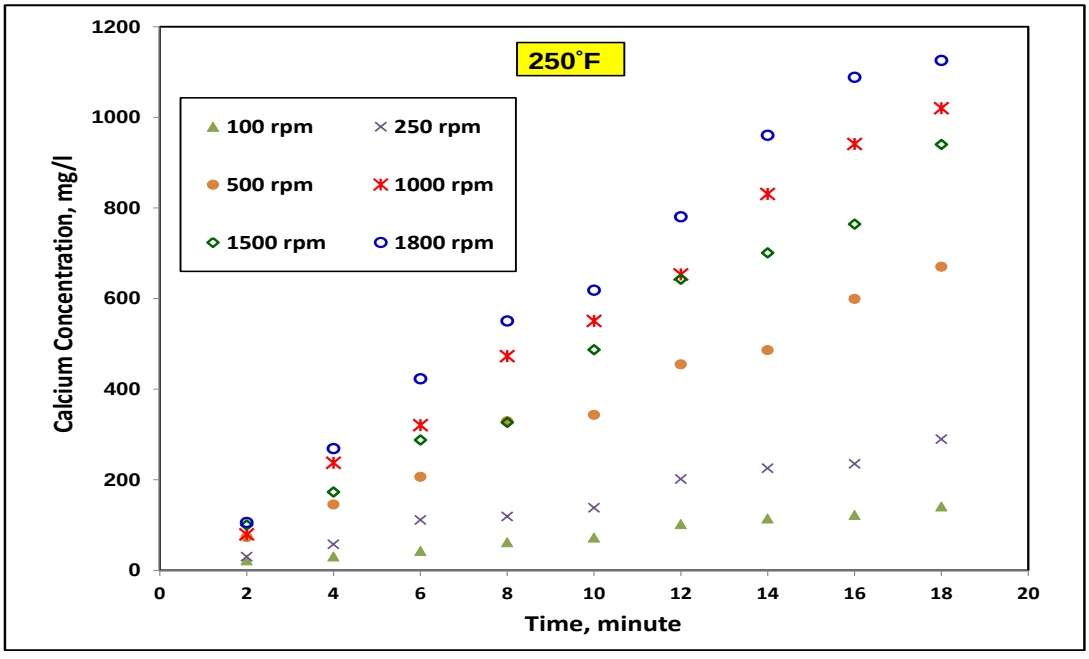

Fig. 4.4: Ca concentration as a function of time for the reaction of GLDA with dolomite at 250°F.

4.5.2 Effects of Mass Transfer on Dolomite Dissolution with GLDA

The dissolution rate of dolomite as a function of the square root of the disk rotational speed is shown in **Fig. 4.5**. Two distinguished regions are noted at 150, 200, and 250°F. At high disk rotational speeds (> 1000 rpm), the dissolution rate is leveling-off and no effect of the disk rotational speed is observed. This indicates a surface reaction controlling phase, in which other parameters such as temperature, acid concentration, and pH can affect the rate of dissolution.

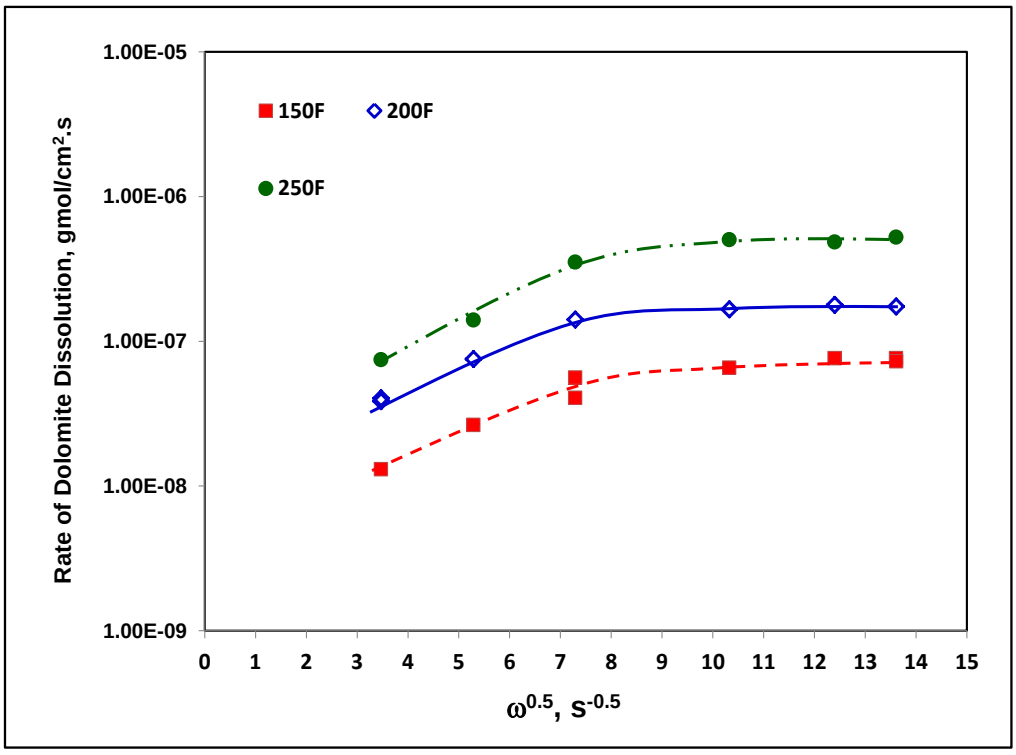

Fig. 4.5: Rate of dolomite dissolution as a function of square root of the disk rotational speed at 150, 200, and 250°F.

Below 1000 rpm, a transition region towards a straight line is observed, which indicates the influence of mass transfer and can be explained by the data obtained in

Figs. 4.2-4 that showed an increase in the calcium produced with increasing the disk rotational speed from 100 to 1000 rpm.

The dissolution rate in the transition region was used to determine the effective diffusivity of GLDA at these temperatures using the following equation. The definition of each parameter in the equation is given in the nomenclature section:

$$R_{MT} = \frac{0.60248(Sc^{-2/3})(\sqrt{\upsilon})(C_b - C_s)}{1+0.2980(Sc^{-1/3})+0.1451(Sc^{-2/3})}\ \omega^{1/2} \quad \text{..... [4.3]}$$

The effective diffusivity coefficients obtained at these temperatures are listed in **Table 4.4**. These data were fitted to the Arrhenius relation and the results are shown in **Fig. 4.6**. The data is consistent with an activation energy 15.9 kcal/mol, which is higher than reported activation energy (3.18-8.88 kcal/mol) if the reaction is solely controlled by mass transfer and therefore, consistent with the observed mutual influence of both mass transfer and at these conditions.

Table 4.4: Effective diffusivity of GLDA at 150, 200, 250°F

T, °F	D_e,cm^2/s
150	1.20E-08
200	5.89E-08
250	3.50E-07

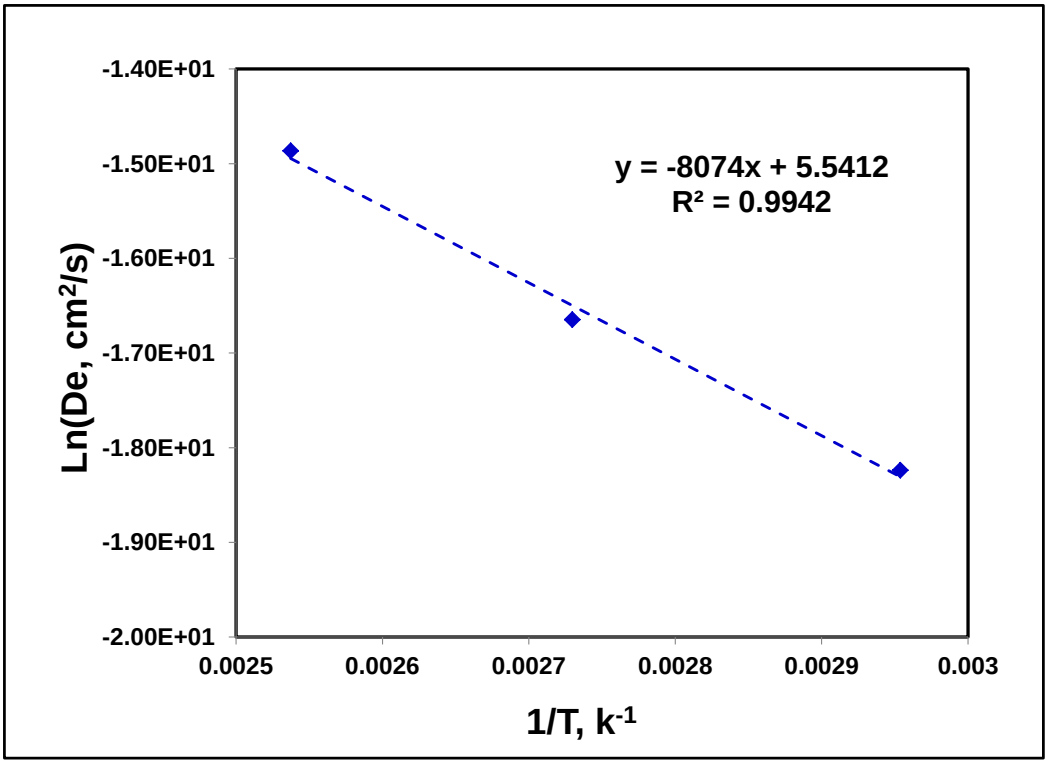

Fig.4.6: GLDA diffusivity fitted to the best of Arrhenius relation.

4.5.3 Effect of Temperature and Surface Reaction

Fig. 4.7 shows a comparison for the rate of dolomite dissolution with GLDA at 150, 200, and 250°F at different disk rotational speeds. From the figure, it is clear that temperature significantly affects the rate and the increasing the temperature increases the rate of dissolution. In a similar fashion to what is shown in Fig. 4.6, the data of the rate of dissolution at disk rotational speeds greater than 1000 rpm (surface reaction limited) were fitted to Arrhenius equation to determine the apparent activation energy for the surface reaction at 150, 200, and 250°F. The data is shown in **Fig. 4.8** and consistent with an apparent activation energy of 9.2 kcal/mol.

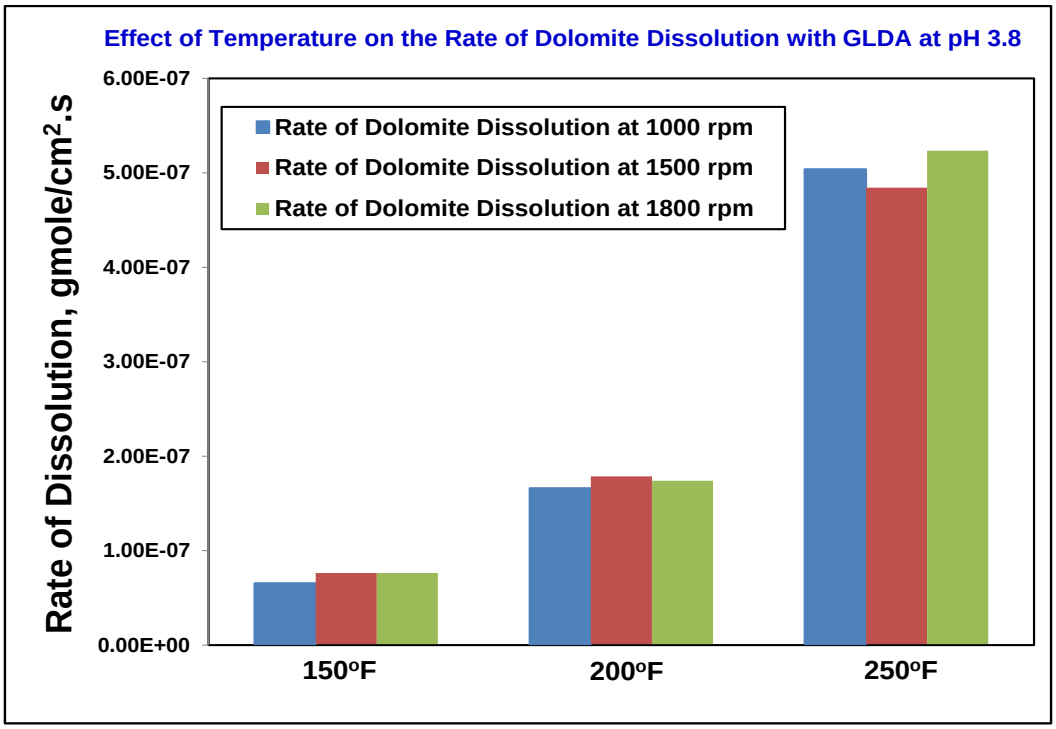

Fig. 4.7: Effect of temperature on the rate of dolomite dissolution with GLDA at pH 3.8.

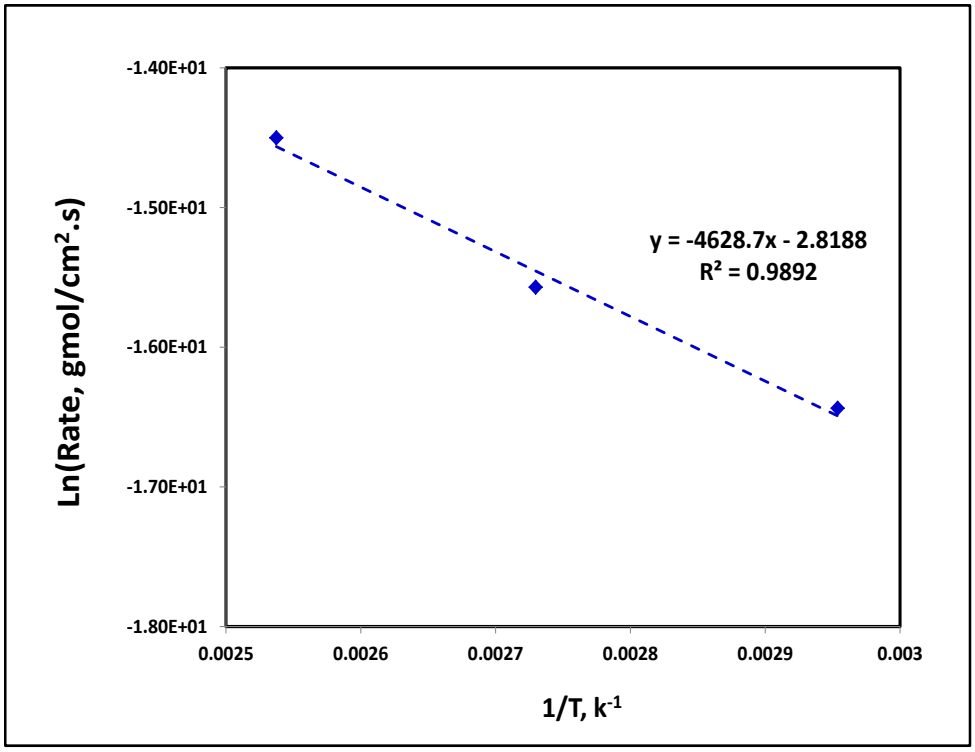

Fig. 4.8: Rate of dolomite dissolution in the surface reaction limiting region fitted to the Arrhenius relation.

It was also interesting to compare the rate of dolomite dissolution with that of calcite with the same acid concentration at the same conditions. This is shown in **Fig. 4.9** for the reaction at 1000 rpm and 150, 200, and 250°F. The data of the calcite dissolution is taken from a previous published work (Rabie et al. 2011b) and was discussed in Chapter 3 as well. It is noted that the dolomite dissolution is significantly lower than calcite dissolution at all temperatures.

The difference between the two rates decreases with increasing the temperature, when the rate of dolomite dissolution is considerable. For instance, the rate of calcite dissolution with GLDA at 150°F is 75 times greater than the rate of dolomite dissolution and 45, and 20 at 200, and 250°F, respectively.

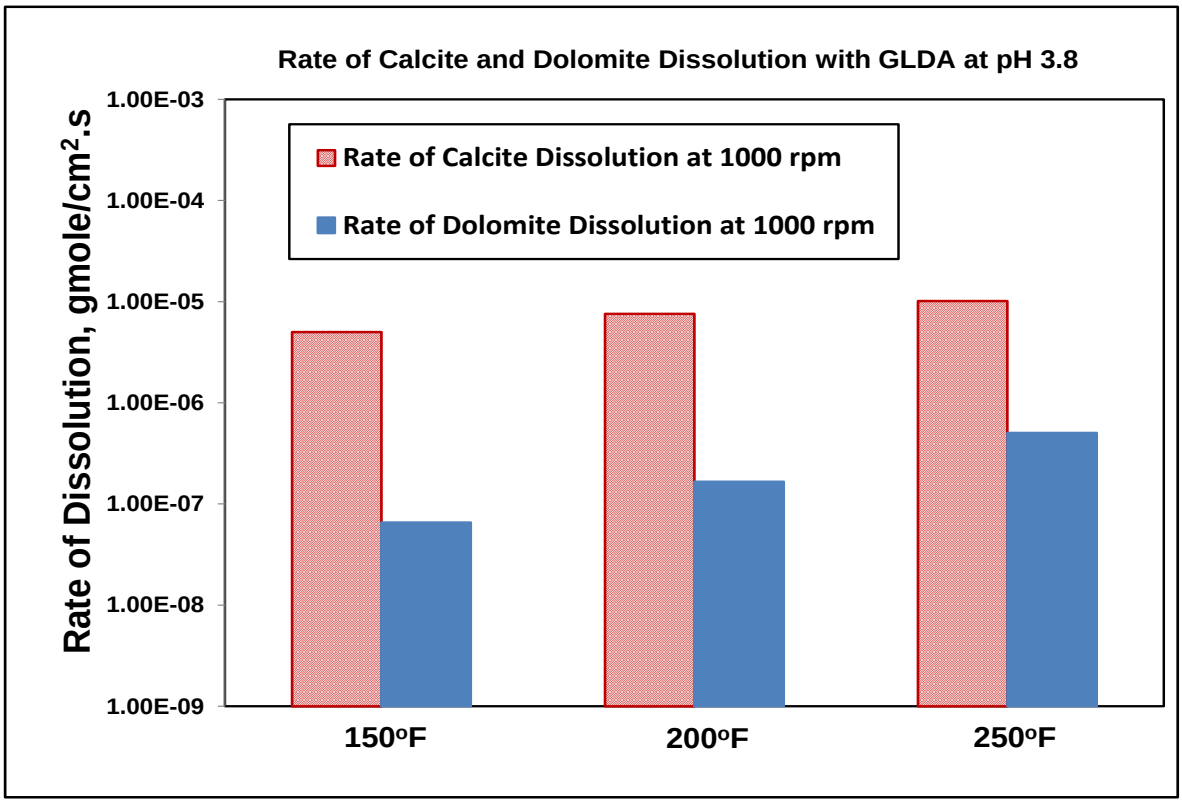

Fig. 4.9: Rate of calcite and dolomite dissolution as at disk rotational speed of 1000 rpm at 150, 200, and 250°F.

Finally, the effect of GLDA concentration on the dolomite dissolution rate was investigated at disk rotational speed of 1500 rpm and temperature of 250°F. Although not expected, increase the GLDA concentration was associated with a reduction in the reaction rate as shown in **Fig. 4.10**. Careful analyzing of these four experiments can give an adequate explanation for these results.

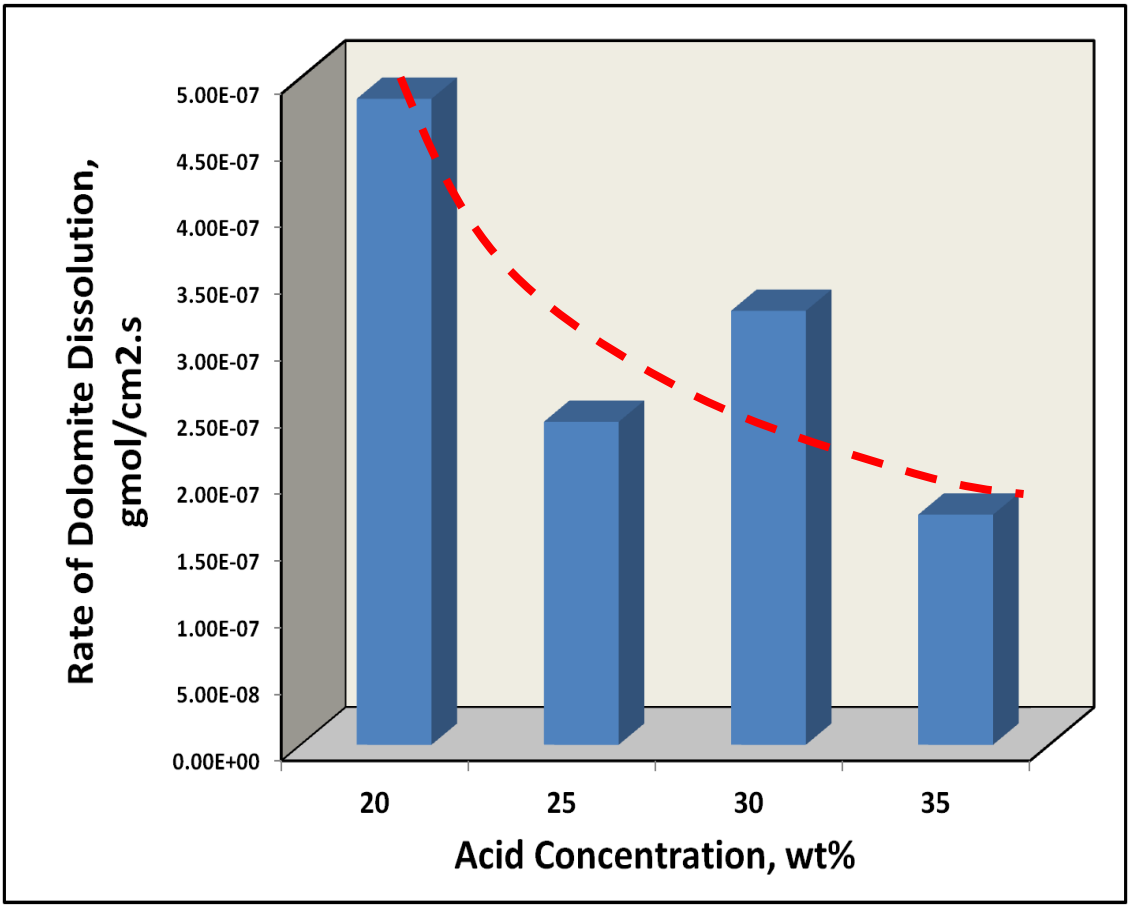

Fig. 4.10: Effect of acid concentration on the rate of dolomite dissolution at disk rotational speed of 1500 rpm and 250°F.

Fig. 4.11 shows the change of calcium concentration inside the rotating disk reactor with time for the four experiments at the four acid concentrations (20, 25, 30, and 35 wt%) and disk rotational speed of 1500 rpm and temperature of 250°F. The results indicate that the initial GLDA solution is not calcium-free, which can be observed by extrapolated the lines to the intersection with the y-axis. Therefore, the calcium concentration in the four initial solutions were measured and added in the figures as shown by the red circles. Extrapolating the data points matches closely the measured

calcium in the initial GLDA solutions and it is observed that the higher the acid concentration, the higher the initial calcium concentration as less dilution is required from the concentrated stock of 40 wt%.

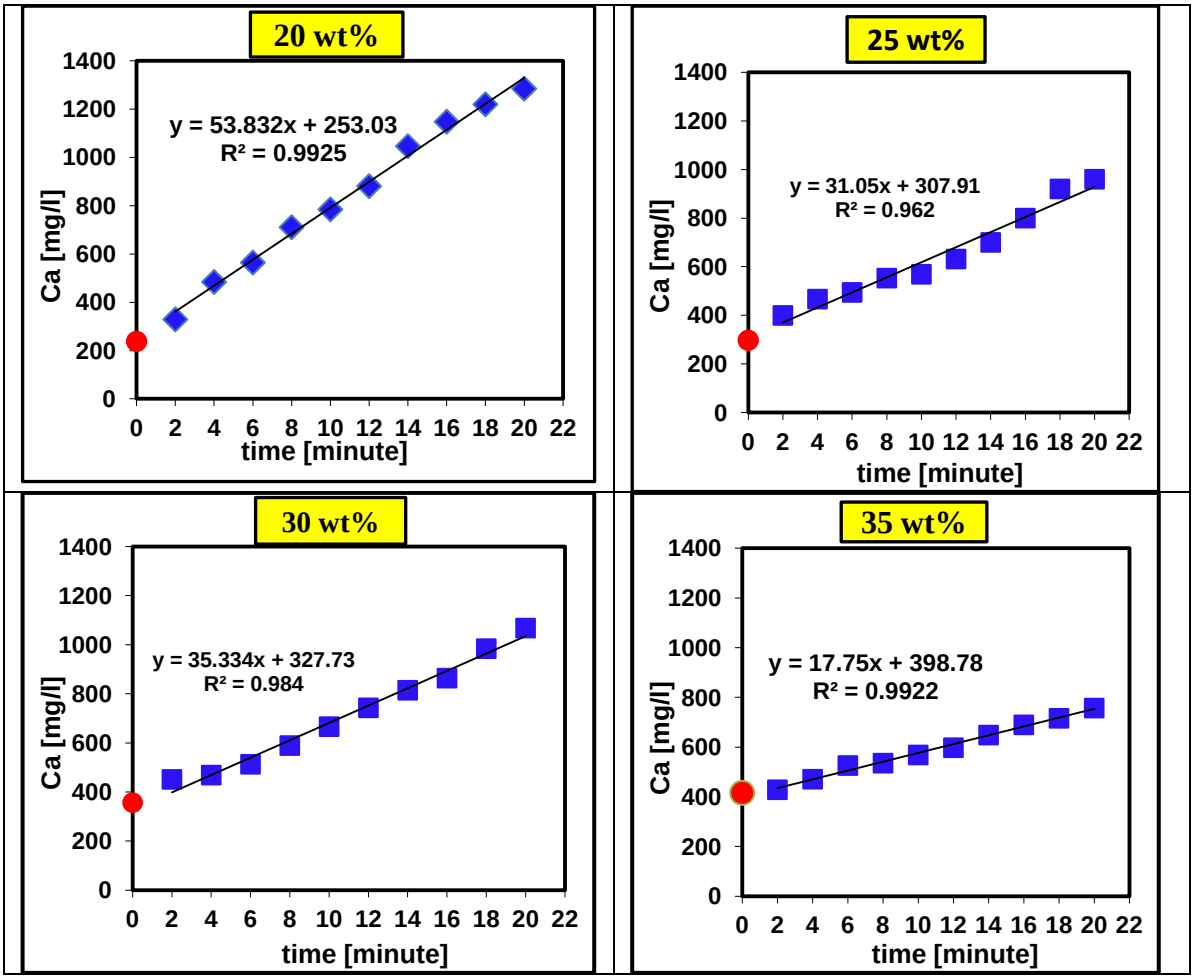

Fig. 4.11: Change of calcium concentration with time for the Dolomite reaction with 20, 25, 30, and 35 wt% GLDA at 1500 rpm and 250°F. (the initial calcium concentration is shown by the red circles on the y-axis)

The data indicates that the presence of calcium in the initial reacting fluid has a reduction effect on the reaction rate and the higher the calcium concentration, the lower the rate. These results match what was reported by Zhang et al. (2007) who conducted

kinetic experiments of dolomite dissolution in water over a temperature range from 25(77) to 250°C (480°F) using a flow through packed bed reactor and three different size fractions of dolomite samples (18–35 mesh, 35–60 mesh, and 60–80 mesh). The authors noted that the dissolution of dolomite is contradicting in most cases. Dissolution of fresh dolomite was non-stoichiometric, the Ca/Mg ratio released to solution was greater than in the bulk solid, and the ratio increases with rising temperatures from 25 to 250°C. The experiments proved that dissolved Ca is a strong inhibitor for dolomite dissolution.

5. HCl-FORMIC IN-SITU GELLED ACID FOR CARBONATE ACIDIZING: CORE FLOOD AND REACTION RATE STUDY*

In highly-heterogeneous carbonate reservoirs and for a large contrast in permeability, several acid systems have been used to enhance the acid diversion for matrix acidizing, such as surfactant-based acids and in-situ gelled acids. In-situ gelled acids are also used to reduce leak-off rate in acid fracturing. The main acid used in this system is HCl. However, high reaction rate and severity of corrosion problems, especially for wells completed with Cr-based tubular, limit the usage of hydrochloric acid especially at high temperatures. On the other hand, mixing organic acids with hydrochloric acid either increases the acid penetration or reduces the necessary strength of HCl and the necessary load of the corrosion inhibitors. A few studies addressed the systems that utilize both advantages.

The objective of this work is to investigate the behavior and the performance of different in-situ gelled HCl-formic acid blends as diverting agents by conducting viscosity measurements, reaction rate measurements using the rotating disk apparatus, and through core flood study. Formic acid was blended with HCl and four in-situ gelled acids were examined. Formic acid concentration varied from 0 to 6.31 wt% and HCl concentration ranged from 0 to 5 wt%.

*: Reprinted with permission from "HCl-Formic In-Situ Gelled Acid for Carbonate Acidizing: Core Flood and Reaction Rate Study" by Ahmed I. Rabie, Ahmed M. Gomaa, and Hisham A. Nasr-El-Din, SPE Paper 140138 presented at the SPE Production and Operations Symposium held in Oklahoma City, Oklahoma, USA, 27–29 March.

Rock samples from Pink Desert limestone were utilized for reaction rate and core flood experiments. The rotating disk apparatus was used to measure the reaction rate at 250^{o}F at disk rotational speeds of 100 and 1000 rpm. The effect of formic acid concentration and zirconium crosslinking on the reaction rate was examined. Core flood experiments were conducted at 250^{o}F using two different rates of injection (2 and 10 cm^{3}/min) and the core samples were imaged using a CT scan technique after each core flood experiment.

Increasing formic acid concentration decreased the reaction rate of HCl-formic in-situ gelled acids with calcite at both low and high disk rotational speeds. This was confirmed by viscosity measurements, which showed that increasing formic acid concentration increased the viscosity of the live acids and decreased the viscosity of the spent acids. Core flood results showed that increasing formic acid concentration in HCl-formic blends reduced acid ability for diversion. In the selected range of acid concentration and for the type of polymer and crosslinking agent used, the in-situ HCl-formic acids behaved more like gelled acids and reached a breakthrough in all core flood experiments. The higher formic acid concentration, the higher pore volume of the acid required to breakthrough.

5.1 Introduction

For heterogeneous reservoirs and for a large contrast in permeability, acid diversion is necessary to enhance the outcome of the matrix acidizing treatments (Woo et al. 1999; Chang et al. 2001; Kalfayan and Martin 2009). Several methods were introduced and tested in the laboratory and applied in the field, such as foam-based acids, surfactant-based acids, and in-situ gelled acids (Smith et al. 1969; Lynn and Nasr-El-Din 2001; Yeager and Shuchart 1997).

In-situ gelled acids are polymer based acids consisting of the acid solution (acid plus a corrosion inhibitor) mixed with a polymer, crosslinker, buffer, and a breaker. When the acid is injected and reacts with formation, pH increases. At pH values of 2 to 3, the polymer is deprotonated and reacts with the crosslinker to form a strongly interconnected network with a very high viscosity. The structure of the solution becomes more like a gel. This gel has the ability to fill and close the highly-permeable zone and force any subsequent injected acid to stimulate the lower-permeable zone. The acid in this formula is used as a diverting agent. The gel structure is then broken when a breaker is activated later in time or at higher pH. The permeability of the plugged zone is regained with the flow back. (Yeager and Shuchart 1997; MaGee et al. 1997; Taylor and Nasr-El-Din 2002; Hill 2005).

One particular example is when the crosslinker contains zirconium, aluminum, or titanium compounds with polyfunctional organic acids. The breaker in this case is a

material that has the ability to form a complex with the organic metallic crosslinker including fluoride, sulfate, phosphate anions, and multi-carboxylated compounds. Calcium fluoride “fluorspar” is normally used as it is readily and naturally available. The breaking mechanism is very simple; the breaker is first coated in water and hydrocarbon insoluble resin and hence can be mixed with the fluid while injecting the fluid in the formation. The coating material delays the release of the breaker so the crosslinker can for the gel with the polymer. At a later time, when the breaker released, the breaker such as CaF_2 forms complexes with the crosslinking agent and therefore breaks the linkages between the crosslinker and the polymer. The gel structure collapses and the viscosity is reduced so the fluid can be flowed back to the well (Boles et. al 1996).

Historically, the main acid used in in-situ gelled acid applictions was hydrochloric acid (HCl). However, the uncontrollable reaction of HCl at elevated temperatures limits its usage in order to avoid the severe corrosion and the probable face dissolution problems if it is used at high concentrations. Organic acids such as acetic, citric, and formic acids have been used to replace HCl. Van Domelen and Jennings (1995) introduced a combination of 9 wt% formic-13 wt% acetic in a gelled form.

Gelled acid are also polymer based acid, however they consist only of the acid solution and the polymer, but they do not have any crosslinker, buffer, or breaker. The acid is used as viscofied system and the viscosity is obtained by the simple addition of the viscous polymer to the acid solution. The acid is used to retard the acid reaction rate

and reduce the acid leak-off in the acid fracturing treatments. The results by Van Domelen and Jennings (1995) showed that the corrosion rate of the gelled acid mixture (formic and acetic acid) is lower than the rate of corrosion of the equivalent 15 wt% gelled HCl and was successfully applied to stimulate the Arun limestone in Indonesia and has been proven effective in terms of both well response and protection of the production equipment.

Another possibility is to mix an organic acid with HCl in order to use an equivalent organic-HCl acid mixture with the same dissolving power of the regular HCl acid but with less HCl concentration. As a result, a controllable reaction with less corrosion can be achieved. Dill and Kneeye (1978) studied the reaction and the corrosion rate of different formic and acetic blends with HCl. The results showed that a minimum corrosion rate was obtained when 1 to 4 wt% of formic acid was mixed with 10 wt% HCl. Unlike the formic acid, increasing the percentage of acetic acid increased the rate of corrosion but still was still than the corrosion if a corresponding HCl is used alone. Several similar lab and field studies have been reported also in the literature (Buijse et al. 2004; Chang et al. 2008).

Welton and Van Domelen (2008) tested and evaluated the chemistry and the rheology properties of gelled and in-situ cross-linked HCl-formic acid blends equivalent to 28% HCl and claimed that HCl and formic acid can be successfully in-situ cross-linked. The authors observed that some synthetic polymer-acid gelling agents provide a

high initial viscosity in HCl-formic acid blends and stated that the gelled HCl-formic acid blends are more robust (than HCl blends) and maintain higher viscosities for longer periods at elevated temperatures.

Nasr-El-Din et al. (2003) examined blends of gelled and in-situ gelled acid blends of 15 wt% HCl – 9 wt% formic acid in the lab and in field treatments. According to the analysis of lab and the flow back samples, the acid mixture was able to effectively stimulate the deep gas wells. However, very limited corrosion packages were successfully able to preserve the tube integrity.

The viscosity of the in-situ gelled acid should be carefully designed for the acidizing treatments. The high viscosity of the in-situ gelled acid will reduce the diffusivity of the hydrogen ion (H^+) to the rock surface and as a result, reduces the rate of reaction of these acids with carbonate. If the reaction does not proceed to a pH value of 2, the crosslinker is inactive and the gel will never form. The presence of the formic acid can significantly affect the reaction and the viscosity of the live and the spent acid, and therefore affect the outcome of the treatment that uses the in-situ gelled formic-HCl mixtures as diversion agents.

5.2 Objectives

The objective of this work is to study the effect of formic acid on the performance of the in-situ gelled HCl-formic acid by conducting viscosity measurements, core flood studies, and reaction rate measurements using the rotating disk apparatus.

5.3 Experimental Studies

5.3.1 Materials

Acid mixtures were prepared from 36.8±0.01 wt% HCl and 88±0.02 wt% formic acid concentrated ACS reagents grade. Acid solutions were prepared using deionized water with a resistively of 18.2 MΩ.cm at room temperature. Polymer and other additives were all oilfield chemicals, and were used without further purification.

5.3.2 Acid Preparation

Four in-situ (crosslinked) gelled acid mixtures (A, B, C, and D) and one gelled acid (E) were tested in this work. The chemical composition of each acid mixture is shown in **Table 5.1.** All acid formulas were prepared with the same polymer and all in-situ gelled acids contained the same crosslinker, breaker, corrosion inhibitor, and buffer concentrations. The composition of the hydrochloric and the formic acids were selected so all the acid systems had an initial acid concentration that is equivalent to 5 wt% HCl (on a molar basis). Based on a previous study (Gomaa and Nasr El-Din 2010b), this acid concentration was optimum to build up the viscosity in the spent acid and hence

provides the best diversion performance. The tested acids have the following composition:

- Acid A: 5 wt% HCl and 0 wt% formic acid, (crosslinked gelled acid)
- Acid B: 3.42 wt% HCl and 2 wt% formic acid
- Acid C: 1.83 wt% HCl and 4 wt% formic acid
- Acid D: 0 wt% HCl and 6.31 wt% formic acid
- Acid E: 5 wt% HCl and 0 wt% formic acid, (gelled acid)

Table 5.1: Formula of in-situ gelled acids tested in the present study.

Chemical	A	B	C	D	E
Formic Acid	0 wt%	2 wt%	4 wt%	6.31 wt%	0 wt%
HCl	5 wt%	3.42 wt%	1.83 wt%	0 wt%	5 wt%
Gelling Agent	20 gpt	20 gpt	20 gpt	20 gpt	20 gpt
Corrosion Inhibitor	4 gpt	4 gpt	4 gpt	4 gpt	4 gpt
Crosslinker	4.5 gpt	4.5 gpt	4.5 gpt	4.5 gpt	-
Breaker.	4 lb/Mgal	4 lb/Mgal	4 lb/Mgal	4 lb/Mgal	-
Buffer	2 gpt	2 gpt	2 gpt	2 gpt	-

5.3.3 Viscosity Measurements

Viscosity measurements for all acid systems were made using an HP/HT viscometer at live and partially neutralized (pH 4-5) conditions. To resist corrosion by the acids, both the rotor (R1) and the bob (B1) of the viscometer were made of Hastelloy C. The viscosity was measured as a function of shear rate from 0.1 to 1020 s^{-1} at 300 psi and in a temperature range from 75 to 250^{o}F.

5.3.4 The Rotating Disk Apparatus

Samples were cut from Pink Desert limestone cores into disks with a diameter of 1.5 in. and a thickness of 0.65 in. Samples were saturated with deionized water for 24 hours under vacuum and the initial porosity was determined, **Table 5.2**. All samples were soaked in 0.1N HCl for 30 to 40 minutes then rinsed thoroughly with deionized water before reaction. This method ensures good reproducibility and eliminates problems associated with preparing the disk surfaces (Fredd and Fogler 1998c). Reaction rate experiments were performed using a rotating disk apparatus. A schematic diagram of the RDR is shown in **Fig. 5.1**.

Table 5.2: Initial core data used for rotating disk experiments.

Run	Acid Type	Disk Rotational Speed, rpm	Porosity, vol.%
1	A	100	27.5
2		1000	29.8
3	B	100	25.5
4		1000	27.2
5	C	100	28.1
6		1000	29.6
7	D	100	26.6
8		1000	28.5
9	E	100	28.9
10		1000	26.8

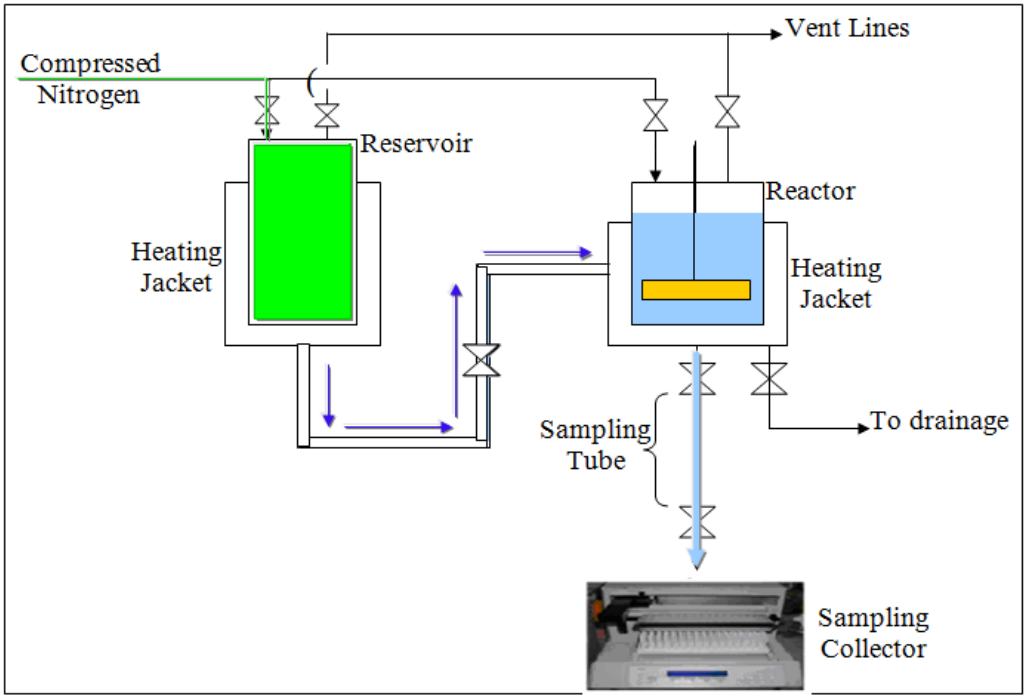

Fig. 5.1: A Schematic diagram for the rotating disk apparatus used for reaction rate measurements.

5.3.5 Core Flood Setup

Eight cylindrical cores with a 1.5-in. diameter and 6-in. length were cut from a Pink Desert limestone block. , **Table 5.3**. Cores were placed inside an oven set at 257^{o}F for 5 hours to be completely dry, and then their weight was measured. Each core was saturated with deionized water under vacuum for 24 hrs. and the porosity was calculated. Deionized water was injected first at different flow rates (5, 10, and 20 cm^3/min) and the initial permeability was determined.

Table 5.3: Initial core data used in core flood study.

Core #	Pore Volume, (-)	Porosity, vol.%	Permeability, md
1	47.0	27.1	80
2	42.9	24.8	85
3	40.7	23.5	75
4	44.7	25.8	73
5	45.4	26.2	83
6	39.5	22.8	71
7	46.5	26.8	80
8	38.2	22.0	82

Core flood experiments were conducted for all acid systems at flow rates of 2 and 10 cm^3/min. A new core was used in each experiment. The cores were imaged using a CT scan technique after each acid injection. A heat jacket was placed around the core holder and was used to heat up the sample to 250^{o}F. Effluent samples were collected throughout the experiment using an automatic fraction collector and density, pH value, and the concentrations of calcium were measured.

5.4 Results and Discussion

5.4.1 Viscosity Measurements

The viscosity of in-situ gelled Acids A, B, C, and D was measured as a function of temperature and shear rate. The results showed a non- Newtonian, shear-thinning behavior. The viscosity and the shear rate relationship for all acids can be described by the power-law model, Eq. 5.1:

$$\mu = K\,\dot{\gamma}^{(n-1)} \quad \text{[5.1]}$$

Where μ is the fluid viscosity (poise), $\dot{\gamma}$ is the shear rate (s^{-1}), n is the power-law index (-), and K is the power-law consistency index ($g.cm^{-1}.s^{n-2}$). **Table 5.4** gives the values of K and n for the four acid blends in live and spent conditions at 250°F.

Table 5.4: Power-law parameters for live and partially neutralized in-site gelled acids A, B, C, and D at 250°F.

System	Formic Acid, wt%	Hydrochloric Acid, wt%	Conditions	K, $mPa.s^n$	n
A	0	5	live	860.4	0.413
			Partially neutralized*	8163.5	0.283
B	3	3.42	live	1809.6	0.374
			Partially neutralized*	3035	0.406
C	4	1.83	live	6127.4	0.26
			Partially neutralized*	1815.5	0.44
D	6.31	0	live	1398.7	0.162
			Partially neutralized*	1353.6	0.351

5.4.2 Viscosity of In-Situ Formic-HCl Gelled Acid at Live Conditions

The viscosity of live Acids A, B, C, and D as a function of shear rate at temperature of 250°F is plotted in **Fig. 5.2**. Following a shear-thinning behavior, increasing the shear rate decreased the viscosity of all acid mixtures. For optimal pumping requirements, in-situ gelled acids are preferred to have a low viscosity at live conditions. However at any specific shear rate, increasing the formic acid concentration enhanced the viscosity of the polymer at live condition. This effect is more significant at low values of the shear rate.

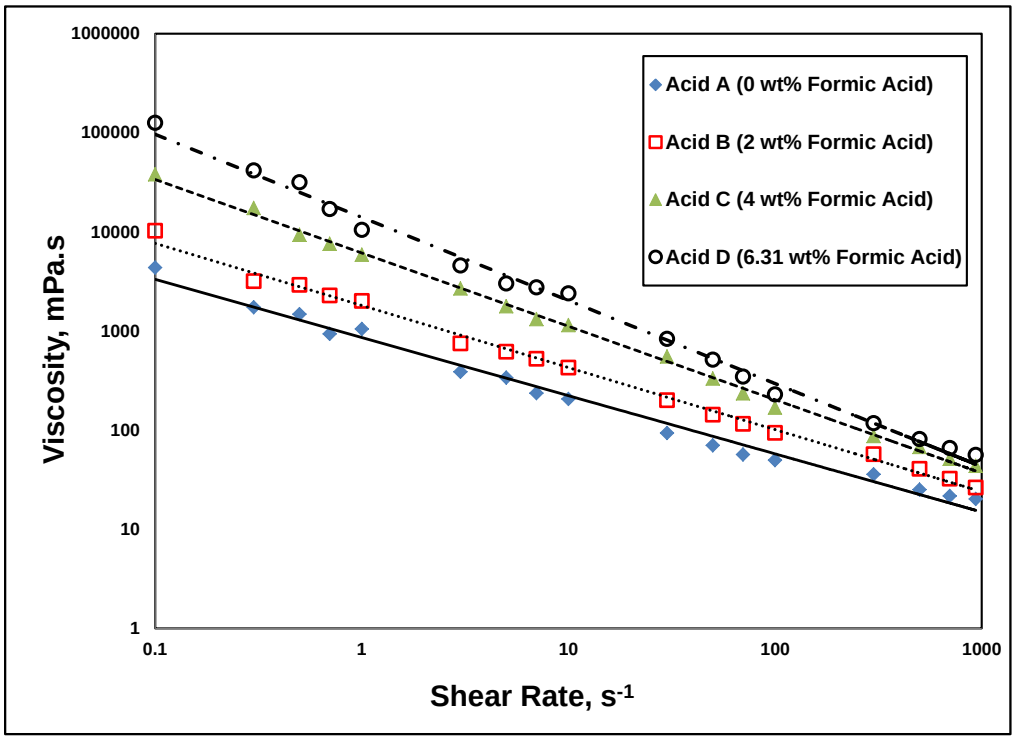

Fig. 5.2: Viscosity of live in-situ gelled Acids A, B, C, and D as a function of shear rate at 250°F.

For instance, the difference between the viscosity of Acid A (0 wt% formic acid) and acid D (6.31 wt% formic acid) reaches two orders of magnitude at shear rate of 0.1 s^{-1}. This effect decreased by the increasing the shear rate and all the acid mixtures have similar viscosity values at shear rate of 1000 s^{-1}.

The effect of temperature on the viscosity of live Acids A, B, C, and D was investigated at a constant shear rate of 100 s^{-1} and in a temperature range of 75-250°F. **Fig. 5.3** shows that increasing the temperature has almost no effect on the viscosity of the all acid mixtures, except a minor drop in the viscosity of live Acid B. At any specific temperature, the higher the formic acid concentration, the higher the viscosity of the acid blend.

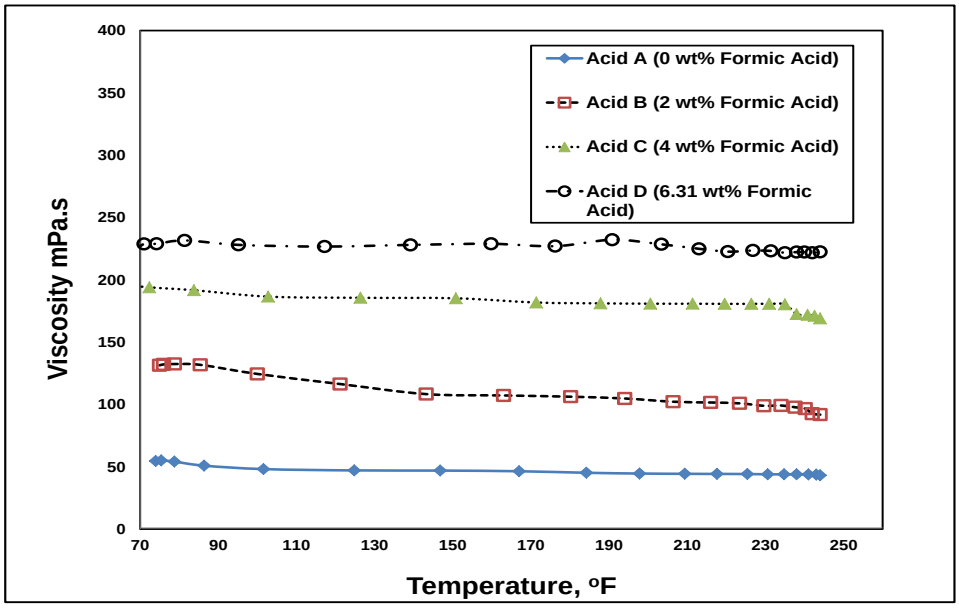

Fig. 5.3: Viscosity of live in-situ gelled Acids A, B, C, and D as a function of temperature at shear rate of 100 s^{-1}.

The effect of formic acid (or other organic acids) on enhancing the viscosity of the live in-situ gelled acids can be probably due to the stability that organic acid adds to the polymer at higher temperatures that prevents fractional chain destruction which causes a reduction in the polymer viscosity. (Van Domelen and Jennings 1995). This claim is confirmed by the results shown in Fig. 5.3, which shows a constant acid viscosity, especially at higher formic acid concentrations.

4.4.3 Viscosity of In-Situ Gelled Acid at Partially Neutralized Conditions

The viscosity of the partially neutralized acid (pH 4-5) was examined for Acids A, B, C, and D as a function of shear rate at temperature of 250^{o}F, **Fig. 5.4**. For better ability to diversion, it is recommended to have the maximum acid viscosity at the neutralized conditions which is the case of Acid A with no formic acid. Adding formic acid to other blends reduced the viscosity. The higher the formic acid concentration, the less viscosity was noted for acid solutions B, C, and D that have 2, 4, and 6.31 wt% formic acid, respectively.

This can be explained by referring to the fact that the presence of the organic acid results in a higher steric hindrance that resists the hydrolysis of the acrylamide group on the side chain which in turns results in less crosslinking (Bryant et al. 1996; Van Domelen and Jennings 1995).

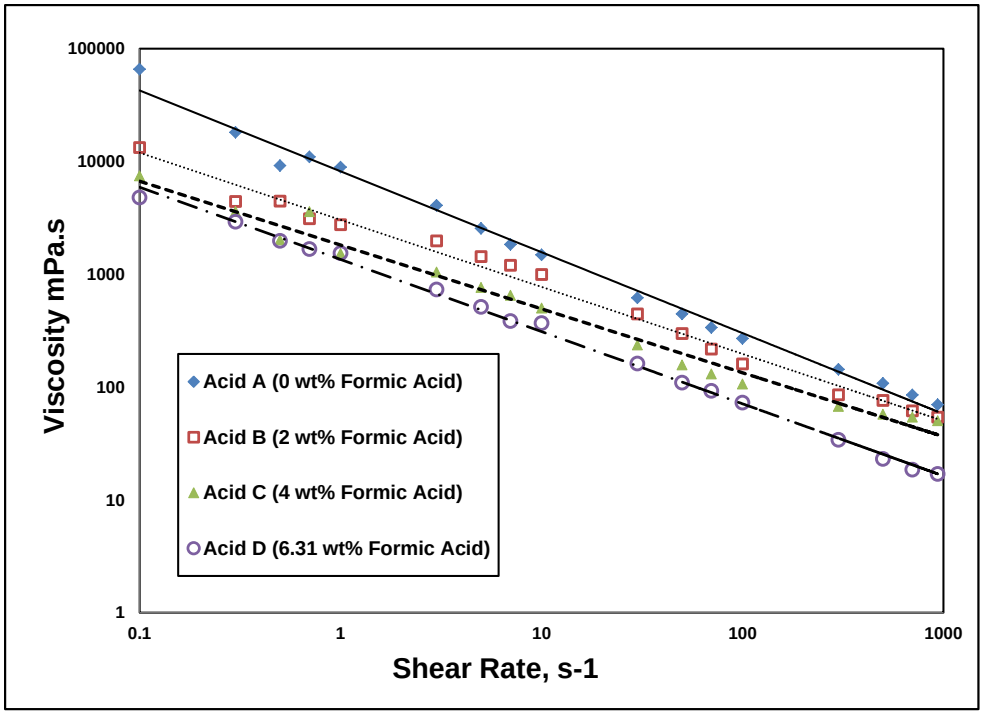

Fig. 5.4: Viscosity of partially neutralized (pH 4-5) in-situ gelled Acids A, B, C, and D as a function of shear rate, 250oF.

The effect of temperature on the viscosity of the spent acid mixtures is shown in **Fig. 5.5**. Increasing the temperature reduced the viscosity of Acid A from 450 mPa.s to 245 mPa.s, when temperature increased from 75 to 250^{o}F. However, temperature did not have a significant effect on the viscosity of the partially neutralized Acids B, C, and D.

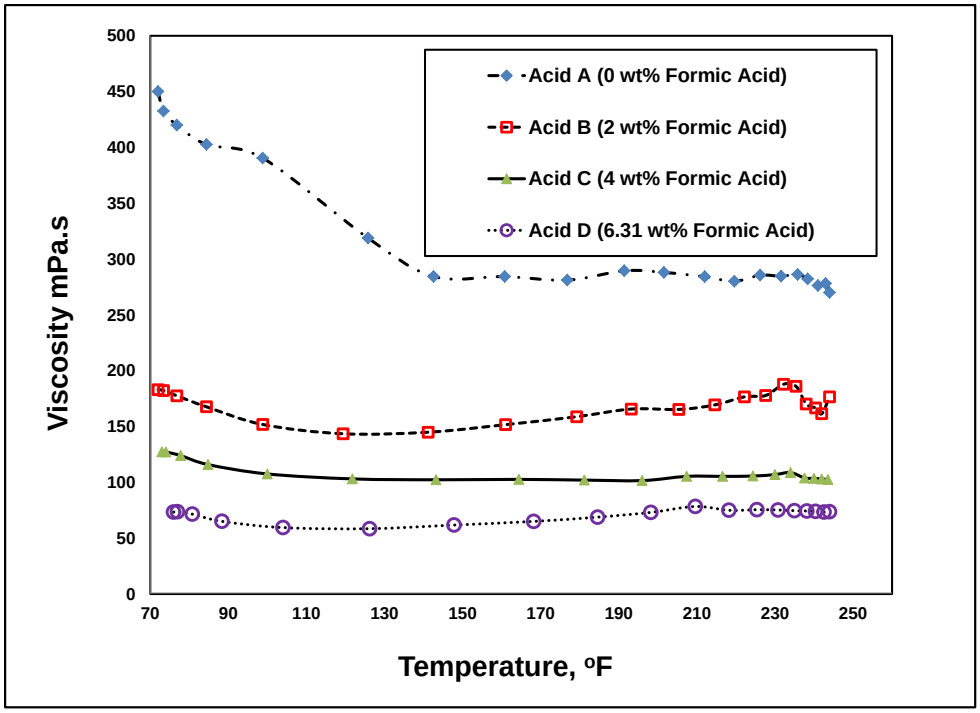

Fig. 5.5: Viscosity of partially neutralized (pH 4-5) neutralized in-situ gelled Acids A, B, C, and D as a function of temperature, 100 s^{-1}.

Fig. 5.6 highlights a comparison between the viscosities of the four acid systems at shear rate of 100 s^{-1} and 250^{o}F. It is worth mentioning that Acid B (2 wt% formic acid) is the only acid system with formic acid that still behaves as an in-situ gelled acid in which the viscosity of the partially neutralized acid is higher than the viscosity of the live acid.

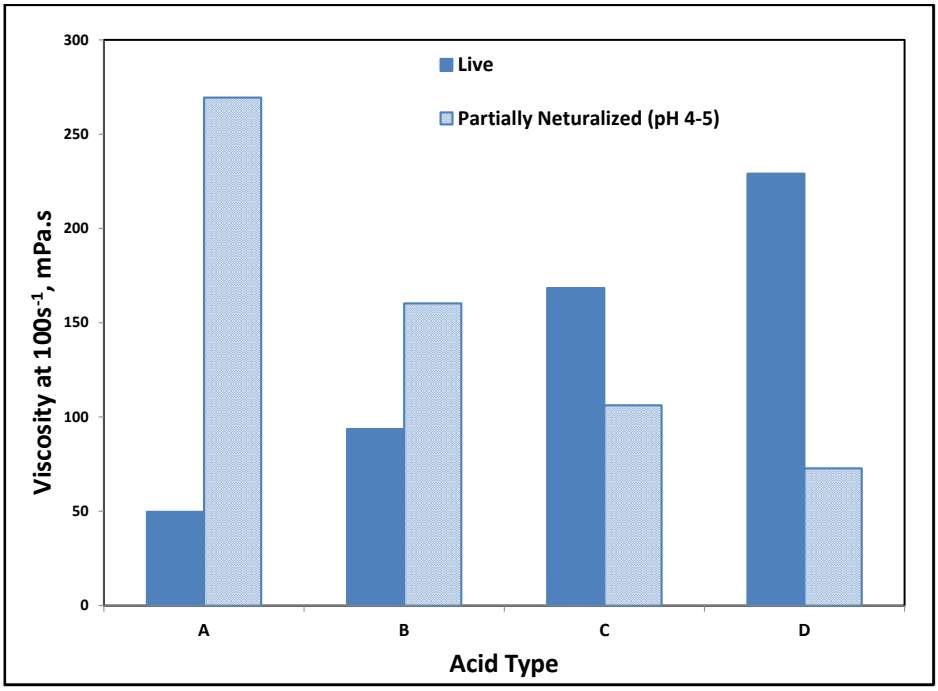

Fig. 5.6: Viscosity of live and partially neutralized (pH 4-5) in-situ gelled Acids A, B, C, and D, 100 s^{-1}, 250^{o}F.

5.4.4 Reaction of In-Situ HCl-Formic with Calcite

The rotating disk apparatus has been widely used for measuring the rate of heterogeneous reactions. For the applications in the oil industry, the rotating disk reactor was used to measure the rate of calcite and dolomite dissolution in the presence of a wide range of acids and aqueous solutions (Lund et al. 1973; 1975; Plummer et al. 1978; Sjoberg and Rickard 1984; Fredd and Fogler 1998a; 1998c). The rotating disk theory and the determination of reaction rate were briefly described in the experimental section and were explained in detail by Rabie et al. (2011a).

For the best explanation of the core flood experiments and the rheology measurements, the reaction rate experiments were conducted at 250^{o}F. Each acid system

was examined at disk rotational speeds of 100, and 1000 rpm, respectively. The rate of reaction can be determined by plotting the calcium produced as a function of the reaction time. The rate of dissolution will then be the slope of the best fitted straight line divided by the initial area of the sample disk taking into account the sample porosity.

Fig. 5.7 illustrates the change in the calcium concentration in the reactor as a function of time for acid systems B, C, and D at disk rotational speed of 100 rpm. As shown in the figure, increasing the formic acid concentration reduced the reaction rate of in-situ gelled HCl-formic acids, which can be explained by the reduction in the viscosity of the live acids as shown in Fig. 5.2. The higher the viscosity, the lower the acid diffusivity to the surface and hence, the lower the rate of reaction.

In addition, increasing the concentration of the formic acid is associated with a reduction in the hydrochloric acid concentration in order to formulate acid mixtures with the same dissolving power as the base Acid A (5 wt% HCl). It is then obvious that a reduction in the reactant concentration will result in a reduction in the rate of reaction. In the case of the rotating disk experiments, the ratio of the acid volume to the volume of the rock sample does not allow the acid to go for complete depletion, therefore the main reactant is the hydrochloric acid and the formic acid probably will not ever react. **Fig. 5.8** compares the rata of reaction of all acid systems A, B, C, and D at 100 rpm.

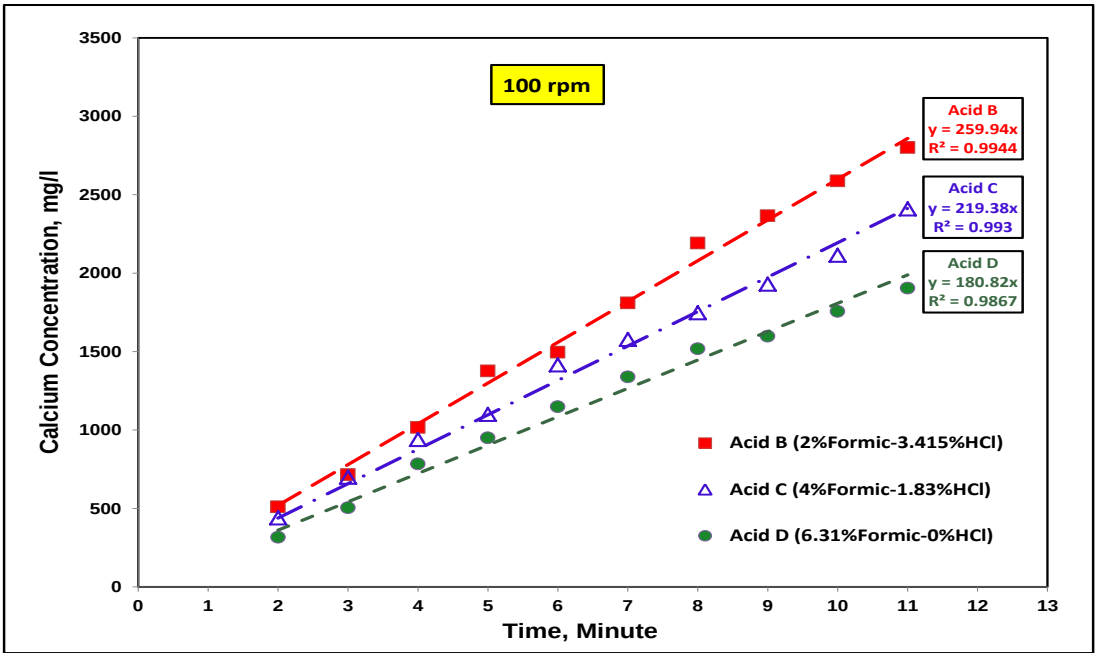

Fig. 5.7: Change in calcium concentration with time for the reactions of Acid B, C, and D with Pink Desert limestone at 250^{o}F and 100 rpm.

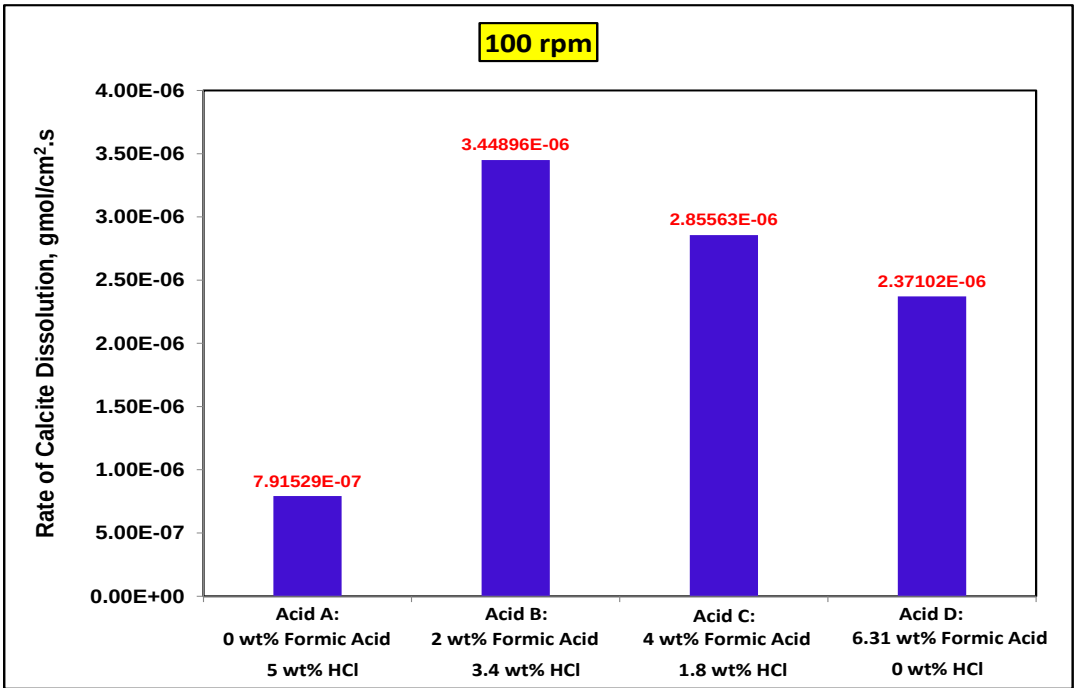

Fig. 5.8: A comparison between the reaction rate of Acids A, B, C, and D with Pink Desert limestone at 250^{o}F and 100 rpm.

Fig. 5.9 shows the change of calcium concentration with the reaction time for acid systems B, C, and D at 1000 rpm. The figure showed a similar behavior to what was obtained at 100 rpm. **Fig. 5.10** shows a comparison between the rate of reaction of these systems with the base Acid A at 1000 rpm.

Figs. 5.8-10 shows a significant reduction when the reaction rate of acid A is compared to the reaction rate of acids B, C, or D at both disk rotational speeds (100 and 1000 rpm). It was then believed that Acids B, C and D more likely react as gelled acids. To confirm this claim, reaction rate of gelled acid system E (0 wt% formic acid- 5 wt% HCl) was measured at disk rotational speeds of 100, and 1000 rpm. Acid system E has the same composition as acid A, but with no crosslinker, buffer, or breaker.

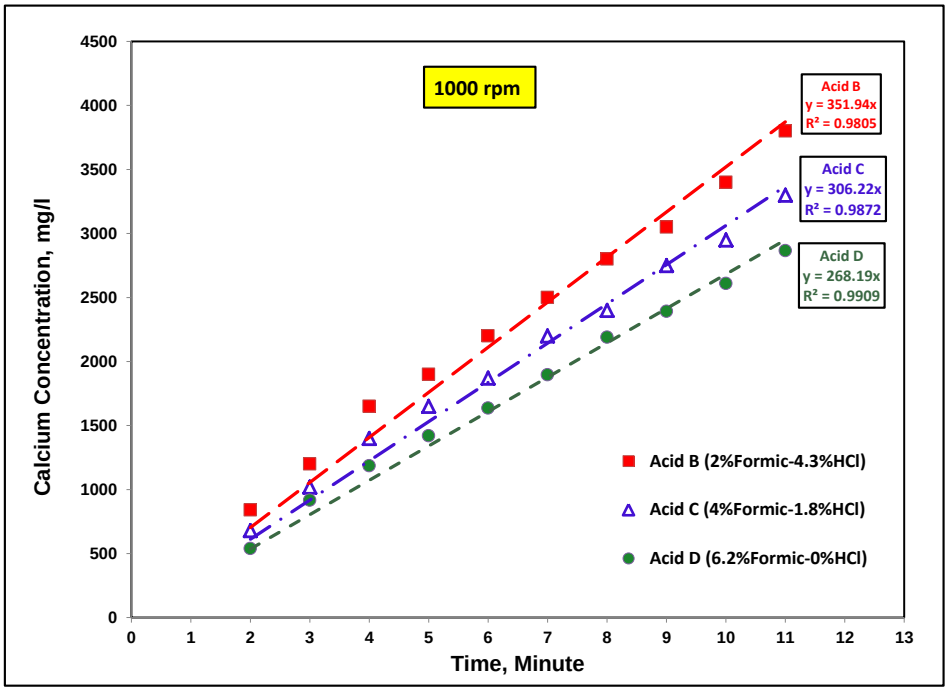

Fig. 5.9: The change in calcium concentration with time for the reactions of Acids B, C, and D with Pink Desert limestone at 250^{o}F and 1000 rpm.

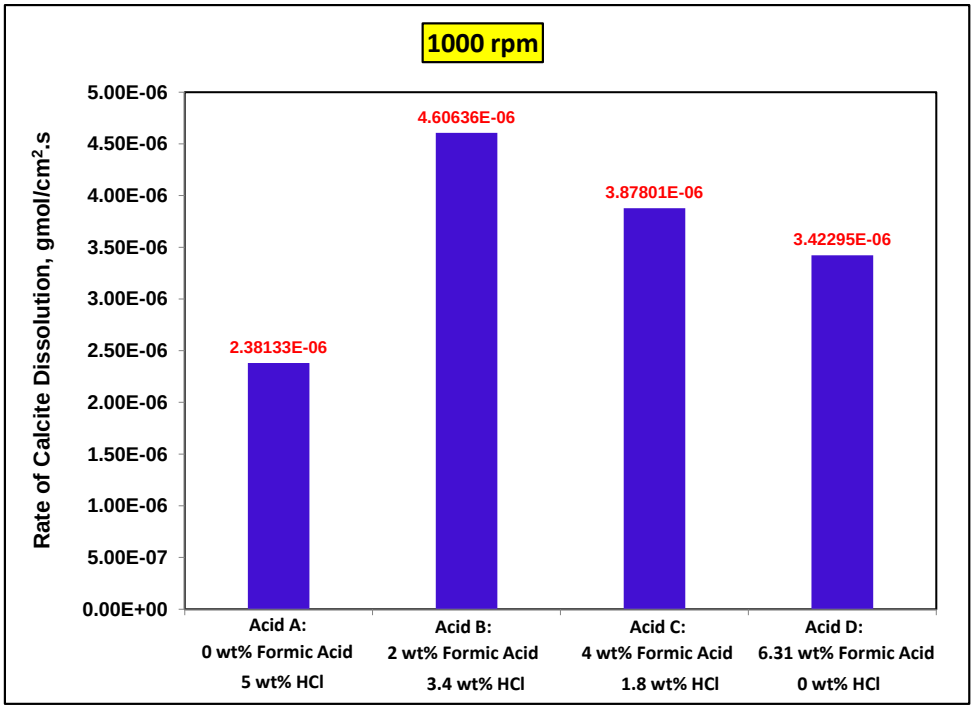

Fig. 5.10: A comparison between the reaction rate of Acids A, B, C, and D with Pink Desert limestone at 250^{o}F and 1000 rpm.

Fig. 5.11 shows that at disk rotational speed of 100 rpm, the rate of reaction of the gelled acid E was $2.5*10^{-6}$ gmol/cm^2.s, which was very close to the rate of reaction of the in-situ gelled Acids C and D ($2.85*10^{-6}$ and $2.37*10^{-6}$ gmol/cm^2.s, respectively). At disk rotational speed of 1000 rpm, the rate of reaction of system E was $5.77*10^{-6}$ gmol/cm^2.s, which was close to the rate of reaction of acid B ($4.6*10^{-6}$ gmol/cm^2.s) as shown in **Fig. 5.12**.

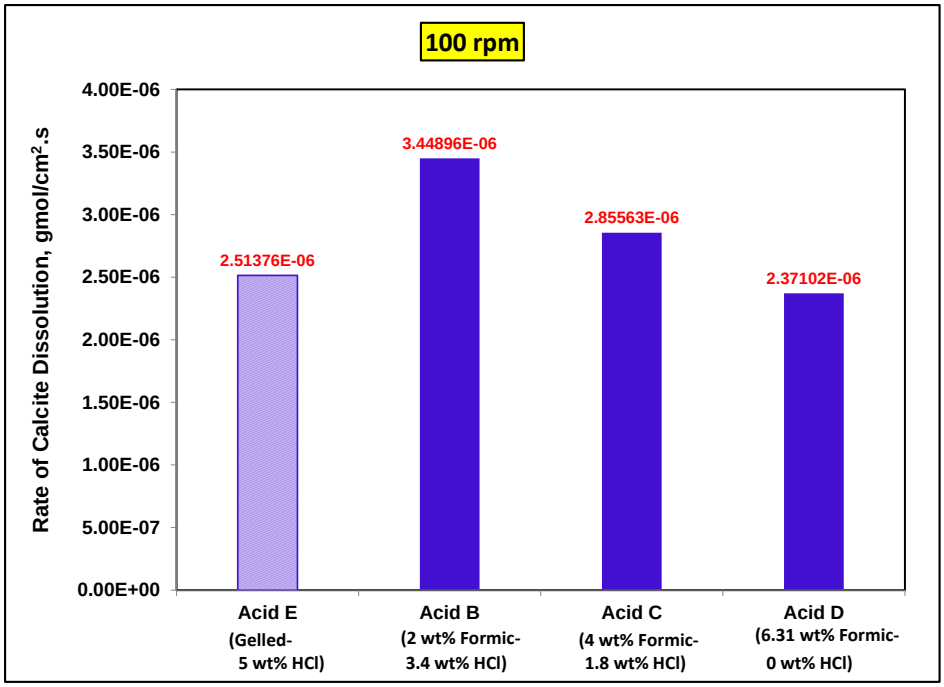

Fig. 5.11: A comparison between the reaction rate of Acids B, C, D, and E with Pink Desert limestone at 250°F and 100 rpm.

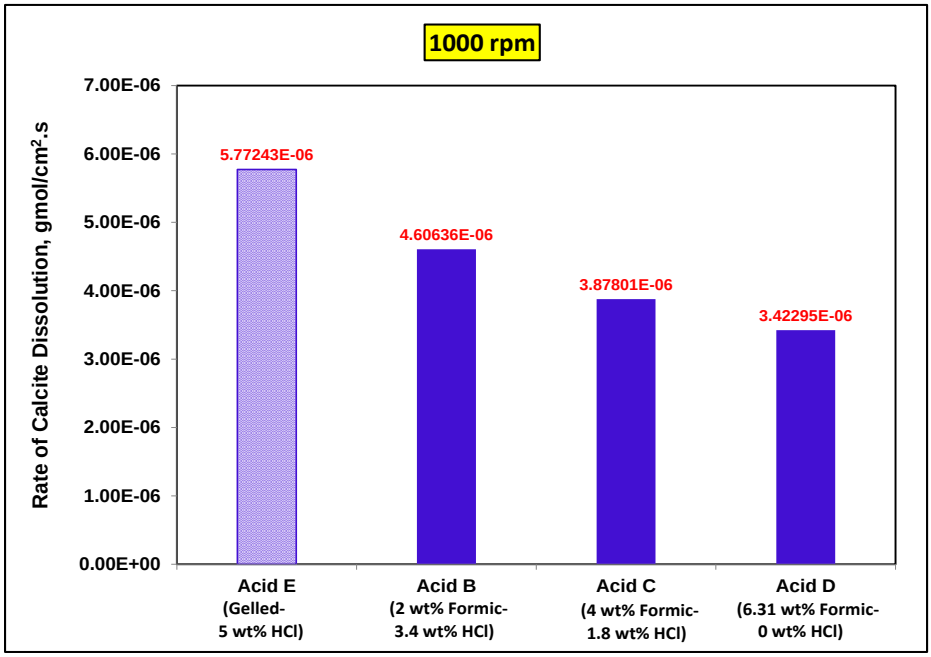

Fig. 5.12: A comparison between the reaction rate of Acids B, C, D, and E with Pink Desert limestone at 250°F and 1000 rpm.

4.4.5 Core Flood Study

Eight experiments were conducted with Acids A, B, C, and D at injection rates of 2 and 10 cm^3/min using Pink Desert carbonate cores, Table 5.3. All experiments were conducted at 250°F while the pressure drop across the core was monitored during the experiment. A new core was used in each experiment.

In the first experiment, water was injected at a rate of 2 cm^3/min in Core 1 to preflush and ensure the saturation of the core. Three pore volumes (PV) of acid A were then injected at the same rate of 2 cm^3/min with no breakthrough. This was followed by a 3.8 PV slug of water injected in the same acid direction.

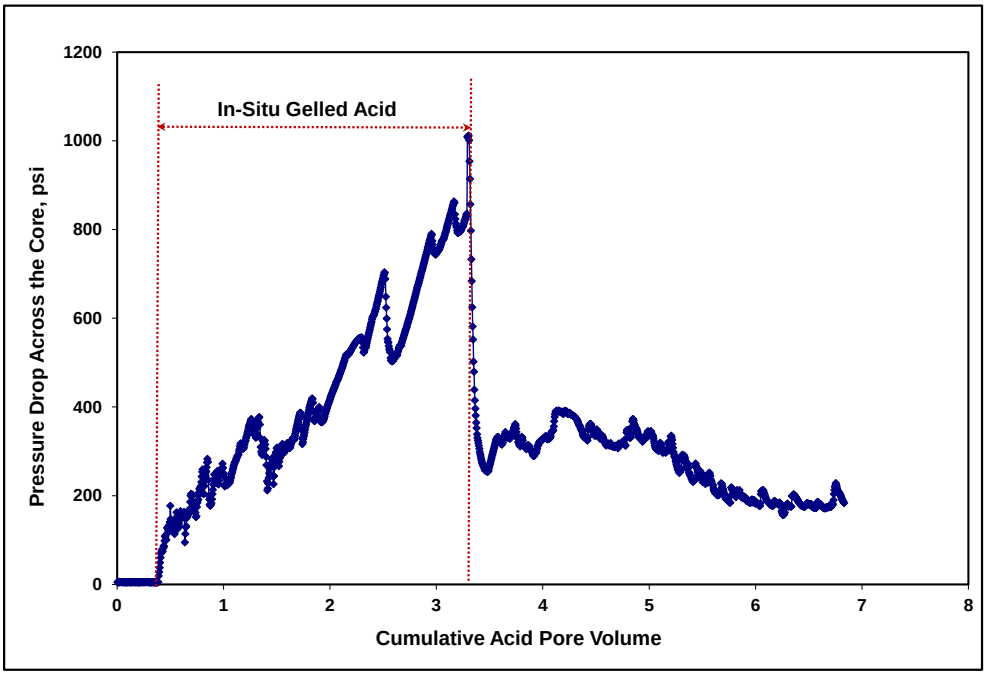

Fig. 5.13: Pressure drop across core 1 as a function of cumulative injected volume of Acid A at injection rate of 2 cm^3/min and 250°F.

Fig. 5.13 shows the change in the pressure drop as a function of the cumulative injected pore volume of acid A. As the acid entered the core, the pressure drop increased due to the higher acid viscosity than water. The pressure drop changed in a cycling manner as it was described by Gomaa et al. (2009). The cycling behavior of the pressure drop indicates that the gel structure was formed and the acid was able to change its direction inside the core. When the gel was formed, the acid loses its mobility and the fresh acid was pressurized utill the point in which the acid was able to penetrate the weakest point in the gel structure and open new channel for flow and therefore the pressure drop goes down and then the cycle repeats. The change of pH and density of the effluent samples are shown in **Fig. 5.14** as a function of the cumulative injected pore volume.

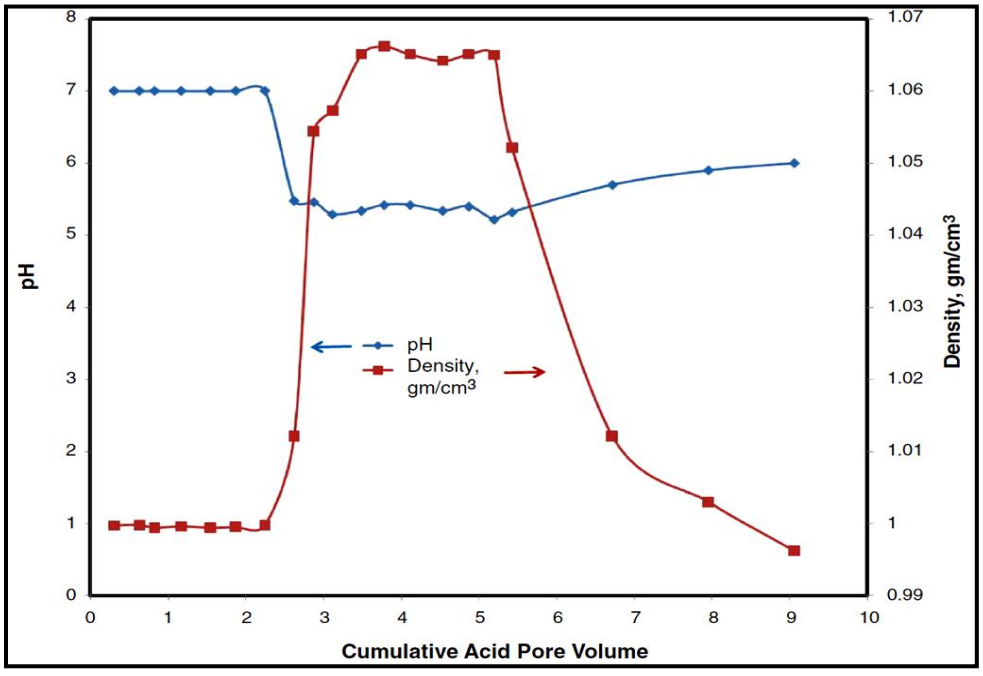

Fig. 5.14: pH and density of the effluent samples as a function of the cumulative acid pore volume of Acid A at injection rate of 2 cm^3/min and 250°F

The second core flood experiment was conducted using the same acid type (acid A) at 10 cm^3/min. After the injection of two pore volumes, the acid achieved a breakthrough which indicates that the acid reacted faster with the core and there was not enough time for proper formation of the gel structure. This effect can be confirmed in **Fig. 5.15**, which shows the pressure drop and illustrates less cycling behavior. In a previous study, Gomaa and Nasr-El-Din (2010a) showed that at 10 cm^3/min, regular, gelled, and in-situ gelled acid (based on iron crosslinker) needed 2.1, 1.4, and 4.2 PV to breakthrough, respectively. In-situ gelled Acid A (based on a zirconium crosslinker) consumed acid volume close to that reported for the regular acid. This means Acid A cannot be used as in-situ gelled acid at a high injection rate.

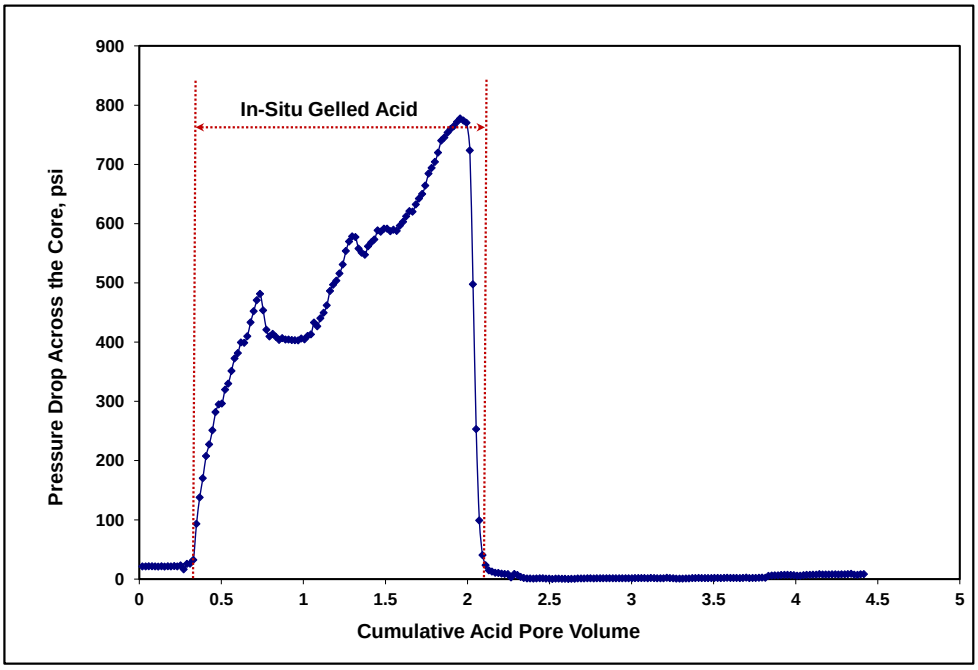

Fig. 5.15: Pressure drop across core 2 as a function of cumulative injected volume of Acid A at injection rate of 10 cm^3/min and 250^{o}F.

Fig. 5.16 shows the pressure drop of Acids B, C, and D as a function of the cumulative injected volume at an injection rate of 2 cm^3/min. As the formic acid concentration increased, the pressure drop across the core was increased and also the volume needed to breakthrough was increased, where a 1.04, 1.23, 1.82 PV was needed for Acids B, C, and D, respectively. The pressure performance was expected because as the formic acid concentration increased, the viscosity of live acid increased as shown in Fig. 5.6.

For Acids B, C, and D, the smaller acid pore volume and smaller pressure drop cycling was evidence that there was no ability of the acid to change its direction inside the core. Same pressure performance was observed at injection rate of 10 cm^3/min for Acids B, C, and D, **Fig. 5.17**.

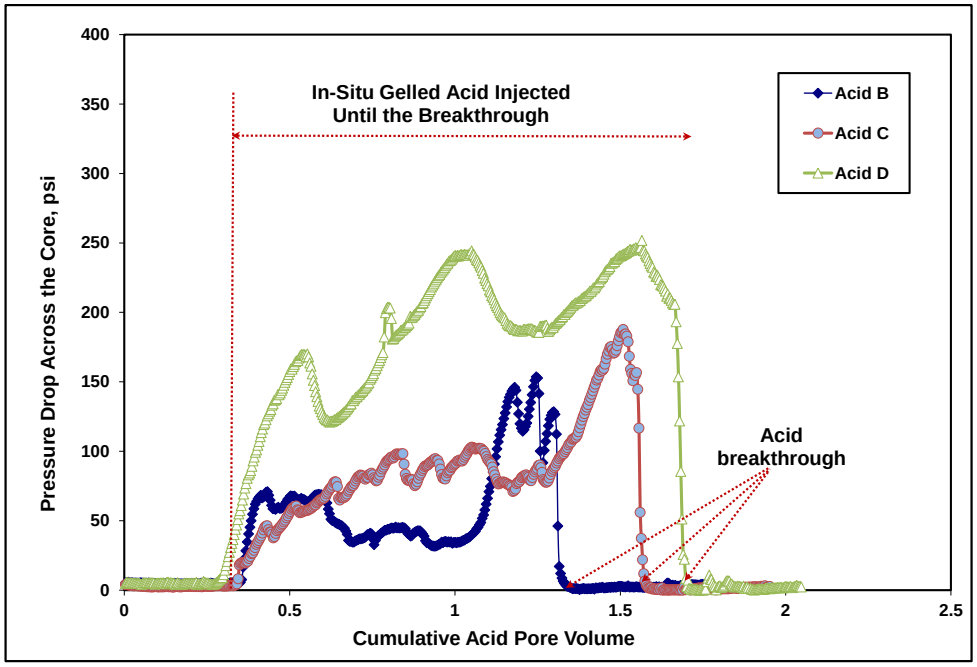

Fig. 5.16: Pressure drop as a function of cumulative volume injected of Acids B, C, and D at injection rate of 2 cm^3/min and 250^oF.

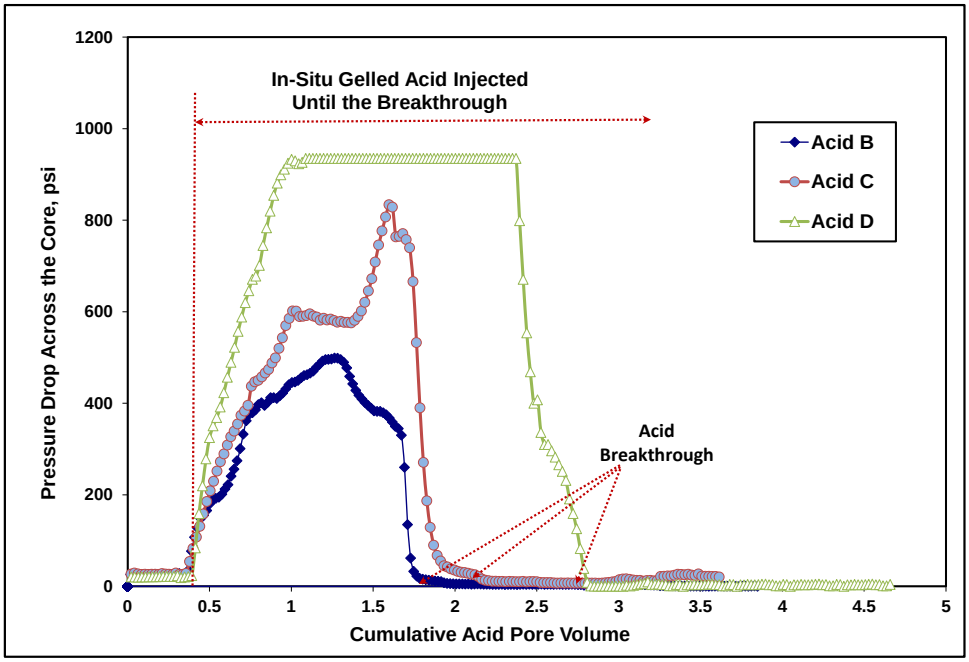

Fig. 5.17: Pressure drop as a function of cumulative volume injected of Acids B, C, and D at injection rate of 10 cm^3/min and 250^oF.

Table 5.5 summarizes acid injection volumes, wormhole propagation rate, and permeability enhancement for Acids A, B, C, and D. Acid breakthrough was achieved in all the core flood experiments except for the first experiment (Acid A at injection rate of 2 cm^3/min.), where the in-situ gelled acid worked effectively. The permeability of first core was reduced from 80 to 1.8 md. The significant permeability reduction was evidence that the gel was formed inside the core. Permeability enhancement, when Acids B, C, and D were used, is due to the acid breakthrough. Table 5.5 shows the pore volume necessary to breakthrough for each acid system (A, B, C, and D) at 2 and 10 cm^3/min.

Table 5.5: Summary of the core flood results.

Acid	Injection Rate, cm^3/min	Initial Permeability, md	Final Permeability, md
A	2	80	1.8
	10	85	Breakthrough
B	2	75	Breakthrough
	10	73	Breakthrough
C	2	83	Breakthrough
	10	71	Breakthrough
D	2	80	Breakthrough
	10	82	Breakthrough

5.4.6 CT Scan

The eight cores investigated in the core flood experiments were scanned using x-ray to visualize the acid propagation and the wormhole formation. To cover the whole length of each core, twenty eight slices with 2 mm thickness and 5 mm separation between slices were selected. Each slice shows a cross-sectional area of the core sample at different lengths. The collection of these slices in order of the longitudinal direction shows the flow path of the acid inside the core.

Analysis of the obtained images showed a cross-sectional area for each slice along the core length. This enabled us to show the difference in the shape of the wormhole when the four acids were injected at various flow rates. **Fig. 5.18** shows the results from the CT scan for the all tested cores.

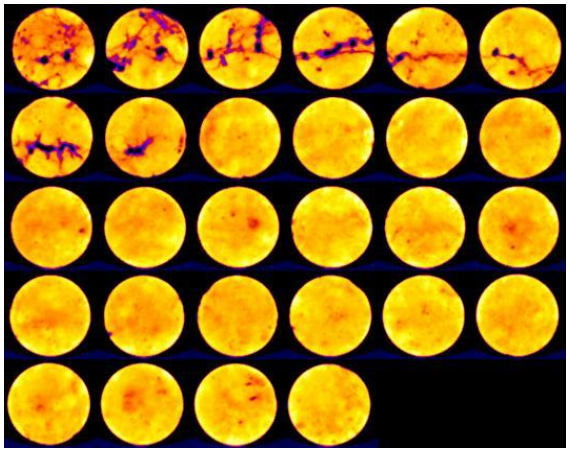

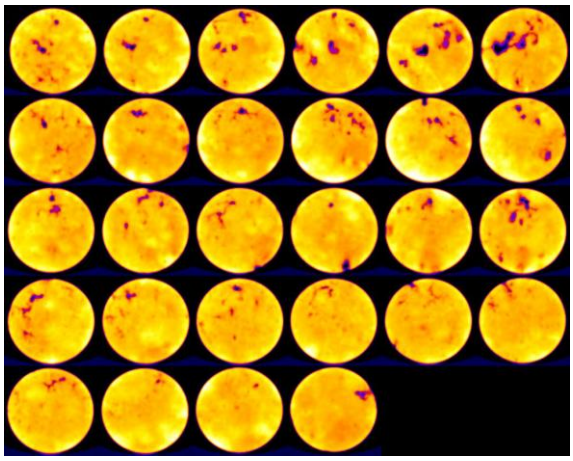

Acid A (0 wt% Formic – 5 wt% HCl): a) 2 cm^3/min | b) 10 cm^3/min

Fig. 5.18: CT scanned images for the tested cores in the core flood study.

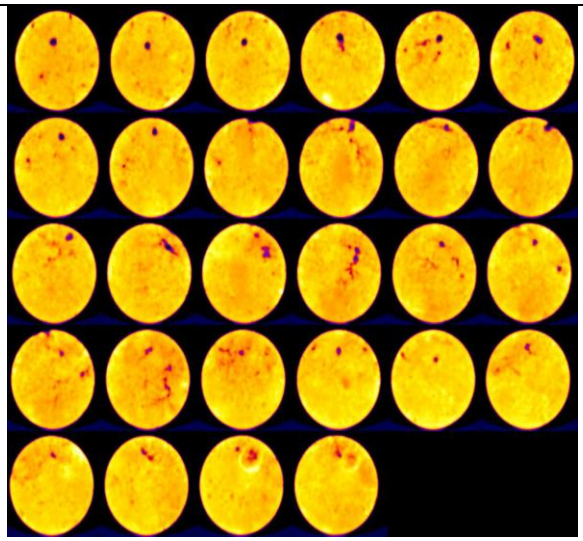

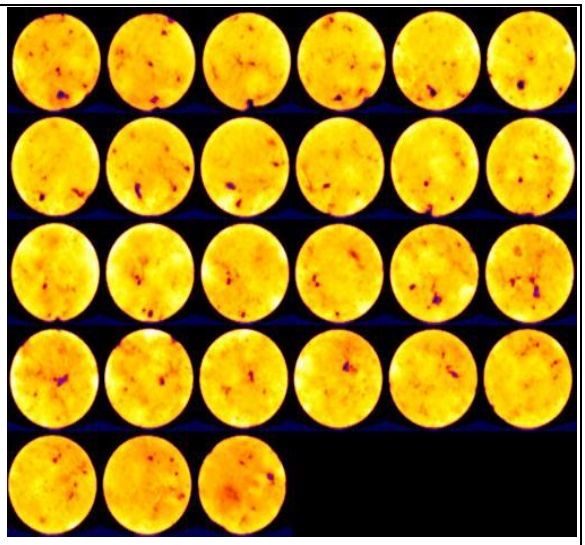

Acid B: (2 wt% Formic – 3.42 wt% HCl: c) 2 cm^3/min

d) 10 cm^3/min

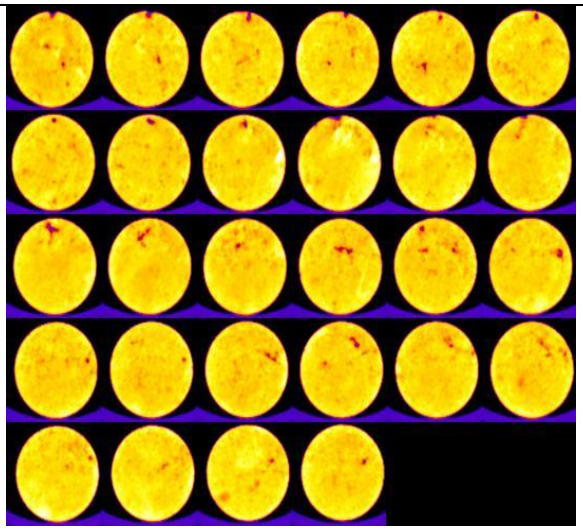

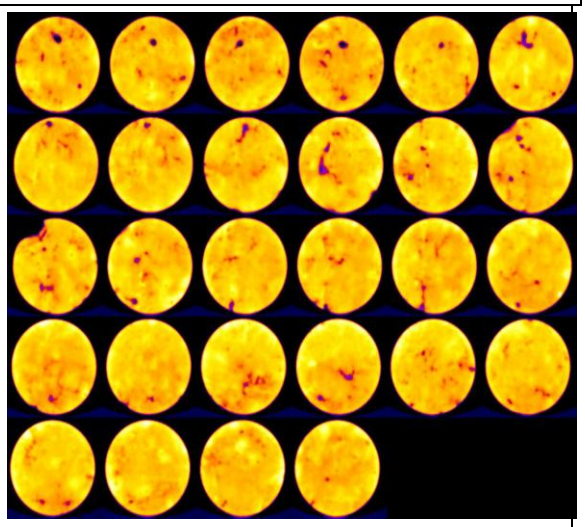

Acid C (4 wt% Formic – 1.83 wt% HCl): e) 2 cm^3/min

f) 10 cm^3/min

Fig. 5.18: CT scanned images for the tested cores in the core flood study, continued.

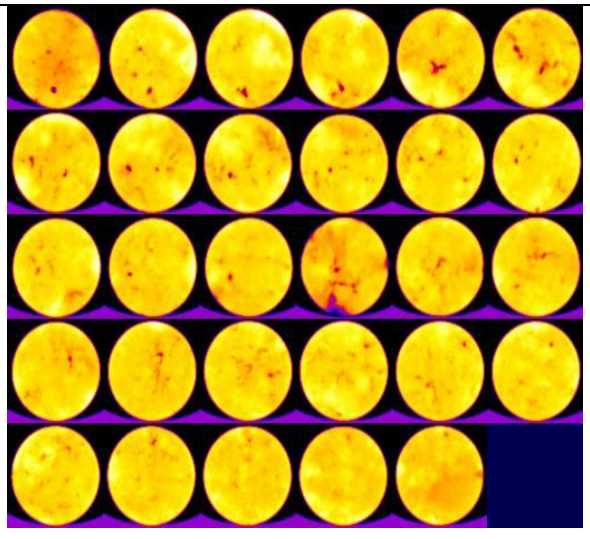

Acid D (6.31 wt% Formic– 0 wt% HCl): g) 2 cm^3/min

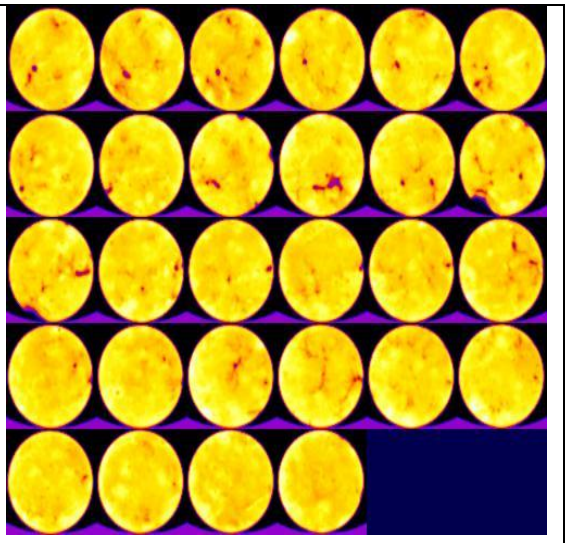

h) 10 cm^3/min

Fig. 5.18: CT scanned images for the tested cores in the core flood study, continued.

In the first experiment in which Acid A (0 wt% formic acid- 5 wt% HCl) was injected at 2 cm^3/min (**Fig. 5.18-a**), the acid did not reach breakthrough. The formed wormhole is then noticed only up to length of 2.4 in. which corresponds to 40% of the total core length. In addition, the images showed that the acid formed several flow paths in the first four slices, which indicates that the acid changed its path. This was mainly due to the gel formation and proves the acid's ability to achieve proper degree of diversion.

Fig. 5.18-b shows the scanned images for Acid A at flow rate of 10 cm^3/min. The figure shows smaller diameter of the wormholes and a breakthrough. This indicates

that the acid did not develop a gel and explains the lower pore volume required to breakthrough.

Figs. 5.18-c and **d** show the scanned images for the experiments in which Acid B was used at a rate 2 and 10 cm^3/min, respectively. At both injection rates, Acid B reached a breakthrough. However at a higher injection rate (10 cm^3/min), the acid consumed 1.54 acid pore volume in comparison to 1.04 at injection rate of 2 cm^3/min. This can be explained by the fact that at higher injection rate, the acid is forced to react over a larger surface area and consume larger amounts of the rock in the radial direction (Fredd and Fogler 1998b). Therefore, it was expected to notice a larger diameter of the wormhole that was created at 10 cm^3/min, and explains the larger pore volume to breakthrough. Acids C and D showed the same behavior as shown in **Figs. 5.18 e-h**. The values of the consumed acid pore volumes are listed in **Table 5.6**.

Table 5.6: Acid pore volumes consumed in each coreflood run.

Acid	Injection Rate, cm^3/min	Acid Volume, PV
A	2	3.00
	10	2.00
B	2	1.04
	10	1.54
C	2	1.23
	10	1.82
D	2	1.82
	10	2.54

6. MEASURING THE REACTION RATE OF LACTIC ACID WITH CALCITE USING THE ROTATING DISK REACTOR*

Lactic acid has been examined in various laboratories and applied in the oil field for acid fracturing, removing drilling fluid filter cake, and functioning as an iron controlling agent. However, the reaction of lactic acid with calcite has not been addressed before. Determination of the reaction rate and the acid diffusion properties is a critical step for successful treatments in matrix acidizing and acid fracturing. Therefore, the objective of this work is to conduct a detailed study on the reaction of lactic acid with calcite. Mass transfer and reaction kinetics are reported for lactic acid-calcite system for this reaction using the rotating disk apparatus.

Core samples of 1.5 in. diameter and 1 in. length were cut from Indiana limestone and were used in the reaction rate experiments. The effect of lactic acid concentration (1, 5, and 10 wt%), temperature (80-250^{o}F), disk rotational speed (100-1800 rpm), and different inorganic salts on the reaction rate was investigated. The diffusion coefficient of 5 wt% lactic acid was determined at low disk rotational speeds and reported at 80, 200, and 250^{o}F. The reaction rate, measured at 1500 rpm over a temperature range from 80 to 250^{o}F was fitted to a power-law rate expression.

---

* Reprinted with permission from "Measuring the Reaction Rate of Lactic Acid with Calcite Using the Rotating Disk Apparatus" by A.I. Rabie, and H.A. Nasr-El-Din, 2011. SPE Paper 140167 presented at the SPE Middle East Oil and Gas Show and Conference held in Manama, Bahrain, 20–23 March.

The activation energy and the rate constant at 80, 150, 200, and 250^{o}F for the reaction of lactic acid with Indiana limestone were reported.

The reaction of lactic acid with calcite was controlled by mass transfer at low disk rotational speeds (up to 500 rpm) and surface reaction limited at higher speeds. The diffusion coefficient increased with increasing temperature. The reaction order was reported to be 0.8225, 0.667, 0.726, and 0.727 at temperatures of 80, 150, 200, and 250°F, respectively. The activation energy was determined as 3.018 kJ/gmol. The presence of other ions such as (Ca, Mg, and sulphate) reduced the reaction rate, which is most likely due to the reduction in the concentration gradient of the product (calcium lactate). The reduction in the concentration gradient will cause a lower rate of diffusion of the calcium generated from the reaction, and hence a lower rate of dissolution.

6.1 Introduction

Lactic acid (α-hydroxypropanoic acid) is an organic acid found in many products of natural origin. Lactic acid is widely used in numerous applications such as the food industry, pharmaceutical applications, and as a natural anti-bacterial agent in disinfecting products. In the polymer industry, lactic acid is the principal building block for polylactic acid (PLA) which has numerous interesting properties including good mechanical properties, thermal stability, processability, and low environmental impact (Carrasco et al. 2010).

In the oil industry, lactic acid was used in acid fracturing, as an iron controlling agent (Smith et al. 1969), and for filter cake removal. In acid fracturing, when the usage of high-reactive acids such as HCl is limited, organic acids, which have lower reactivity, can be used to replace HCl and mitigate the consequences of uncontrolled reaction and corrosion problems at high temperatures. Still et al. (2007) introduced a method that can be applied to overcome these two problems. Acids are pumped in a solid precursor form that is hydrolyzed by water at downhole conditions. The solid precursors included compounds such as the cyclic dimer of lactic acid (lactide) and polylactic acid (PLA). The in-situ generated acid in this case is lactic acid.

Nasr-El-Din et al. (2009) applied this method to acid-fracture a deep high-temperature gas reservoir in a carbonate formation in Saudi Arabia. The application involved the usage of an ester of lactic acid in the form of solid beads as acid precursor, which reacted with water via hydrolysis at bottomhole temperatures to produce lactic acid (Nasr-El-Din et al. 2007).

Lactic acid was also used as filter cake removal agent. One way introduced by Almond et al. (1995) was to generate the acid *in-situ* by utilizing enzymes instead of the bacterial cells that were used previously. The system uses enzymes to catalyze the conversion of suitable substrates to generate organic acids in place. Another way published recently (Willberg and Dismuke 2009; Al-Otaibi et al. 2006; 2008) was to use an ester as precursor for lactic acid that had several advantages over the previous

cleaning techniques. It was also more efficient than using precursors for other organic acids. Several studies have addressed similar techniques (Al-Moajil et al. 2007; 2008; Rostami and Nasr-El-Din 2010).

Although these different applications reveal the potential of lactic acid as a good candidate to accomplish several tasks in the oil industry, the fundamentals of the reaction of lactic acid with calcite were not previously studied.

6.2 Objectives

The objectives of this work are to utilize the usage of the rotating disk apparatus to: (1) identify the different reaction regimes that control the lactic acid-calcite reaction; (2) investigate the effect of disk rotational speed, acid concentration, and temperature on the rate of dissolution; (3) report quantitatively the mass transfer properties and the kinetics of the reaction of lactic acid with calcite at different temperatures; and (4) examine the effect of Na^+, Mg^{2+}, and sulfate ions on the rate of reaction by preparing the acid using seawater.

6.3 Dissociation of Lactic Acid

Lactic acid (LA) is a weak acid which partially dissociates in water resulting in lactate ion ($CH_3CH(OH)CO_2^-$) or (L^-) and H^+. The dissociation reaction can be written as follows:

$$LA \leftrightarrow H^+ + L^-, \qquad K_a = 1.38 \times 10^{-4} \quad \text{..... [6.1]}$$

where K_a is the acid dissociation constant at 25°C (Dean 1999), which can be defined as:

$$K_a = \frac{[H^+][L^-]}{[LA]} \quad \text{..... [6.2]}$$

Eq. 6.2 is most commonly rearranged in a logarithmic form as:

$$pK_a = pH + log\frac{[L^-]}{[LA]} \quad \text{..... [6.3]}$$

where pK_a is equal to $-\log_{10}K_a$. Depending on pH, lactic acid is either present as acid in its non-dissociated form (LA) at low pH or in the ion form (L^-) at higher pH. The pH at which 50% of the acid is dissociated is numerically equal to the pK_a value, which is equal to 3.86 for lactic acid (Dean 1999).

At pH greater than 3.86, the majority of lactic acid will be dissociated and present as lactate. If the pH is below this value, most of the acid will be in the un-ionized form. The percentage of dissociation of a weak acid can be determined by measuring and substituting the solution pH in Eq. 6.3.

In the current study, the concentrations of the lactic acid used were 1, 5, and 10 wt%. At these concentrations, the pH of the live acid at 25^{o}C was measured and was found to be 2.3, 2.2, and 2.12, respectively.

It is worth mentioning that the dissociation constant is an equilibrium constant that depends on temperature. The pKa values of acetic, formic, and lactic acids as function of temperatures are listed in **Table 6.1**, (Dean 1999).

Table 6.1: Lactic acid dissociation constants determined at 80, 150, 200, and 250^{o}F.

	Temperature, °C °F	25	30	35	40	50
		77	86	95	104	122
Acetic Acid	pK_a	4.756	4.757	4.762	4.769	4.787
	% Acid Dissociation	0.419	0.418	0.415	0.412	0.404
Formic Acid	pK_a	3.750	3.752	3.758	3.766	3.782
	% Acid Dissociation	1.33	1.33	1.32	1.30	1.28
Lactic Acid	pK_a	3.86	3.861	3.867	3.873	3.895
	% Acid Dissociation	1.18	1.17	1.16	1.15	1.12

6.4 Reaction Kinetics of Lactic Acid with Calcite

The reaction of calcite with different aqueous solutions has been a subject of interest for many researchers (Lund et al. 1973; 1975; Plummer et al. 1978; Sjoberg and Rickard 1984). Three surface reactions occur simultaneously (Plummer et al. 1978). These reactions include dissolution by hydrogen ion reaction, water reaction, and calcite reaction with carbonic acid:

$$H^+ + CaCO_3 \leftrightarrow Ca^{2+} + HCO_3^- \quad \text{..... [6.4]}$$

$$H_2CO_3 + CaCO_3 \leftrightarrow Ca^{2+} + 2HCO_3^- \quad \text{..... [6.5]}$$

$$H_2O + CaCO_3 \leftrightarrow Ca^{2+} + HCO_3^- + OH^- \quad \text{..... [6.6]}$$

When the partial pressure of CO_2 over the reaction mixture is less than 0.1 atm, the concentration of H_2CO_3 is negligible and the hydrogen ion attack shown by Eq. 6.4 represents the main reaction at low pH. At high pH, Eq. 6.6 represents the dominant reaction of water dissolution. The reaction represented by Eq. 6.5 is considered only when CO_2 partial pressure is > 0.1 atm and the pH is > 5. Because the pH of the reaction of calcite with lactic acid in this study was below 2.3, the main reaction on the calcite surface is described by Eq. 6.4, and the reaction of lactic acid with calcite can be written as follows:

$$LA \leftrightarrow H^+ + L^- \quad \text{..... [6.7]}$$

$$H^+ + CaCO_3 \leftrightarrow Ca^{2+} + HCO_3^- \quad \text{..... [6.8]}$$

$$2L^- + Ca^{2+} \leftrightarrow CaL_2 \quad \text{..... [6.9]}$$

The rate of this surface reaction (R_s) is assumed to be similar to that reported for HCl and other organic acids, namely, a power-law expression as shown in Eq. 6.10

(Lund et al. 1975; Williams et al. 1979; Alkattan et al. 1998; Buijse et al. 2004; Alkhaldi et al. 2010a).

$$R_s = k\,[H_s^+]^n \quad \text{[6.10]}$$

However, in the case of a reaction of lactic acid (a weak acid) Eq. 6.7 should be combined with Eq. 6.10 because the acid is not totally dissociated at the calcite surface and the resultant reaction is reversible. Therefore, the rate expression should consider the backward reaction of weak acid in Eq. 6.8 and it can be written as (Buijse et al. 2004):

$$R_s = k_f[H^+]_s^n - k_b\,[Ca^{2+}]_s^n[\mathrm{HCO_3^-}]_s^n \quad \text{[6.11]}$$

Buijse (2004) stated that for pH values less than 4, the contribution of the backward reaction can be neglected. The concentration of the hydrogen ions on the surface can be related to the total acid concentration in the bulk (C_b) (Alkhaldi et al. 2010b):

$$[H^+]_s = \sqrt{K_a.C_b} \quad \text{[6.12]}$$

Substitution of Eq. 6.12 into Eq. 6.10 results in a final form of the rate expression of the reaction of a weak acid with calcite, Eq. 6.13:

$$R_s = k_f\,[K_a.C_b]^{n/2} = k_r\,[C_b]^{n/2} \quad \text{..... [6.13]}$$

where k_f is the reaction rate constant for the forward reaction shown in Eq. 6.8, and k_r is the apparent reaction constant which is equal to $k_f.K_a^{n/2}$. Eq. 6.13 will be used to study the kinetics of the reaction of 1, 5, and 10 wt% lactic acid with calcite at 80, 150, 200, and 250^{o}F with kinetic parameters reported below.

6.5 Experimental Studies

Core samples from blocks of Indiana limestone were cut into disks with 1.5 in. diameter and 0.65 in. thickness. The procedure reported by Fredd and Fogler (1998) was followed. One surface of each sample was first polished with sand paper then soaked in 0.1N HCl for 30 to 40 minutes, then rinsed thoroughly with deionized water before reaction. This method ensures good reproducibility and eliminates problems associated with preparing the disk surfaces. Samples were saturated under vacuum in water and the weight of the samples were measured before and after saturation. The average porosity was 13.25 vol%. **Table 6.2** gives the dimenssions and the measured porosity of all samples used in the reaction experiments.

Table 6.2: Measured porosity for all samples used in the reaction experiments.

Sample #	Diameter, in.	Thickness, in.	Porosity, vol.%
1	1.50	1.00	13.39
2	1.47	1.01	13.62
3	1.46	1.00	13.39
4	1.46	1.01	13.70
5	1.46	0.98	13.65
6	1.46	1.01	13.52
7	1.46	1.02	12.96
8	1.46	0.86	14.28
9	1.46	0.96	13.50
10	1.47	0.99	13.81
11	1.46	1.00	12.07
12	1.46	0.99	13.28
13	1.47	0.98	13.48
14	1.46	0.98	13.59
15	1.46	0.99	12.84
16	1.47	1.00	13.35
17	1.46	0.99	15.36
18	1.49	0.99	12.82
19	1.46	0.98	13.22
20	1.46	0.81	13.73
21	1.47	0.96	11.89
22	1.46	0.74	13.69
23	1.47	0.98	13.26
24	1.46	0.98	13.28
25	1.46	0.98	13.97

6.6 Results and Discussion

Rotating disk experiments were conducted over a wide range of disk rotational speeds (100-1800 rpm) and in a temperature range of 80-250^{o}F. The calcium concentration of all samples was measured using the Perkin-Elmer atomic absorption instrument. The rate of calcite dissolution is determined from the rate of production of calcium with time and the initial surface area of the disk. The data obtained from the

rotating disk study was used to report the mass transport properties and the reaction kinetics at different temperatures. The reproducibility of data was tested at different temperatures and acid concentrations and is shown in **Fig. 6.1**.

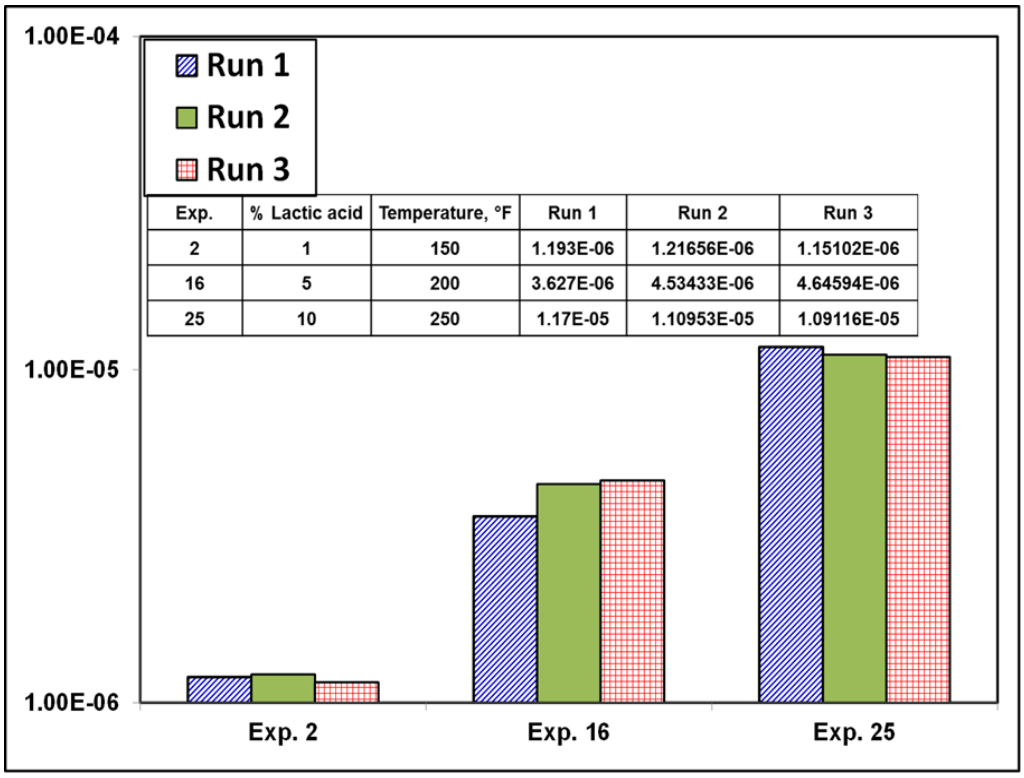

Exp.	% Lactic acid	Temperature, °F	Run 1	Run 2	Run 3
2	1	150	1.193E-06	1.21656E-06	1.15102E-06
16	5	200	3.627E-06	4.53433E-06	4.64594E-06
25	10	250	1.17E-05	1.10953E-05	1.09116E-05

Fig. 6.1: Testing the reproducibility of data for the reaction of lactic acid with Indiana limestone using the rotating disk reactor.

6.6.1 Effect of Disk Rotational Speed on the Dissolution Rate of Lactic Acid with Calcite

The rate of calcite dissolution by 5 wt% (0.56M) lactic acid was measured over a range of disk rotational speeds and temperatures and is shown in **Fig. 6.2**. At 80°F, the data showed a plateau for almost the whole range of disk rotational speeds and the average rate of dissolution in this range was 7.423×10^{-7} gmol/cm^2.s. The data indicates

that at this temperature the reaction of lactic acid is mainly controlled by the kinetics of the surface reaction unless the disk rotational speed is below 500 rpm.

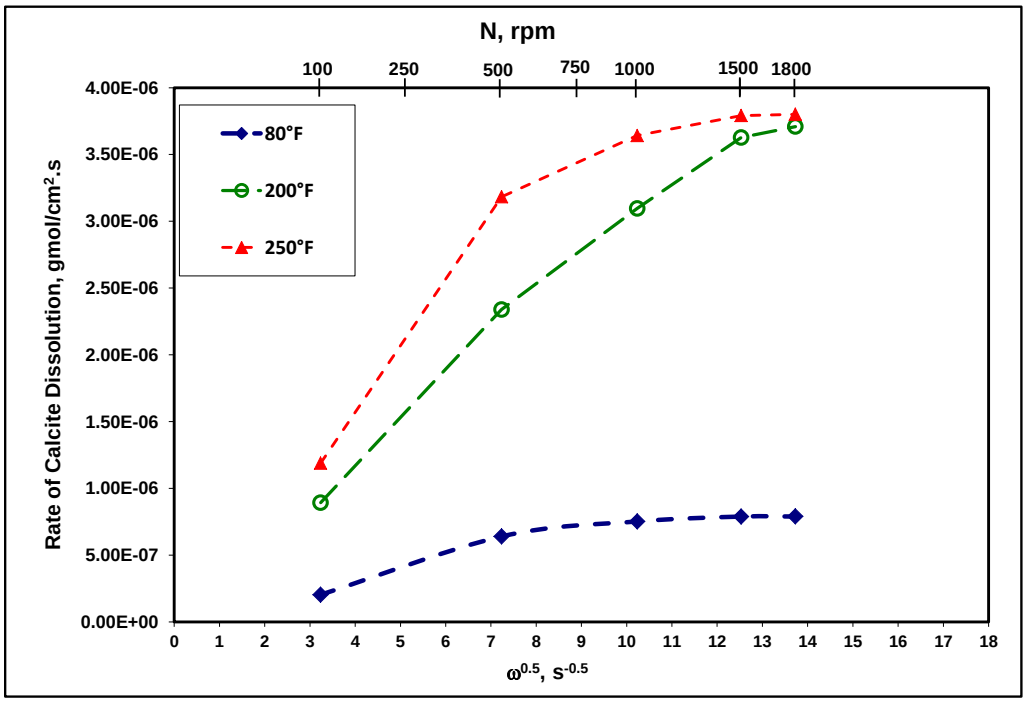

Fig.6.2: Reaction of 5 wt% lactic acid with Indiana limestone at 80, 200, and 250°F.

Increasing the temperature to 200 and 250°F showed a dependence of the rate of dissolution on the disk rotational speed up to 1500 rpm, but the rate of dissolution then started to level off at 1500 rpm. This can be shown alternatively in **Fig. 6.3**, which illustrates the change of the concentration of the produced calcium with time for the reaction of 5 wt% lactic acid at 200°F. An increase in the calcium concentration is noted with increasing the disk rotational speed from 100 to 500, and 1000 rpm. The data points for the reactions at 1500, and 1800 rpm, however, are overlapping indicating that there is no effect of the disk rotational speed on the reaction above 1500 rpm.

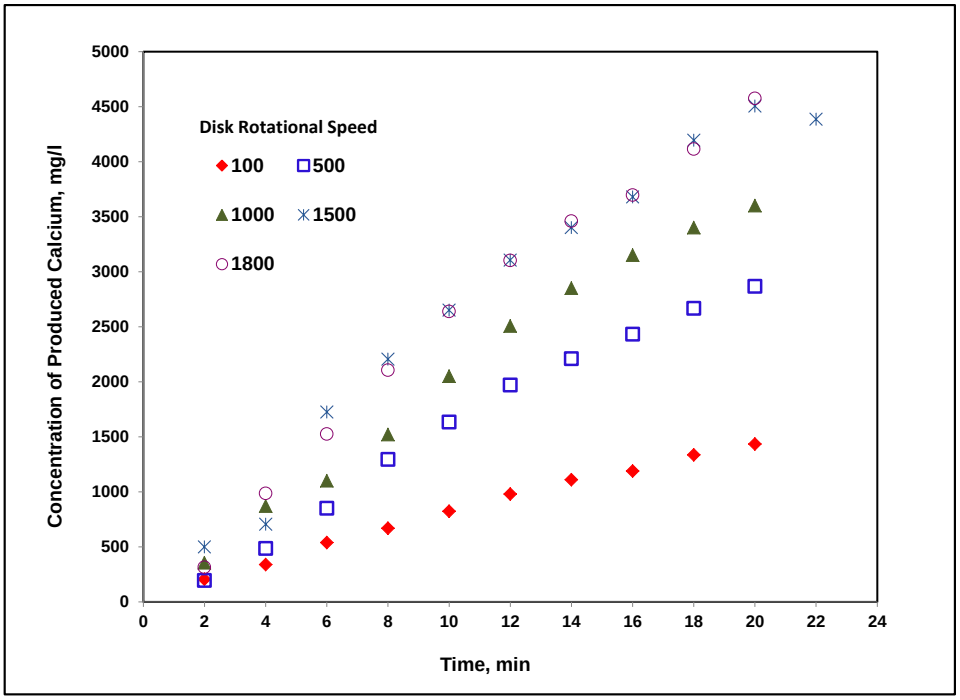

Fig. 6.3: Reaction of 5 wt% lactic acid with Indiana limestone at 200°F.

The results in Figs. 6.2-3 indicate that the reaction is controlled by both mass transfer to the surface and the kinetics of the reversible reaction on the surface. This can be confirmed by determining the acid diffusion at these conditions assuming negligible concentration on the surface using the data in the mass transfer region.

A linearization of the rate dissolution equation in the mass transfer region described in Chapter 4, Eq. 4.3, should yield a straight line with a theoretical slope of ½ if the reaction is controlled by the diffusion to the surface. A plot of the rate of dissolution versus the disk rotational speed on a natural logarithmic scale is shown in **Fig. 6.4** for the reaction of lactic acid at 80, 200, and 250°F.

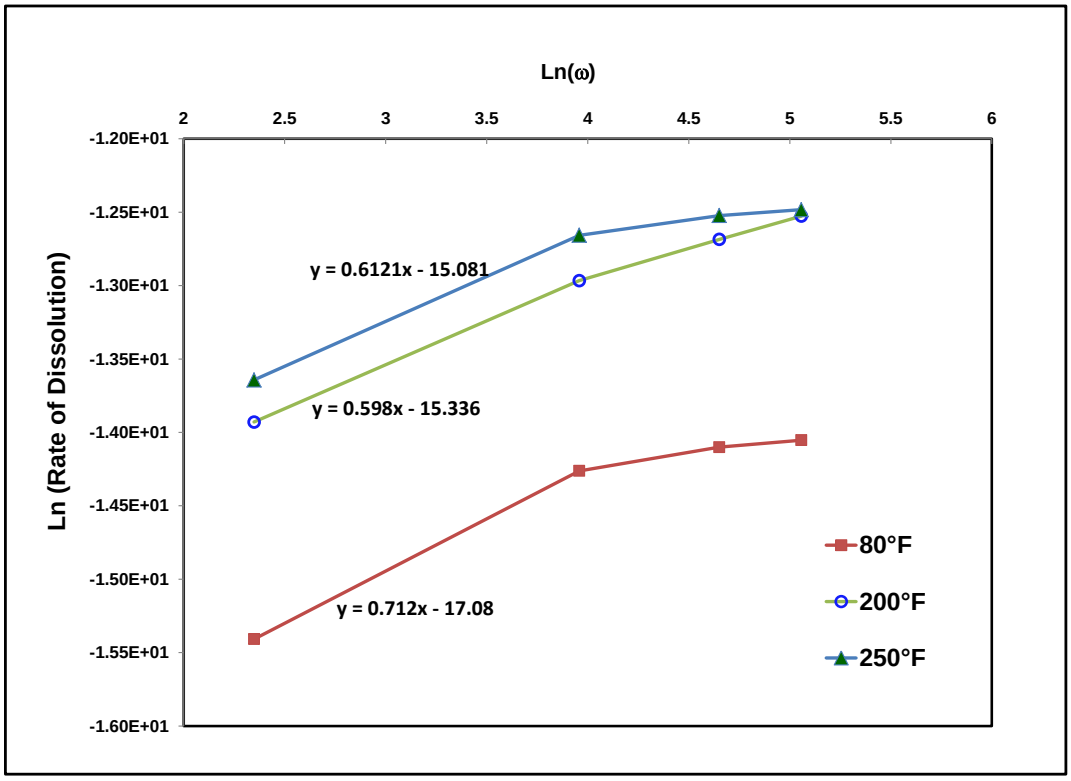

Fig 6.4: Linerization of the rate dissolution data for the reaction of 5 wt% lactic and calcite at 80, 200, and 250^{o}F.

As shown in the figure, the mass transfer is the main controlling mechanism for the reaction of 5 wt% lactic acid at 80°F below 500 rpm in which the slope of the rate of dissolution is 0.712. Therefore, the data points in this range were used to determine the effective diffusivity of the lactic acid at 80°F using Eq. 4.3 and the density and the viscosity of solutions of 5 wt% lactic acids at 80°F. The effective diffusivity was calculated at this temperature and was found to be 1.23×10^{-6} cm^2/s.

A similar approach was applied to the data obtained for the reaction of 5 wt% lactic acid with calcite at 200 and 250^{o}F. The data shown in Fig. 6.4 is consistent with a slope of 0.59 and 0.61, respectively, which gave an effective diffusivity of 5 wt% lactic acid at 200 and 250°F as 8.915×10^{-6} and 1.45×10^{-5} cm^2/s, respectively.

The acid diffusivity data were fitted to the best Arrhenius relation and the result is shown in **Fig. 6.5**. The data are consistent with activation energy of 6.19 kcal/mol that is higher than the reported value of 3-4 kcal for the reactions that are solely controlled by mass transfer of the reactant to the surface (Sjoberg and Rickard 1984; Fredd and Fogler 1998a) indicating the mutual influence of both mass transfer of the reactant and the products and the kinetics of the reversible reaction on the surface. Similar results were obtained by Fredd and Fogler (1998a) for the reaction of acetic acid with calcite.

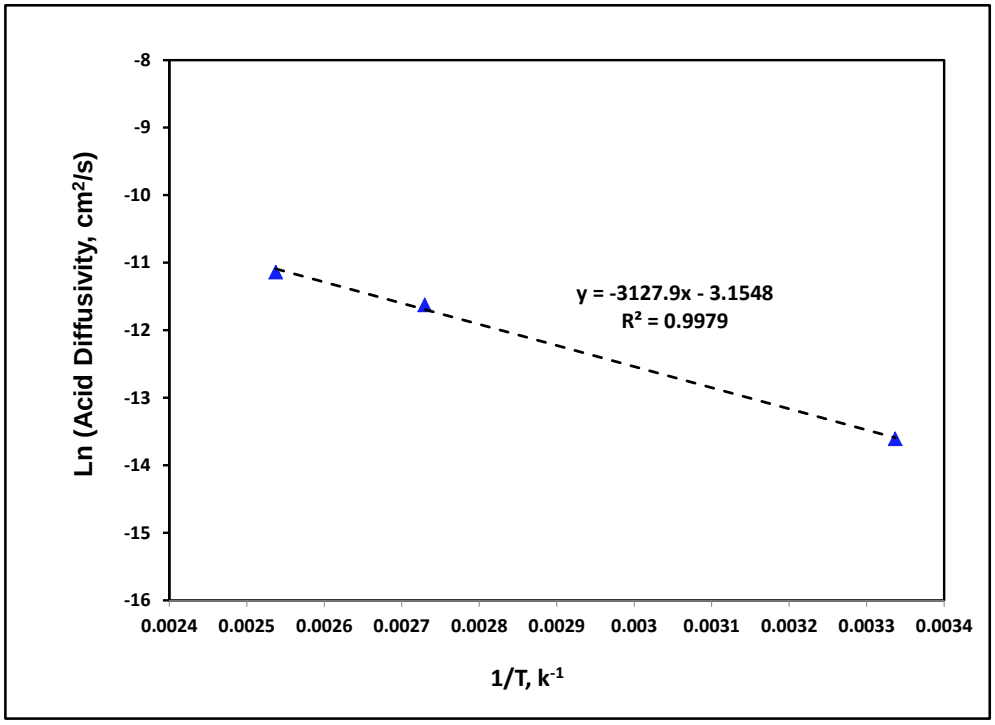

Fig 6.5: Effective acid diffusivity as a function of temperature where the data are fitted to the best of Arrhenius realtion.

Arrhenius equation was first proposed by Van Hoff in 1884 to correlate the dependence of the reaction rate constant on temperature. Five years later, Swedish chemist Svante Arrhenius provided a physical justification and interpretation. Arrhenius argued that for reactants to transform into products, they must first acquire a minimum amount of energy, called the activation energy E_a.

From a mathematical point of view and at an absolute temperature T, the fraction of molecules that have a kinetic energy greater than E_a can be calculated from statistical mechanics. The concept of activation energy explains the exponential nature of the relationship.

The calculations for reaction rate constants involve an energy averaging over a Maxwell-Boltzmann distribution with E_a as lower bound and take a final form of incomplete gamma functions, which turn out to be proportional to $e^{\frac{-Ea}{RT}}$.

Physically, the interpretation of the Arrhenius relation depends on the collision theory which was developed by Max Trautz and William Lewis in the years 1916-18. In this theory, the suitable particles of the reactant hit with each other. Only a certain percentage of the sum of the collisions causes noticeable or significant chemical change; these successful changes are called successful collisions. The successful collisions have enough energy, also known as activation energy, at the moment of impact to break the preexisting bonds and form all new bonds. This results in the products of the reaction.

Increasing the concentration of the reactant particles or raising the temperature, results in more collisions and more successful collisions, and therefore, increases the rate of reaction and leads to an expression very similar to the Arrhenius equation.

Many researchers have also used the Arrhenius relation to fit other physical and chemical processes that are showing significant dependence on temperature such acid diffusion, population of crystal vacancies, and creep rates. Perhaps the reason that the diffusivity can also mathematically described by the Arrhenius relation is the similarity of the basic physical phenomena that leads to the chemical reaction or the flux of the

diffusive particles. The random collision was explained in case of chemical reaction in the preceding paragraph, and the same phenomenon was proposed for the molecular diffusion.

As shown in **Fig. 6.6**, initially there are solute molecules on the left side of the red barrier. When the barrier is removed, solute molecules diffuse to fill the whole container. The movement of the particles due to the difference in the concentration between the two chambers is associated with particle-to-particle collisions that lead to the final state of equilibrium when the molecules fill the whole chamber, which is known as "random walk" theory and therefore, molecular diffusion is mathematically described as a function of the mean free path (the path that molecules are taking before they collide with each other) and the velocity as follows:

$$D = \frac{1}{3} l v \quad \text{..... [6.14]}$$

Where the mean free bath and the velocity are defined, in gas diffusion, as follows:

$$l = \frac{k_B T}{\sqrt{2}\,\pi\, d^2\, P} \quad \text{..... [6.15]}$$

$$v = \sqrt{\frac{8\, k_B T}{\pi\, m}} \quad \text{..... [6.16]}$$

Where:

k_B: Boltzmann constant, J K^{-1}

T: Temperature, K

d: Particle diameter, m

P: Pressure, N/m^2

m: Particle mass, kg

The effect of particle collisions is more pronounced when the diffusing molecules exist initially at relatively high concentration, which is referred to as "collective diffusion". In that case, high concentration is associated with more molecular density and hence, higher number of collisions and higher diffusion coefficient.

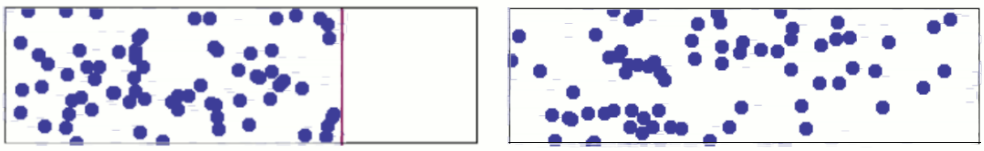

a) Before diffusion b) After diffusion

Fig. 6.6: Particle collisions lead to molecular diffusion.

Another case in which collision is controlling the diffusivity is the case of gas or liquid diffusing through small pores (such as internal pores in a catalyst) in which the length of the pore is comparable to (or smaller than) the mean free bath of the particles as shown in **Fig. 6.7**. This diffusion is known as Knudsen diffusivity and the diffusion coefficient is defined as:

$$D_{KA} = \frac{d_{pore}}{3}\sqrt{\frac{8\,k_B N T}{\pi\,M_A}} \quad \text{..... [6.17]}$$

Where:

d_{pore}	Pore diameter, m
k_B:	Boltzmann constant, J K^{-1}
N	Avogadro number, (6.023E23 molecules/mol)
T:	Temperature, K
M_A	Molecular weight of the diffusing particles

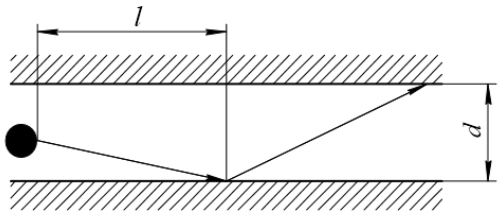

Fig 6.7: Schematic diagram for a condition in which Knudsen diffusivity is applied.

The discussion mentioned above show the physical basis for fitting the acid diffusivity for Arrhenius correlation. However, other correlations were reported for diffusion in liquids as well. Wilke and Chang (1955) proposed another correlation based on data published for 251 solute-solvent systems. The effect of the solute, solvent and temperature was described by the following correlation:

$$D = 7.4 \times 10^{-8} \frac{T \times (xM)^{\frac{1}{2}}}{\mu \times V^{0.6}} \quad \text{..... [6.18]}$$

Where:

D	Diffusion coefficient, cm^2/s
x:	Solvent association parameter, - (= 2.6 for water)

M Solvent molecular weight

μ: Viscosity of solution, cP

V Molecular volume of solute at normal boiling point, $cm^3/gmol$

Wilke and Change proposed fitting the data to a log-log plot between $(\frac{D}{T} \times 10^8)$ and $\frac{\mu \times V^{0.6}}{(M)^{\frac{1}{2}}}$, which results in a straight line in which increasing the parameter on the x-axis should yield decreasing in the y-axis parameter.

Diffusivity data for 5 wt% lactic acid in the mass transfer region was fitted as mentioned by Wilke and Change and the calculation is shown in **Table 6.3**. The data showed very good agreement with the proposed correlation as shown in **Fig. 6.8**.

Table 6.3: Calculations necessary to fit the diffusivity data for 5 wt% lactic acid to Wilke and Change Correlation.

x (water) =		2.6	V, $cm^3/gmol$ =	1786	M (5 wt% lactic acid) =	17.14
t, °c	t, °F	T, K	D, cm^2/s	LHS (D/T)*10^8	viscosity, cp	RHS
26.66667	80	299.6	1.23E-06	0.4105474	0.89	11.91316
93.33333	200	366.3	8.92E-06	2.43516244	0.27	3.614103
121.1111	250	394.1	1.45E-05	3.67926922	0.21	2.810969

The diffusivity of 5 wt% of lactic acid was previously fitted to Arrhenius relation and showed also a good agreement. Accordingly, more data point might be required to reach a unique correlation for acid diffusivity. It is also noted here that using Arrhenius correlation requires the knowledge of only one variable, which is the temperature, while

using the Wilke and Change correlation requires the knowledge of the temperature, solute molecular volume, solvent molecular weight, and the solution viscosity.

It is also interesting to remember that the solution viscosity is also a strong function of temperature and if the final form approaches exponential-like function, this will explain why both correlations were able to fit the data.

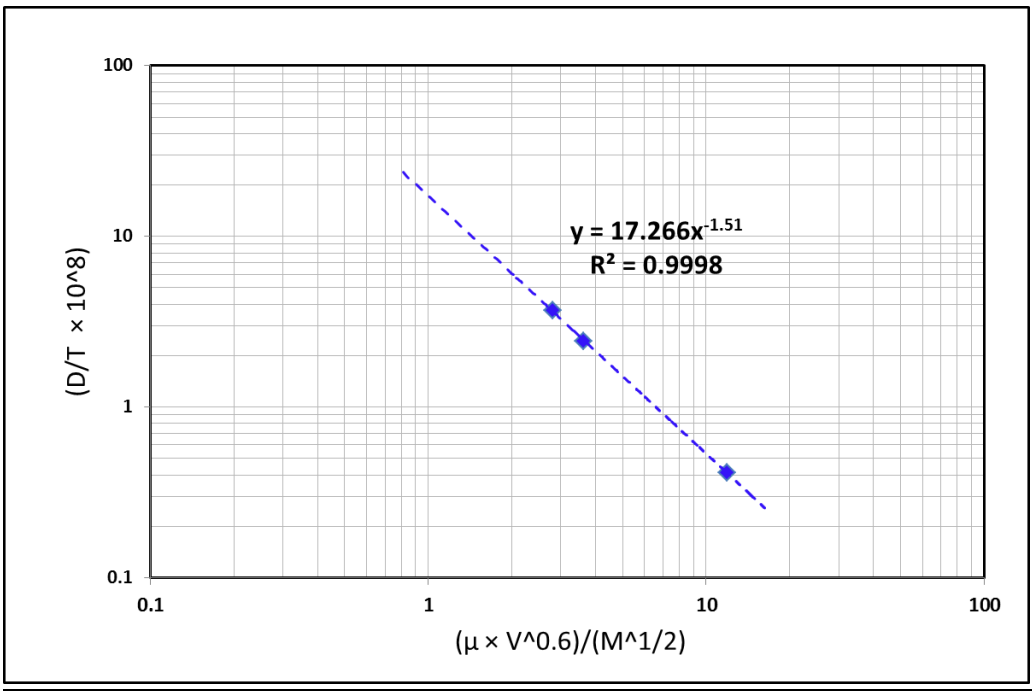

Fig. 6.8: Fitting the diffusivity data for 5 wt% lactic acid to the correlation proposed by Wilke and Change 1995.

The assumption of neglected acid concentration on the surface was then investigated. A linear regression method was used to determine the acid diffusivity (D) and the acid concentration on the surface (C_s). At each temperature, the experimental rate data as a function of the disk rotational speed was fitted to the mass flux equation, Eq. 6.14, and an Excel solver was used to determine the diffusivity and the acid concentration on the surface so the data matches the equation.

$$R_{MT} = \frac{0.60248(Sc^{-2/3})(\sqrt{\upsilon})(C_b - C_s)}{1+0.2980(Sc^{-1/3})+0.1451(Sc^{-2/3})}\ \omega^{1/2} \quad \text{..... [6.19]}$$

Only the data that fall in the mass transfer region was used for this regression (i.e. the data that fits a straight line if the rate is plotted vs. the square root of the disk rotational speed). The analysis showed that C_s is around 10e-6 gmol/cm^3. The acid diffusivity that was calculated from this analysis is compared to that previously calculated assuming a negligible concentration on the surface. A comparison is shown in **Table 6.4**. This analysis confirms that for the reaction of 5 wt% lactic acid at 200 and 250°F, the assumption of neglecting the acid concentration on the surface is valid.

Table 6.4: Investigating the assumption of negligible acid concentration on the rock surface on determining the acid diffusivity.

T, °F	D, cm2/s	D*,cm2/s
200	8.92E-06	8.50E-06
250	1.45E-05	1.50E-05

D*: Diffusivity calculated assuming negligible surface concentration

A comparison between the diffusivity of the 5 wt% lactic acids at 80, 200 and 250^{o}F with previously published data for HCl and different types of organic acids is listed in **Table 6.4.** The diffusivity of 5 wt% lactic acid is the lowest at room temperature when compared with all other acids including acetic and citric acids at the same acid strength. Increasing the temperature to 200, and 250^{o}F increases the acid diffusivity as it enhances the ion mobility. However, the values of the diffusion coefficients of 5 wt% lactic acid at 200 and 250^{o}F are less by almost one order of magnitude than the reported values for HCl with the same molar strength.

Table 6.5: Comparison between the diffusivity of the 5 wt% lactic acid at 200 and 250^{o}F with previously published data for weak acids and HCl.

Type of Acid	Concentration, M	Temperature, ^{o}C	Diffusivity, cm^2/s	Ref.
HCl	0.50 M	25^{o}C	3.6x10^{-5}	Kung (1998)
	0.56 M	93.33^{o}C (200^{o}F)	8.3x10^{-5}	Conway (1999)
	0.56 M	121^{o}C (250^{o}F)	1.1x10^{-4}	Conway (1999)
Formic Acid	0.5 M	25^{o}C	3.0x10^{-5}	Kung (1998)
Acetic Acid	0.5 M	25^{o}C	1.15x10^{-5}	Vitagliano and Lyons (1956)
Citric Acid	0.25 M	25^{o}C	6.46x10^{-6}	Muller and Stockes (1957)
	0.26 M (5 wt%)	40^{o}C	6.8x10^{-6}	Alkhaldi (2010b)

	0.39 M (7.5 wt%)	50^{o}C	4.5x10^{-6}	Alkhaldi (2010b)
Lactic Acid	0.56 M (5 wt%)	26.67^{o}C (80^{o}F)	1.23x10^{-6}	Current Study
	0.56 M (5 wt%)	93.33^{o}C (200^{o}F)	8.92x10^{-6}	Current Study
	0.56 M (5 wt%)	121^{o}C (250^{o}F)	1.45x10^{-5}	Current Study

It is worth mentioning that for lactic acid at 5 wt% and temperatures 80-250^{o}F, the acid diffusion coefficient determined from this study represent an effective diffusivity that lump the diffusion of H^{+}, L^{-}, and LA at equilibrium.

6.6.2 Kinetic Study of the Reaction of Lactic Acid with Calcite

The results obtained in Fig. 6.2 shows that the kinetics study (when the rate of dissolution is independent on the disk rotational speed) can be conducted using the rate of dissolution obtained at rotational speeds of 1500 rpm or higher. The kinetics of the surface reaction of lactic with calcite can be studied by measuring the dissolution rate as function of the temperature and acid concentration in the bulk solution.

Eq. 6.13 gives the rate of dissolution as a function of the initial acid concentration in the bulk solution (C_b) and the temperature. Although not explicitly shown in the equation, the effect of temperature on the rate of dissolution can be understood from the effect of temperature on the reaction rate constant. This is described by Arrhenius equation as follows:

$$k_f = A \cdot e^{-E_a/RT} \quad \text{..... [6.15]}$$

Increasing temperature significantly increases the rate of reaction due to the exponential relation shown above. The rate of dissolution was measured at a disk rotational speed of 1500 rpm and for 1, 5, and 10 wt% lactic acid over a temperature range of 80-250^{o}F. The effect of the initial acid concentration is shown in **Fig. 6.6**.

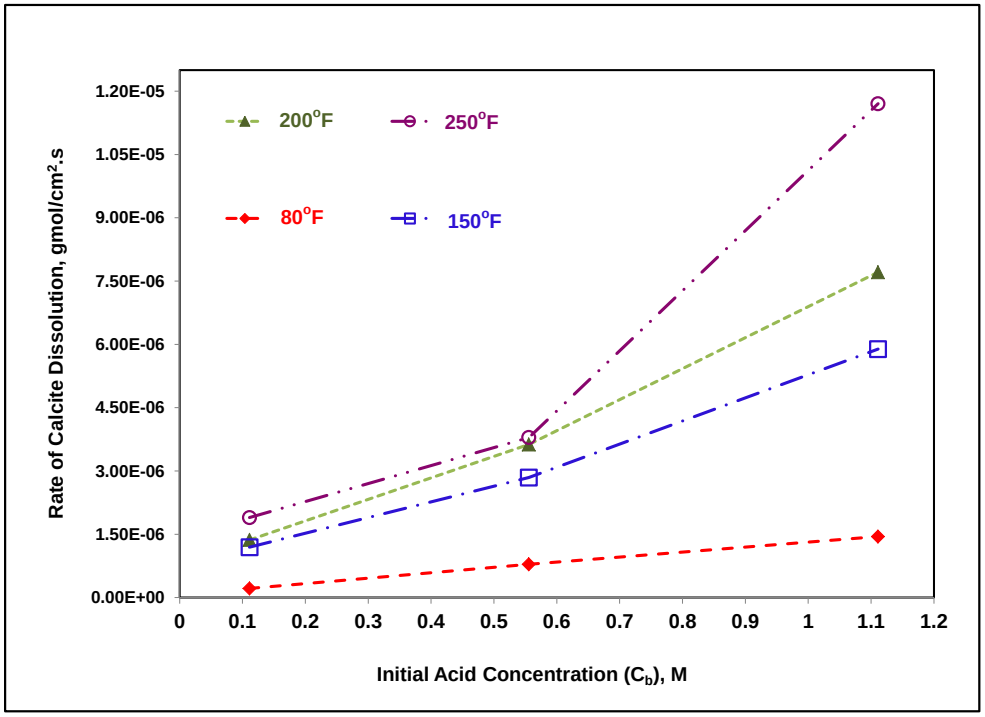

Fig 6.9: Effect of the initial acid concentration on the rate of dissolution for the reaction of lactic acid and calcite at temperature range of 80-250^{o}F.

Increasing the acid concentration increased the rate of dissolution and the relation is not linear in general, unless the reaction is first order. Linearization of Eq. 6.13 can be written in the following form:

$$Ln(R_s) = Ln(k_r) + \left(\frac{n}{2}\right) Ln(C_b) \quad \text{..... [6.16]}$$

A plot of the rate of dissolution versus the acid concentration on a natural log scale should yield a straight line, the slope of which represents the reaction order that is equal to n/2, while the reaction rate constant (k_f) can be determined from the intercept. **Fig 6.7** shows the linearization of the data obtained for the reaction of 1, 5, and 10 wt% of lactic acid with Indiana limestone at 80^{o}F. For consistency of units, the acid concentration is used on a molar basis. The data is consistent with an order of reaction of 0.8225 (n=1.645) and a forward reaction constant of 0.571 gmol$^{0.1775}$.cm$^{0.4675}$.s^{-1}.

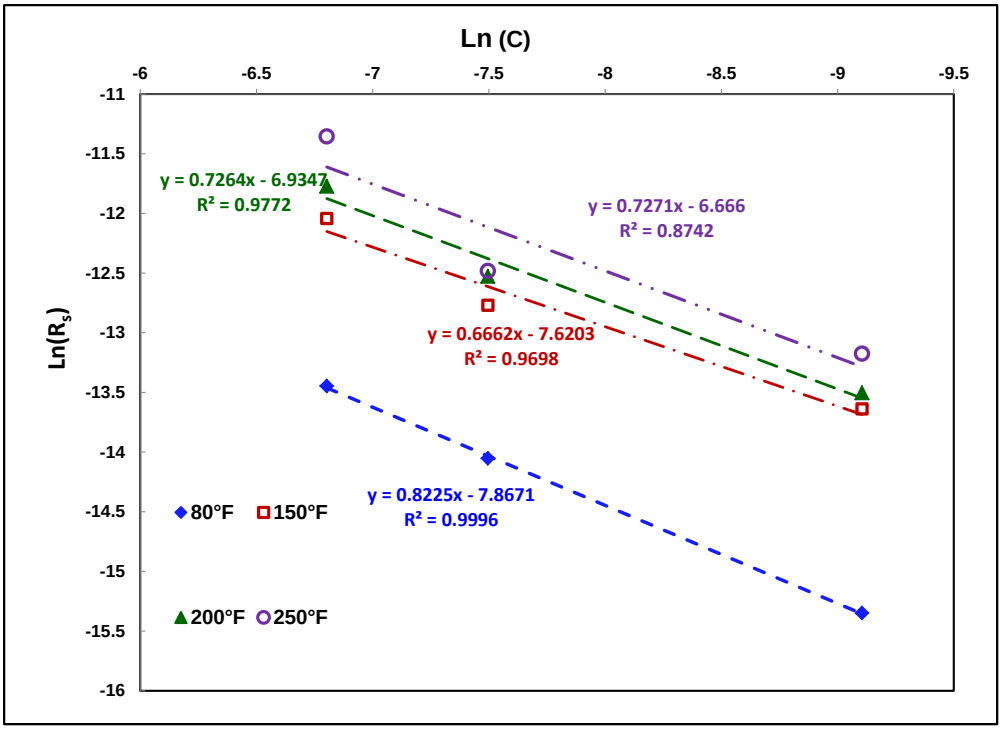

Fig 6.10: Kinetic data for the reaction of lactic acid with Indiana limestone at 80, 150, 200, and 250^{o}F.

Data obtained for the reaction of lactic acid at 150, 200, and 250^{o}F was treated in a similar approach and the results are shown in Fig. 6**.** The numerical values for the reaction order, the reaction rate constant, and the dissociation constant over a temperature range of 80-250^{o}F are listed in **Table 6.5**.

Table 6.6: Data for the reaction kinetics and the dissociation constant of lactic acid with Indiana limestone over a temperature range of 80-250^{o}F.

T,^{o}F	Slope	n	Intercept	K_a	k_f, $gmol^{(1-n/2)}/cm^{(2-3n/2)}.s$
80	0.826	1.645	-7.867	1.387E-04	0.571
150	0.666	1.334	-6.420	1.272E-04	0.646
200	0.726	1.452	-6.935	1.197E-04	0.687
250	0.727	1.454	-6.866	1.137E-04	0.773

The results showed an increase in the reaction rate constant and a decrease in the dissociation constant with increasing temperature. The effect of temperature on the rate of dissolution is shown in **Fig. 6.8** for 1 wt% lactic acid which clearly indicates that the rate increases with increasing temperature. A similar effect was noted at lactic acid concentrations of 5, and 10 wt% as shown in Fig. 6.7.

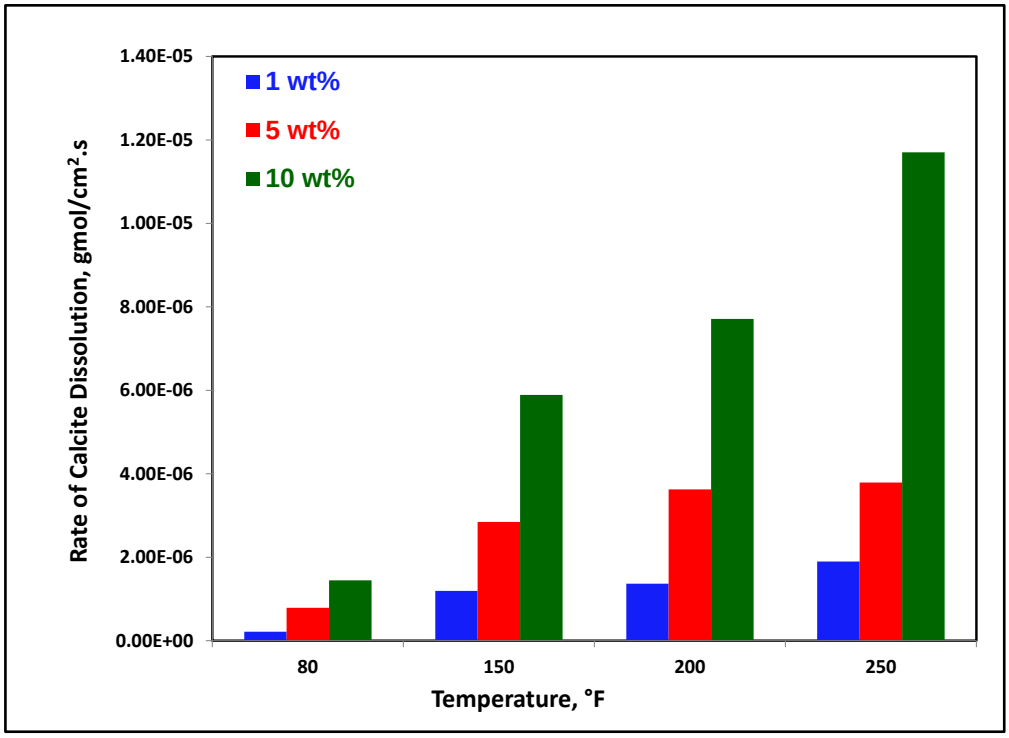

Fig 6.11: Effect of temperature on the reaction rate of 1, 5, and 10 wt% lactic acid with Indian limestone at 1500 rpm.

The activation energy of the lactic acid reaction with Indiana limestone is determined by plotting the log of the reaction rate constant (k_f) versus the reciprocal of temperature as shown in **Fig. 6.9**. The data obtained from the figure is consistent with a pre-exponential constant (A) equals to 1.89 $gmol^{(1-n/2)}/cm^{(2-3n/2)}$.s and activation energy equals to 3.018 kJ/gmol. Few experiments were conducted to study the reaction of lactic acid with dolomite as well. Silurian dolomite cores were used for the reaction of 5 wt% lactic acid at 1500 rpm over a temperature range of 80-250°F as shown in **Fig. 6.10**.

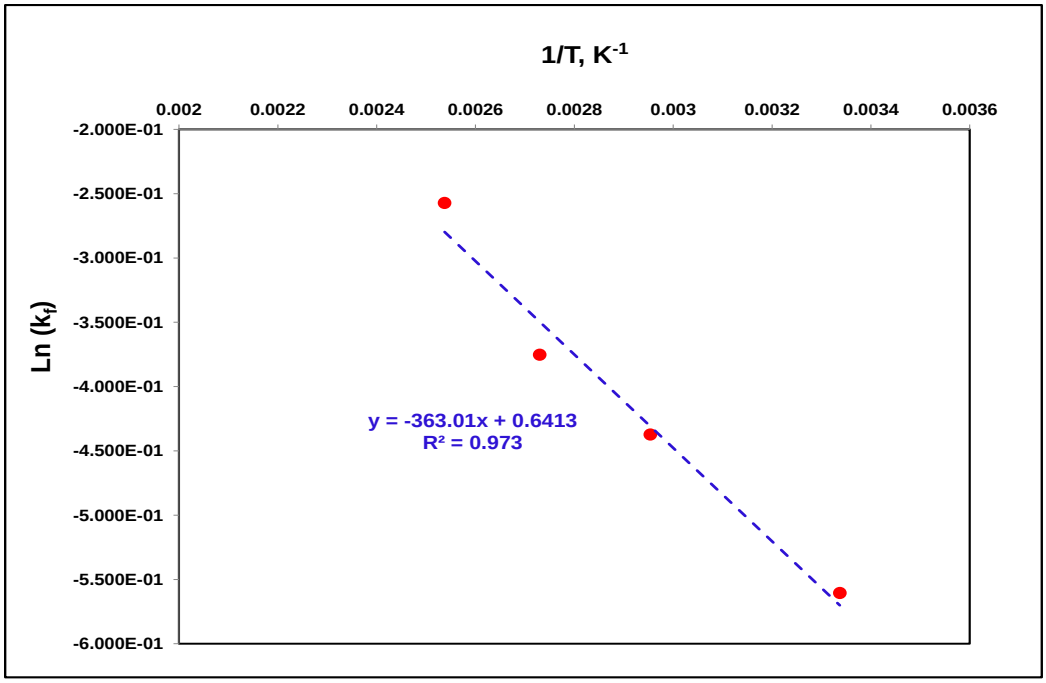

Fig 6.12: Reaction rate constant (k_f) as a function of temperature for the reaction between lactic acid and Indiana limestone.

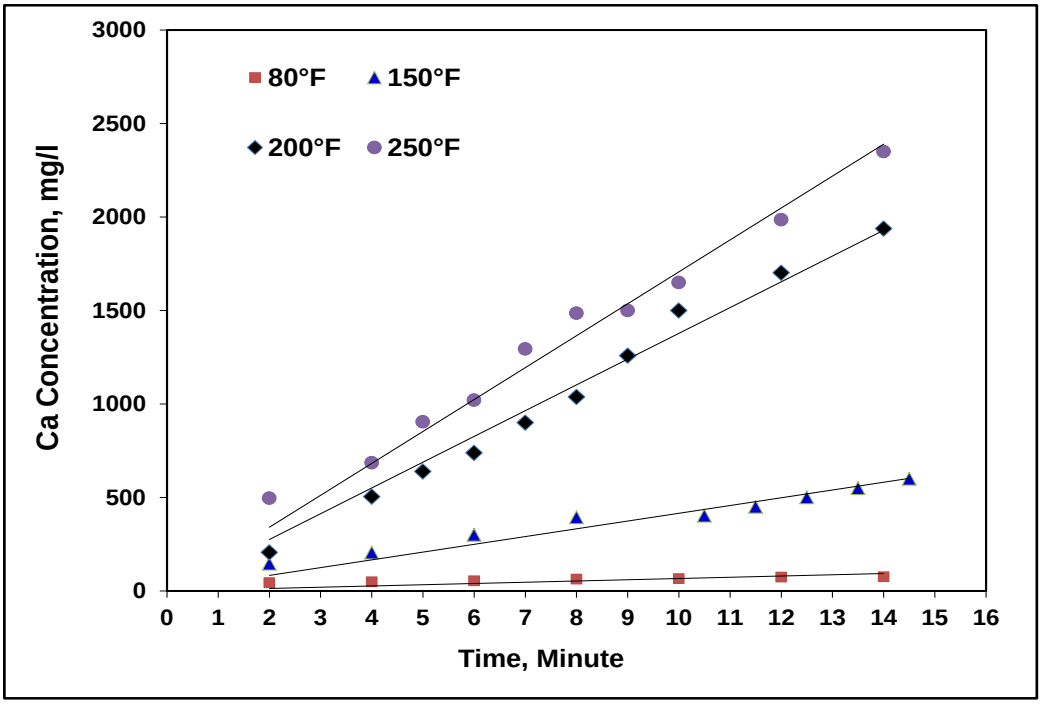

Fig. 6.13: Reaction of 5 wt% lactic acid with dolomite at 1500 rpm.

Increasing the temperature increased the rate of reaction and a significant difference between the reaction of lactic acid with calcite and dolomite was noticed at lower temperatures (80 and 150°F). The difference becomes smaller at higher temperatures (200 and 250°F), **Fig. 6.11**.

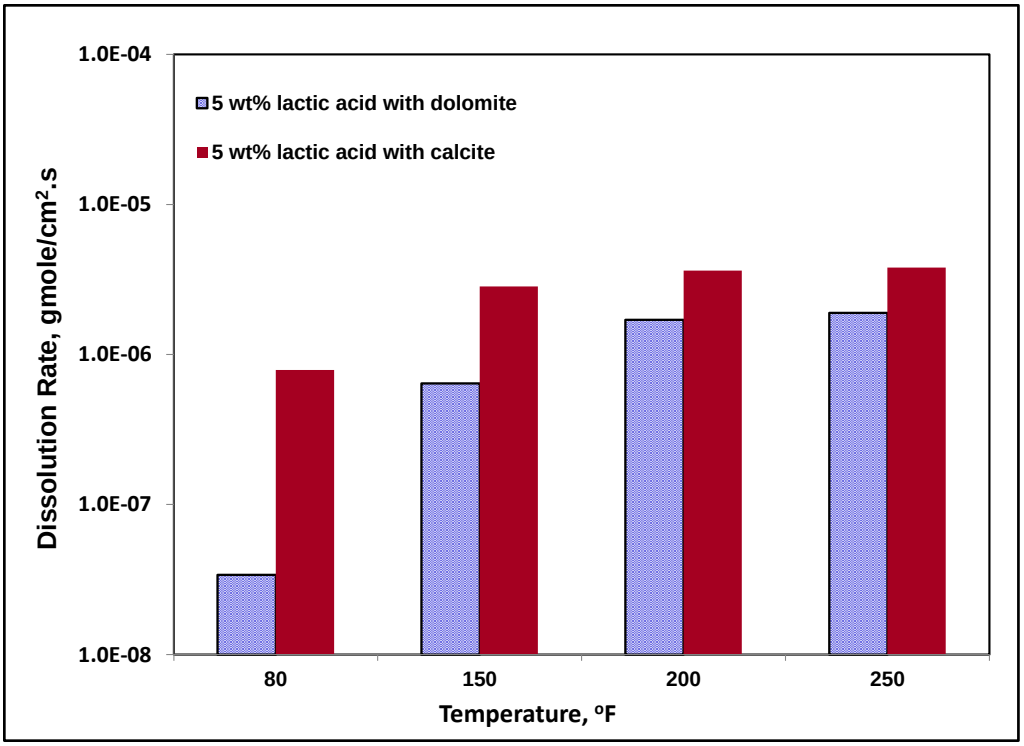

Fig 6.14: Effect of temperature on the reaction rate 5 wt% lactic acid with Indiana limestone and dolomite at 1500 rpm.

6.6.3 Effect of Presence of Na+, Mg2+, and Sulfate Ions on the Rate of Dissolution

Different factors may affect the rate of dissolution of a mineral with acids including temperature, acid concentration, and the disk rotational speed as discussed above. However, the high salinity of the water used to prepare the acid may affect the rate of reaction as well. This is mainly because of the hindering effect that these additional ions can cause on the acid mobility and diffusivity. In the current study, the effect of Na^{+}, $Mg^{2+,}$ and sulfate was investigated by preparing the acid in seawater that has a composition typical of that presents in the Gulf area in Saudi Arabia (Ba-Taweel et al. 2006).

Two conditions were selected to illustrate the effect of the presence of ions on the rate of dissolution; one at low temperature (80^{o}F) with low rotational speed (500 rpm), and the other was at high temperature (250^{o}F) and high disk rotational speed (1500 rpm). The two experiments were conducted for the same acid concentration of 5 wt% lactic acid.

Fig. 6.12 shows the change of the calcium concentration with time for the first case (80^{o}F and 500 rpm). The data obtained for the reaction of 5 wt% lactic acid prepared in deionized water was added for comparison. Fig. 6.12 shows a lower rate of calcium ion generation when the acid was prepared in seawater. The same comparison is shown in Fig. 6.12 for the reaction of 5 wt% lactic acid at 250^{o}F and 1500 rpm. It is

worth mentioning that because the seawater initially has a significant calcium concentration, the figures were plotted on a basis of free calcium.

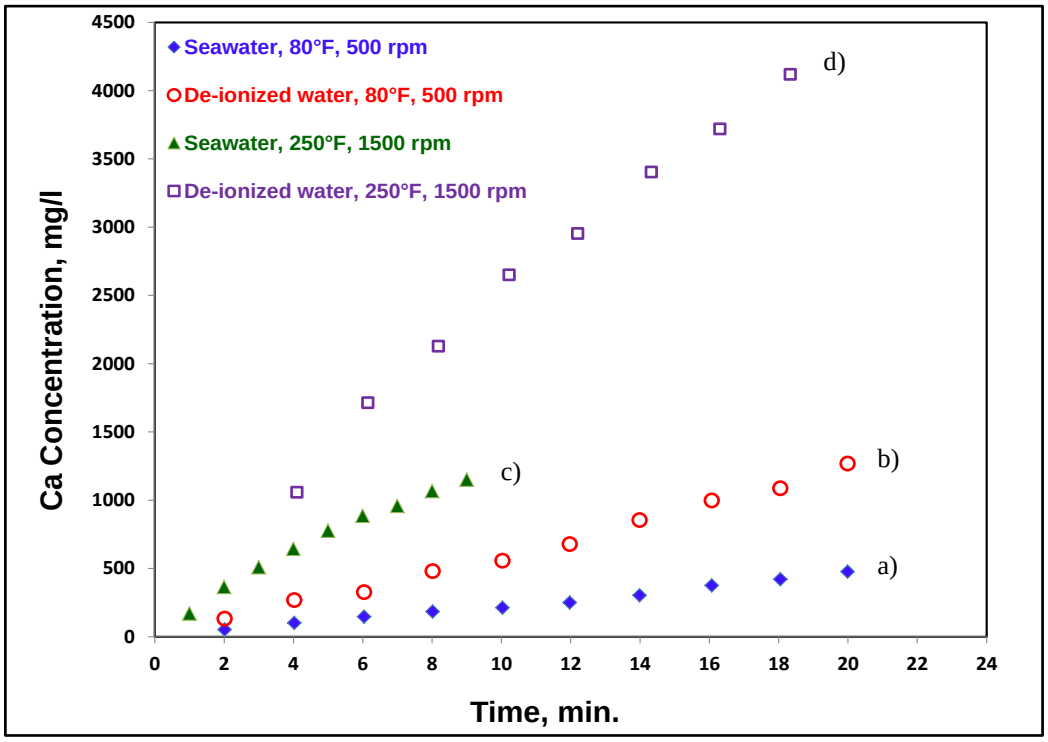

Fig 6.15: Change of Calcium Concentration with time for the reaction of 5 wt% lactic acid at: a) 80°F, 500 rpm, seawater, b) 80°F, 500 rpm, de-ionized water, c) 250°F, 1500 rpm, seawater, and d) 250°F, 1500 rpm, de-ionized water.

The rate of dissolution was determined for both cases and is shown in **Fig. 6.13.** The results were graphically compared to those obtained when the acid was prepared in deionized water. From the results shown in Fig. 16-13, it is clear that the presence of salts such as sodium chloride, calcium chloride, magnesium chloride, and sodium sulfate exhibits an adverse effect on the rate of dissolution by lactic acid. This is most likely due to the reduction in the concentration gradient of the product (calcium lactate) because of

the increase in the concentration of other ions such as calcium, magnesium, and sulphate ions in solutions. This reduction in the concentration gradient will cause a lower rate of diffusion of the calcium generated from the reaction, and hence a lower rate of dissolution.

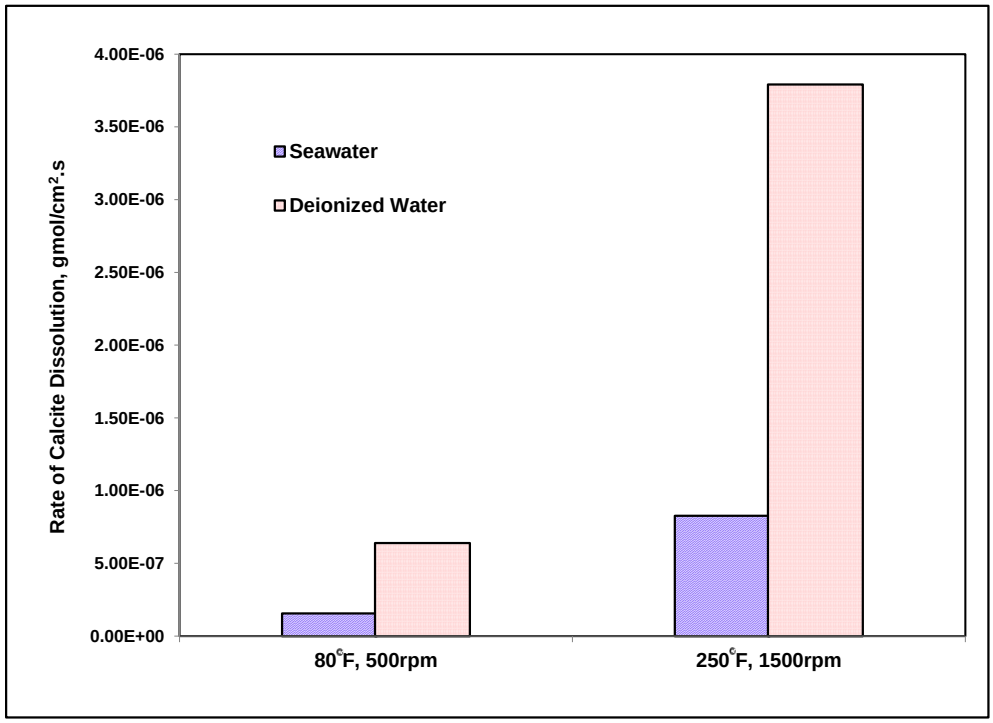

Fig 6.16: Comparison between the rate of dissolution for the reaction of 5 wt% lactic acid with calcite when the acid was prepared using deionized water (dotted), and seawater (dashed).

7. CONCLUSIONS

In this chapter, conclusions from each case study are summarized separately in the same order of listing them in the dissertation

7.1 Reaction of GLDA with Calcite

Based on the rotating disk and the core flood experiments, the following conclusions are made:

1- Reaction of GLDA with calcite is a mass transfer limited up to 1800 rpm.

2- Increasing temperature significantly increased the dissolution rate. The rate of dissolution at pH 3.8, 1000 rpm, and 80^{o}F increased 6 times when the temperature was increased to 200^{o}F.

3- 0.6M GLDA reacted faster at pH of 1.7. At this pH, GLDA reacts as polyprotic acid and the dominant mechanism is hydrogen ion attack.

4- The reaction at pH 3.8, and 13 became less dependent on the disk rotational speed, which indicated that at these pH values the kinetics of the surface reaction play a key role in the overall rate.

5- Increasing temperature increased both the rate of chelation and hydrogen attack reactions with a reduction in the influence of the chelation.

6- Increasing the disk rotational speed did not have a significant effect on the rate of the chelation reaction.

7- The values of the diffusion coefficients from the reaction study of 0.6M GLDA was combined with core flood data to determine the Damköhler number. In all experiments, there was an optimum Damköhler number that corresponded to a minimum pore volume required to break through the core.

8- In the core flood study, increasing temperature or decreasing the pH increased the optimum Damköhler number with a reduction in the minimum pore volume required to breakthrough.

7.2 Reaction of GLDA with Dolomite

1- Dolomite dissolution is a surface reaction limited at 150, 200, and 250°F at disk rotational speeds greater than 500 rpm.

2- Below 500 rpm, a transition region was noted that reveals a mutual influence of mass transfer and surface reaction affects the dolomite dissolution.

3- GLDA diffusivity in the transition region is consistent with an apparent activation energy of 15 kcal/mol, while the rate data of the surface reaction limited region is consistent with activation energy of 9.2 kcal/mol.

4- The rate of calcite dissolution with GLDA is higher than the rate of dolomite dissolution by a factor varying from 20 to 75, depending on the temperature of reaction.

7.3 HCl-Formic In-Situ Gelled Acid for Carbonate Acidizing

The performance of four different HCl-formic in-situ acid solutions was investigated by viscosity measurements, reaction rate, and core flood studies. Based on the results obtained, the following conclusions can be drawn:

1) The presence of formic acid in formic-HCl solutions increased the viscosity of the live acid and reduced the viscosity of the partially neutralized (pH 4-5) acids compared to the viscosity of in-situ HCl gelled acid with the same acid molar concentration.

2) Increasing formic acid concentration to 2, 4 and 6 wt% significantly increased the viscosity of the live acid and reduced the viscosity of the spent acid to a point that the viscosity of the spent acid became higher than the viscosity of the live acid for acids B and C.

3) The reaction rate of in-situ HCl-formic gelled acids is higher than the reaction rate of the in-situ HCl and the higher the formic acid concentration, the higher the reaction rate.

4) The reaction rate of the HCl-formic in situ gelled acids is comparable to the reaction rate of the gelled acid indicating the negative effect of the presence of formic acid on the proper development of the gel structure.

5) 5 wt% HCl in-situ gelled acid was the only acid that was able to achieve an efficient degree of gelation and diversion at a low rate of injection.

6) Core flood study showed that the wormhole propagation rate reduced by increasing formic acid concentration or increasing the acid injection rate.

7.4 Reaction of Lactic Acid with Calcite

Mass transport and kinetic study was conducted to understand the reaction of lactic acid with Indiana limestone using the rotating disk apparatus and the following are the main conclusions:

1- At low temperature ($80^{o}F$), the reaction of lactic acid with calcite was mainly controlled by the kinetics of the surface reaction, unless the disk rotational speed

was very low (< 500 rpm) in which the rate of dissolution is controlled by mass transfer.

2- At higher temperatures (200 and 250^{o}F), the dependence of the rate of dissolution on the disk rotational speed increased up to 1500 rpm. Above this value of rotational speed the reaction was limited by the surface kinetics.

3- In the mass transfer region, the lactic acid diffusivity was determined and reported at low temperature (80^{o}F) and higher temperatures (200 and 250^{o}F) and was found to be $1.23x10^{-6}$, $8.92x10^{-6}$, and $1.45x10^{-5}$ cm^2/s, respectively.

4- The reaction rate data at 1500 rpm was fitted to a power-law kinetic expression and the reaction rate order and the reaction rate constant was determined at 80, 150, 200, and 250^{o}F. At these temperatures, the reaction rate constants were 0.571, 0.646, 0.687, and 0.773 $gmol^{(1-n/2)}/cm^{(2-3n/2)}$.s, respectively.

5- The activation energy of the reaction of lactic acid with Indiana limestone is determined and found to be equal to 3.018 kJ/gmol and the pre-exponential constant (A) was equal to 1.89 $gmol^{(1-n/2)}/cm^{(2-3n/2)}$.s.

6- The reaction of 5 wt% lactic acid with Indiana limestone was reduced when the acid prepared by seawater indicating a negative effect of the presence of sodium,

magnesium, and sulfate salts on the rate of reaction. Therefore it is not recommended to prepare the acid in seawater for offshore stimulation purposes.

NOMENCLATURE

A	=	pre-exponential constant in Arrhenius equation
C_b	=	reactant concentration in the bulk solution, gmol.cm^{-3}
C_s	=	reactant concentration at the surface, gmol.cm^{-3}, gmol.cm^{-3}
d	=	average wormhole diameter, cm
Da	=	Damköhler number, -
D_e	=	effective diffusion coefficient cm^{2}.s^{-1}
E_a	=	reaction activation energy, J/gmol
J	=	mass flux, gmol.cm^{-2}.s^{-1}
k_f	=	reaction rate constant, gmol$^{(1-n/2)}$/cm$^{(2-3n/2)}$.s
k_{sr}	=	surface reaction constant, cm.s^{-1}
K_a	=	acid dissociation coefficient, -
K_m	=	reactant mass transfer coefficient, cm.s^{-1}
l	=	wormhole length, cm
Q	=	injection volumetric flow rate, cm^{3}.s^{-1}
r_D	=	rate of calcite dissolution, gmol.cm^{-2}.s^{-1}
R	=	universal gas constant, = 8.314 J/(gmole.^{o}K)
R_s	=	rate of surface reaction, gmol/cm^{2}.s
R_{MT}	=	rate of mass transfer, gmol/cm^{2}.s
Sc	=	Schmidt number, -
ΔH	=	change in enthalpy, J/gmol

ΔE = activation energy, J/gmol

υ = kinematic viscosity, $cm^2.s^{-1}$

ω = disk rotational speed, s^{-1}

μ = fluid viscosity, Pa.s

ρ = fluid density, $kg.m^{-3}$

REFERENCES

Alkattan, M., Oelkers, E., Dandurand, J., and Schott, J. 1998. An Experimental Study of Calcite and Limestone Dissolution Rates as a Function of pH from 1 to 3 and Temperature from 25 to 80^{o}C. *Chemical Geology*, **152**:199-214.

Al-khaldi, M.H., Nasr-El-Din, H. A., Mehta, S., and Al-Aamri, A. 2007. Reaction of citric acid with calcite. *Chemical Engineering Science*, **62**(21): 5880-5896.

Al-khaldi, M.H., Nasr-El-Din, H.A., and Sarma., H. 2010a. Kinetics of the Reaction of Citric Acid With Calcite. *SPE Journal.*, **15**(3): 704-713.

Al-khaldi, M.H., Sarma., H.K., and Nasr-El-Din, H.A. 2010b. Diffusivity of Citric Acid During its Reaction With Calcite. *Journal of Canadian Petroleum Technology*, **49**(8): 43-52.

Al-Moajil, A.M., Nasr-El-Din, H.A., and Al-Aamri, A.D. 2007. Evaluation of In-situ Generated Acids for Filter Cake Clean Up. Paper SPE 107537 presented at the European Formation Damage Conference held in Scheveningen, Netherlands, 30 May–1 June.

Al-Moajil, A.M., Nasr-El-Din, H.A., and Al-Yami, A. 2008. Removal of Filter Cake Formed by Manganese Tetraoxide Based-Drilling Fluids. Paper SPE 112450 presented at the SPE International Symposium and Exhibition on Formation Damage Control, Lafayette, Louisiana, USA, 13-15 February.

Almond, S.W., Harris, R.E., and Penny, G.S. 1995. Utilization of Biologically Generated Acid for Drilling Fluid Damage Removal and Uniform Acid Placement across Long

Formation Intervals. Paper SPE 30123 presented at the SPE European Formation Damage Conference, The Hague, Netherlands, 15-16 May.

Al-Otaibi, M.B. and Nasr-El-Din, H.A. 2008. Use of Ester as a precursor to clean Formate Drill-in Fluid Damage in Horizontal Wells" paper SPE 127514, *SPE Drilling and Completion*, **24**(3): 404-412.

Al-Otaibi, M.B., Al-Moajil A.M., and Nasr-El-Din, H.A. 2006. In-situ Acid System to Clean-up Drill-in Fluid Damage in High Temperature Gas Wells. Paper SPE 103846 presented at the IADC/SPE Asia Pacific Drilling Technology Conference and Exhibition held in Bangkok, Thailand, 13–15 November.

Anderegg, G., and Podder, N. 1975. Pyridine-Derivatives as Complexing Agents .10. Thermodynamics of Complex-Formation of N,N'-Bis-(2-Pyridylmethyl)-Ethylenediamine and of Two Higher Homologues. *Journal of Coordination Chemistry*. **4**:297

Arena, G., Musumeci, S., and Purrello, R. 1983. Calcium-Edta and Magnesium-Edta Complexes - Stability-Constants and Their Dependence on Temperature and Ionic-Strengt. *Thermochimica Acta*. **61**(2): 129-138.

Barron, A.N., Hendrickson, A.R., and Wieland, D.R. 1962. The Effect of Flow on Acid Reactivity in a Carbonate Fracture. *Journal of Petroleum Technology*, 409-415, AIME, 225.

Ba-Taweel, M.A., Al-Anazi, H., Al-Otaibi, M., Ballan, A., and Hilab, V. 2006. Core Flood Study of Injectivity Decline by Mixing Produced Oily Water with Seawater in

Arab-D Reservoir. Paper SPE 106356 presented in SPE Technical Symposium of Saudi Arabia Section. Dhahran, Saudi Arabia, 21-23 May.

Boles, J.L., Metcalf, A.S., and Dawson, J.C. 1996. Coated Breaker for Cross-linked Acid. United States Patent 5497830, 12 March.

Bryant, S.L., Rabaioli, M.R., and Lockhart, T.P. 1996. Influence of syneresis on permeability reduction by polymer gels. *SPE Production & Facilities*. **11**(4): 209-215.

Buijse, M., de Boer, P., Breukel, B., and Burgos, G. 2004. Organic Acids in Carbonate Acidizing. *SPE Production & Facilities* **19** (3): 128–134. SPE-82211-PA. doi: 10.2118/82211-PA.

Busenberg, E. and Plummer, L.N. 1982. The Kinetics of Dissolution of Dolomite in CO_2-H_2O Systems at 1.5-Degrees-C to 65-Degrees-C and O-Atm to 1-Atm PCO_2. *American Journal of Science*, 282 (1): 45-78

Carrasco, F., Pages, P., Gamez-Perez, J., Santana, O., and Maspoch, M. 2010. Kinetics of the Thermal Decomposition of Processed Poly(Lactic Acid). *Polyemr Degradation and Stability*. In press. Accepted 29 July 2010.

Chang, F., Nasr El-Din, H.A., Lindvig, T., and Qiu, X.W. 2008. Matrix Acidizing of Carbonate Reservoirs Using Organic Acids and Mixture of HCl and Organic Acids. Paper SPE 116601 presented at the Annual Technical Conference and Exhibition. Denver, Colorado, USA.

Chang, F., Qu, Q., and Frenier, W. 2001. A Novel Self-Diverting-Acid Developed for Matrix Stimulation of Carbonate Reservoirs. Paper SPE 65033 presented at the

International Symposium on Oilfield Chemistry held in Houston, Texas, 13–16 February.

Conway, M.W., Asadi, M., Penny, G.S., Change, F. 1999. A Comparative Study of Straight/Gelled/Emulsified Hydrochloric Acid Diffusivity Coefficient Using Diaphragm Cell and Rotating Disk. Paper SPE 56532 presented at the Annual Technical Conference and Exhibition, Houston, Texas, USA, 3-6 October.

Craggs, A., Moody, G., and Thomas, J. 1979. Calcium Ion-Selective Electrode Measurements in the Presence of Complexing Ligands. *Analyst.* **104**(1243): 961-972.

Dean, J.A., 1999. Lange's Handbook of Chemistry. 15th ed. McGraw–Hill. ISBN 0-07-016384-7.

Dill, R.W., and Keeney, B.R. 1978. Optimizing Hcl-formic acid mixtures for high temperature stimulation. Paper SPE 7567 presented at the Annual Fall Technical Conference and Exhibition. Houston, Texas,

Economides, M.J. and Nolte, K.G. 1989. Reservoir Stimulation. Prentice Hall, New Jersey. 13-01- 13-12

Ellision, B.T. 1969. Mass Transfer to a Rotating Disk. PhD Thesis University of California, Berkeley.

Finneran, D.W., and Morse, J.W. 2008. Calcite dissolution kinetics in saline waters. *Chemical Geology*, **268**: 137-146.

Fogler, H.S., Lund, K., and Mccune, C.C. 1975. Acidization 3. Kinetics of Dissolution of Sodium and Potassium Feldspar in Hf-Hcl Acid Mixtures. *Chemical Engineering Science*, **30**(11): 1325-1332.

Fredd, C.N. and Fogler, H.S. 1998a. The Kinetics of Calcite Dissolution in Acetic Acid Solutions. *Chemical Engineering Science.*, **53** (22): 3863–3874.

Fredd, C.N. and Fogler, H.S. 1998b. The Influence of Chelating Agents on the Kinetics of Calcite Dissolution. *Journal of Colloid and Interface Science.* **204**(1): 187-197.

Fredd, C.N. and Fogler, H.S. 1998c. Influence of Transport and Reaction on Wormhole Formation in Porous Media. *American Institute of Chemical Engineering.* **44** (9): 1933-1949.

Fredd, C.N. 2000. Reservoir Stimulation: Appendix: Advances in Understanding and Predicting Wormhole formation. 3rd edition, Prentice Hall, A16-1: A16-18.

Frenier, W.W., Brady, M., Al-Harthy, S., Arangath, R., Chan, K.S., Flamant, N., and Samuel, M. 2004. Hot oil and gas wells can be stimulated without acids. *SPE Production & Facilities*. **19**(4): 189-199

Frenier, W.W., Fredd, C.N. and Chang, F. 2001. Hydroxyaminocarboxylic Acids Produce Superior Formulations for Matrix Stimulation of Carbonates. Paper SPE 68924 presented at the European Formation Damage Conference, The Hague, The Netherlands, 21-22 May. DOI: 10.2118/68924-MS.

Gautelier, M., Oelkers, E.H., and Schott, J. 1999. An experimental study of dolomite dissolution rates as a function of pH from 0.5 to 5 and temperature from 25 to 80°C. *Chemical Geology.* **157**: 13–26.

Glasbergen, G., Kalia, N, and Talbot, M. 2009. The Optimum Injection Rate for Wormhole Propagation: Myth or Reality? Paper SPE 121464 presented at the 2009

European Formation Damage Conference, Scheveningen, The Netherlands, 27-29 May.

Gomaa, A.M. and Nasr-El-Din, H.A. 2010a. New Insights into Wormhole Propagation in Carbonate Rocks Using Regular, Gelled and In-Situ Gelled Acids. Paper SPE 133303 presented at the SPE Production and Operations Conference and Exhibition, Tunis, Tunisia, 8–10 June.

Gomaa, A.M. and Nasr-El-Din, H.A. 2010b. New Insights into the Viscosity of Polymer-Based In-Situ Gelled Acids. *Journal of SPE Production & Operations*. **25** (3): 367-375.

Gomaa, A.M., Mahmoud, M., and Nasr-El-Din, H.A. 2009. When Polymer-based Acids can be used? A Core Flood Study. Paper IPTC 13739 presented at the SPE International Petroleum Technology Conference, Doha, Qatar, 7–9 December.

Hansford, G.S. and Litt, M. 1968. Mass Transport from a Rotating Disk into Power-Law Liquids. *Chemical Engineering Science*, **23**: 849-864.

Hill, D.G. 2005. Gelled Acid. United States Patent Application Publication, US2005/0065041 A1, Mar. 24.

Huang, T., McElfresh, P.M., and Gabrysch, A.D. 2003. Carbonate Matrix Acidizing Fluids at High Temperatures: Acetic Acid, Chelating Agents or Long-Chained Carboxylic Acids? Paper SPE 82268 presented at the SPE European Formation Damage Conference, Netherlands 13-14 May.

Hung, K.M., Hill, A.D., and Sepehrnoori, K. 1989. A Mechanistic Model of Wormhole Growth in Carbonate Matrix Acidizing and Acid Fracturing. *Journal of Petroleum Technology*, **41**(1): 59-66

Jamialahmadi, M. and Muller-Steinhagen, H. 1991. Reduction of Calcium-Sulfate Scale Formation during Nucleate Boiling by Addition of EDTA. *Heat Transfer Engineering*. **12**(4):19-26.

Kalfayan, L.I., and Martin, A.N. 2009. The Art and Practice of Acid Placement and Diversion: History, Present State and Future. Paper SPE 124141 presented at the Annual Technical Conference and Exhibition, New Orleans, Louisiana, USA, 4-7 October.

Khodadoust, A.P., Reddy, K.R., and Maturi, K. 2005. Effect of different extraction agents on metal and organic contaminant removal from a field soil. *Journal of Hazardous Materials*. **B117**: 15-24.

Kline, W.E. and Fogler, H.S. 1981, Dissolution Kinetics - Catalysis by Strong Acids. *Journal of Colloid and Interface Science*, **82**(1): 93-102.

Kung, M.S. 1998. Flow and reaction of weak acids in carbonate porous media. MS thesis, University of Michigan, Ann Arbor, Michigan.

LePage, J.N., De Wolf, C.A., Bemelaar, J.H., and Nasr-El-Din, H.A. 2011. An Environmentally Friendly Stimulation Fluid for High Temperature Applications. *SPE Journal*. **16**(1): 104-110.

Levich, V.G. 1962. Physicochemical Hydrodynamics, Prenctice-Hall, Englewood Cliffs, New Jersey, 78-83.

Lund, K., Fogler, H.S., and McCune, C.C. 1973. Acidization I: The Dissolution of Dolomite in Hydrochloric Acid, *Chemical Engineering Science*, **28**: 681-700.

Lund, K., Fogler, H.S., McCune, C.C. and Ault, J.W. 1975. Acidization–II. The Dissolution of Calcite in Hydrochloric Acid. *Chemical Engineering Science* **30**(8): 825–835. doi: 10.1016/0009-2509(75)80047-9.

Lynn, J.D. and Nasr-El-Din, H.A. 2001. A Core-Based Comparison of the Reaction Characteristics of Emulsified and In-Situ Gelled Acids in Low Permeability, High Temperature, Gas Bearing Carbonates. Paper SPE 65386 presented at the SPE International Symposium on Oilfield Chemistry, Houston, Texas, USA, February 13-16.

MaGee, J., Buijse, M.A., and Pongratz, R. 1997. Method for Effective Fluid Diversion when Performing a Matrix Acid Stimulation in Carbonate Formations. Paper SPE 37736 presented at the Middle East Oil Show, Bahrain, 15-18 March.

Mahmoud, M.A., Nasr-El-Din, H.A., De Wolf, C.A., LePage, J.N. 2010a. An Effective Stimulation Fluid for Deep Carbonate Reservoirs: A Core Flood Study. Paper SPE 131626 presented at the 2010 International Oil and Gas Conference, Beijing, China, 8-10 June.

Mahmoud, M.A., Nasr-El-Din, H.A., De Wolf, C.A., LePage, J.N. 2010b. Optimum Injection rate of A new chelate that can be used to stimulate carbonate reservoirs. Paper SPE 133497 presented at the 2010 SPE Annual Technical Conference and Exhibition, Florence, Italy, 19-22 September.

Mahmoud, M.A., Nasr-El-Din, H.A., De Wolf, C.A., LePage, J.N. and Bemelaar, J.H. 2011. Evaluation of a New Environmentally Friendly Chelating Agent for High-Temperature Applications. *SPE Journal*. **16**(3): 559-574.

Martell, A.E. and Calvin, M. 1956. Chemistry of Metal Chelate Compounds. Prentice-Hall, New Jersy, USA..

Moore, R.E., Bischof, A.E., Robins, J.D., and Brenneman, D.R. 1972. One-Step Anhydrite Scale Removal. *Journal of Material Protection and Performance*. **11**(3): 41-44.

Muller, G.T. and Stokes, R.H. 1957. The Mobility of the Undissociated Citric Acid Molecule in Aqueous Solutions. *Transacion of the Faraday Society*. **53**: 642–645. doi: 10.1039/tf9575300642.

Nasr-El-Din, H.A., Driweesh, S.M., and Muntasheri, G.A. 2003. Field Application of HCl-Formic Acid System to Acid Fracture Deep Gas Wells Completed with Super Cr-13 Tubing in Saudi Arabia. Paper SPE 84925 presented at the International Improved Oil Recovery Conference held in Kuala Lumpur, Malaysia, 20-21 October

Nasr-El-Din, H.A., Al-Mohammad, A.M., Al-Aamri, A.M. and Al-Fuwaires, O. 2008. Reaction of Gelled Acids with Calcite. *SPE Production & Operations*, **23**(3): 353-361.

Nasr-El-Din, H.A., Al-Zahrani, A., Garzon, F.O., Giraldo, C.A.F., I., Al-Hakami, M., and Al-Marri, H.M. 2009. Acid Fracturing of Gas Wells by Use of an Acid Precursor in the Form of Solid Beads: Lessons learned From First Field Application. SPE paper 110895, *SPE Production & Operation*s: May, 320-335.

Nasr-El-Din, H.A., Al-Zahrani, A., Still, J., Lesko, T., and Kelkar, S. 2007. Laboratory Evaluation of An Innovative System For Fracture Stimulation of High-Temperature Carbonate Reservoirs. Paper SPE 106054 presented at the International Symposium on Oilfield Chemistry, Houston, 28 February–2 March.

Newman, J. 1966. Schmidt Number Correction for the Rotating disk. *Journal of Physical Chemistry*, **70**(4): 1327-1328.

Nierode, D.E. and Williams, B.B. 1971. Characteristics of Acid Reactions in Limestone Formations. *Journal of Society of Petroleum Engineering*, **11**(4): 406-418.

Peters, R.W. 1999. Chelant extraction of heavy metals from contaminated soils. *Journal of Hazardous Materials*. **66:**151-210.

Plummer, L.N., Wigley, T.L., and Parkhurst, D.L. 1978. Kinetics of Calcite Dissolution in CO_2-Water Systems at 5-Degrees-C to 60-Degrees-C and 0.0 to 1.0 atm CO_2. *American Journal of Science.* **278**:179-216.

Pokrovsky, O.S., Golubev, S.V., and Schott, J. 2005. Dissolution kinetics of calcite, dolomite and magnesite at 25 degrees C and 0 to 50 atm pCO_2. *Chemical Geology*, **217**(3-4): 239-255.

Pokrovsky, O.S., Golubev, S.V., Schott, J., and Castillo, A. 2009. Calcite, dolomite and magnesite dissolution kinetics in aqueous solutions at acid to circumneutral pH, 25 to 150 degrees C and 1 to 55 atm pCO_2: New constraints on CO_2 sequestration in sedimentary basins. *Chemical Geology*, **265**(1-2): 20-32.

Polettini, A., Pomi, R., Rolle, E., Ceremigna, D., De Propris, L., Gabellini, M., and Tornato, A. 2006. A kinetic study of chelant-assisted remediation of contaminated dredged sediment. *Journal of Hazardous Materials*. B137:1458-1465.

Rabie A.I., Gomaa A.M., and Nasr-El-Din H.A. 2011a. Reaction of In-situ Gelled Acids with Calcite: Reaction Rate Study. *SPE J.* **16** (4): 981-992. SPE 133501-PA.

Rabie, A.I, and H.A. Nasr-El-Din. 2011c. Measuring the Reaction Rate of Lactic Acid with Calcite and Dolomite Using the Rotating Disk Apparatus. Paper SPE-140167 presented at the 17th SPE Middle East Oil & Gas Show and Conference (MEOS), Manama, Bahrain, 25-28 September.

Rabie, A.I, Mahmoud, M.A, and Nasr-El-Din, H.A. 2011b. Reaction of GLDA with calcite: Reaction Kinetics and Transport Study. SPE 139816 presented at the 2011 International Symposium on Oil Field Chemistry, Woodland, TX, USA, 11-13

Rabie, A.I., Gomaa A.M., and H.A. Nasr-El-Din. 2012. HCl-Formic In-Situ Gelled Acid for Carbonate Acidizing: Core Flood and Reaction Rate Study. *SPE Production & Operation*, **27** (2): 170-184.

Roberts, L.D. and Guin, J.A. 1974. The effect of surface kinetics on the fracture acidizing. *SPE Journal*, **14** (4): 385-395.

Rostami, A. and Nasr-El-Din, H.A. 2010. Optimization of a Solid-acid Precursor for Self- destructing Filter Cake. Paper SPE 139087 presented at the 2010 SPE Eastern Regional Meeting held in Morgantown, West Virginia, USA, 12-14 October.

Sayed, M.A., and Nasr-El-Din, H.A. 2012. Reaction Rate of Emulsified Acids and Dolomite. Paper SPE 151815. Presented at the International Symposium and Exhibition on Formation Damage Control, Lafayette, Louisiana, 15-17 February.

Schechter, R.S. 1992. Oil Well Stimulation. Prentice Hall, New Jersey. 403-425.

Sjoberg, E.L. and Rickard, D.T. 1984. Calcite Dissolution Kinetics - Surface Speciation and the Origin of the Variable pH-Dependence. *Chemical Geology*, **42**(1-4): 119-136.

Smith, C.F., Crowe, C.W., and Nolan, T.J. III. 1969. Secondary Deposition of Iron Compounds Following Acidizing Treatments. SPE *Journal of Petroleum Technology*, **21**(9): 1121-1129.

Still, J.W., Dismuke, K., and Frenier, W.W. 2007. Generating acid downhole in acid fracturing. US Patent No. 7,166,560.

Taylor, K.C. and Nasr-El-Din, H.A. 1999. A systematic study of iron control chemicals-part 2. Paper SPE 50772 presented at the International Symposium on Oilfield Chemistry, Houston, Texas, 16-19 February.

Taylor, K.C. and Nasr-El-Din, H.A. 2002. Coreflood Evaluation of In-Situ Gelled Acid. Paper SPE 73707 presented at the International Symposium and Exhibition on Formation Damage held in Lafayette, Louisiana, U.S.A., 20–21 February.

Taylor, K.C. and Nasr-El-Din, H.A. 2003. Laboratory Evaluation of In-Situ Gelled Acids for Carbonate Reservoirs. *SPEJ*, **8**(4): 426-434.

Taylor, K.C., Al-Ghamdi, A.H., and Nasr-El-Din, H.A. 2004. Measurement of Acid Reaction Rates of a Deep Dolomitic Gas Reservoir. *Journal of Canadian Petroleum Technology* **43** (10): 49–56.

Van Domelen, M.S. and Jennings, A.R. 1995. Alternate Acid Blends for HPHT Applications. Offshore Europe, Aberdeen, United Kingdom, 5-8 September.

Van Ginkel, G.G., Geets, R. and Nguyen, P.D. 2005. Biodegradation of L-Glutamatediacetic acid by Mixed Cultures and an Isolate. *Biodegradability of chelating Agents*. ACS Symposium Series Volume 910, pp: 183-194.

Vitagliano, V. and P.A. Lyons. 1965. Diffusion in Aqueous Acetic Acid Solutions. *Journal of the American Chemical Society*, 1956. **78**(18): p. 4538-4542.

Welton, T.D. and Van Domelen, M.S. 2008. High-Viscosity-Yield Acid Systems for High-Temperature Stimulation. *SPE Production & Operations*. **23**(2): 177-183.

Williams, B.B., Gidley, J.L., and Schechter, R.R. 1979. Acidizing Fundamentals, Monograph Series, SPE, Richardson, Texas.

Willberg, D. and Dismuke, K. 2009. Self-destructing Filter Cake. US Patent No. 7482311.

Woo, G.T., Lopez, H., Metcalf, A.S., and Boles, J. 1999. A New Gelling System for Acid Fracturing. Paper SPE 52169 presented at the Mid-Continent Operations Symposium held in Oklahoma City, Oklahoma, 28-31 March.

Yeager, V. and Shuchart, C. 1997. In-Situ Gels Improve Formation Acidizing. *Oil & Gas Journal.* **95:** 70-72.

Zenger, D.H., Dunham, J.B., Ethington, R.L., 1980. Concepts and models of dolomitization. Special Publication-SEPM **28**: 320-333

Zhang, R., Hu, S., Zhang, X., and Yu, W. 2007. Dissolution Kinetics of Dolomite in Water at Elevated Temperatures. *Aquatic Geochemistry*, **13**(4): 309-338.